8-2017

Evaluation and Uncertainty Quantification of VS30 Models Using a Bayesian Framework for Better Prediction of Seismic Site Conditions

Andrew West Brownlow
Clemson University, abrownlow21@gmail.com

EVALUATION AND UNCERTAINTY QUANTIFICATION OF V_{S30} MODELS USING A BAYESIAN FRAMEWORK FOR BETTER PREDICTION OF SEISMIC SITE CONDITIONS

A Dissertation
Presented to
the Graduate School of
Clemson University

In Partial Fulfillment
of the Requirements for the Degree
Doctor of Philosophy
Civil Engineering

---

by
Andrew West Brownlow
August 2017

Accepted by:
Dr. Qiushi Chen, Committee Chair
Dr. C. Hsein Juang, Co-chair
Dr. Ronald D. Andrus
Dr. Jie Zhang

ABSTRACT

The time-averaged shear-wave velocity in the top 30 meters of subsurface material (V_{S30}) is a widely used parameter when estimating the potential for amplification of seismic waves. Situations often arise where a design V_{S30} value needs to be chosen from multiple proxy-based V_{S30} models. This dissertation seeks to assist with the problem of model selection and to improve the overall prediction of V_{S30} through implementation of a Bayesian framework for model ranking. Furthermore, this dissertation investigates the effects of uncertainty on the model ranking results.

In this work, probabilistic methods are developed and implemented to assess the performance of multiple proxy-based V_{S30} models. The methodology utilizes Maximum Likelihood Estimation (MLE) to evaluate how well a model (or set of models) can predict the sample data against which it is being evaluated. Bayesian Information Criterion (BIC) is used to quantify the relative performance of multiple candidate V_{S30} models. The proposed method can provide a performance ranking for situations when one model is superior as well as when multiple models show comparable levels of performance. With ranking results, a new V_{S30} database comprised of a superior set of V_{S30} predictions based on known information can be obtained, and this is illustrated through the development of a new synthetic V_{S30} database for California. The method is also applied to other regions of the country, specifically the Seattle and Puget Sound area and the Salt Lake City, Ogden, and Provo area to further demonstrate the new method and explore its applicability to areas with limited data. Enhanced site condition maps for those regions are also developed.

To strengthen confidence in predictions and designs, civil engineers have started to explicitly consider uncertainty in their calculations. The Bayesian method for model ranking presented herein is also presented in a modified form to allow users to include appropriate, available uncertainty information. The effects of uncertainty on the updated site conditions map for California are investigated, and recommendations for appropriate use of uncertainty information in model ranking applications are made.

Finally, the new synthetic database is used to inform the hazard information needed when performing a CPT-based liquefaction hazard quantification calculation. Its application is explained alongside an illustrative example in the San Francisco Bay area.

DEDICATION

For Melissa

ACKNOWLEDGMENTS

The research performed during the process of developing this dissertation was supported as part of a research project funded by AIG. I am very grateful that AIG was able to provide the catalyst and resources that made this dissertation a reality.

As with all PhDs, my degree would not have happened without a significant support group who all contributed to my success. I wish I could thank everyone individually here, but there are some significant contributors to whom I am indebted.

I must first thank my wife, Melissa, for her steadfast support throughout this arduous process. She has been a primary facilitator of my success, and I cannot thank her enough for her patience and understanding.

To my advisors, thank you so much for your patience and willingness to help answer my seemingly endless questions. Your support and guidance has been invaluable, and I have grown tremendously thanks to your instruction. Dr. Hsein Juang first invited me to pursue a PhD after watching a presentation I gave in one of his classes. I am ever grateful for the opportunity that he provided. Dr. Zhang Jie has been a tremendous resource on whom I could rely when I had challenging questions and source of endless positive encouragement. Dr. Qiushi Chen, the chair of my committee, has helped drive my progress, offering helpful words and prodding me along to make this dissertation a reality. Dr. Ron Andrus gave invaluable critiques and drove me to understand the fundamentals of both my work and the applications thereof, and I am incredibly grateful for the motivation and direction that he provided.

I must also acknowledge Alireza Shahjouei and Mohammad Javanbarg, both of whom provided the baseline research project and pointed guidance that led to this dissertation. Ali and I worked hard together to thoroughly refine the scope of this work to be sure my research would lead to something meaningful.

A person who deserves far more credit than she ever receives, but without whom I may never have successfully navigated the confusing and chaotic world of university politics is Kristi Baker. I am eternally grateful for her constant, cheerful willingness to help me accomplish whatever task was at hand and keep me moving towards my goal.

Finally, I want to thank the Clemson Men's Ultimate team: The Joint Chiefs of Waft, for keeping me sane and painfully aware of my age throughout my journey.

TABLE OF CONTENTS

LIST OF TABLES

LIST OF FIGURES

Figure Page

CHAPTER 1

INTRODUCTION

1.1 PROBLEM STATEMENT

Earthquakes are among nature's most powerful, devastating natural phenomena. The specific phenomenon referred to as an earthquake can occur due to natural processes or powerful explosions, and is characterized by transmission of kinetic energy through the surface of the earth as seismic waves. There are multiple types of seismic waves, and each wave manifests in different ways, but the end result is some degree of potentially damaging ground motion. These damages can include structural damage from the actual ground motion, but also damages that can result from hazards triggered by the earthquake including liquefaction, fire, landslides, and flooding.

Significant effort and resources have been dedicated to understanding and predicting earthquakes and earthquake-induced hazards. Ground motion prediction equations (GMPEs) (e.g., those found in Douglas 2011) have been developed for decades; they are an attempt to help engineers and stakeholders anticipate the risks associated with earthquake shaking. An important component to ground motion prediction is the potential for amplification of seismic energy, expressed via amplification factors. Borcherdt (1994) recommended a relationship for estimating site amplification based on V_{S30}, the time-averaged shear wave velocity to 30 meters depth. Boore et al. (1993, 1994) utilized V_{S30} in ground motion prediction equations, and was a catalyst for widespread adoption of V_{S30} in site condition assessments. Because of its popularity as a parameter for seismic site

response characterization, it is desirable to estimate the value at locations where V_{S30} measurement data are not available. Although there are currently multiple models available for estimating V_{S30} there is no clear guidance for which model produces the best results at a location of interest.

1.2 OBJECTIVES

The objective of this research is to develop a tool to evaluate and quantify the impact of proxy-based V_{S30} models, including explicit consideration of uncertainty, using a Bayesian framework to facilitate better prediction of seismic site conditions. In addition to its use in GMPEs, seismic design codes (e.g. FEMA 2015) utilize V_{S30} to suggest site amplification factors. This research also presents a method for explicit consideration of uncertainties in both benchmark data and in candidate models when evaluating competing proxy-based V_{S30} models for their predictive capacity.

There are known limitations to the use of V_{S30} as an indicator of seismic site conditions (e.g., Mucciarelli and Gallipoli, 2006, Castellaro et al. 2008), and this dissertation should not be interpreted as an endorsement for site characterization using V_{S30}. However, the fields of seismic engineering design and hazard mitigation consistently use V_{S30} for site classification purposes. Therefore, it is still desirable to improve the existing methods for estimating V_{S30} in the absence of measurement data.

1.3 MOTIVATIONS

Currently, various proxy-based methods are used for estimation of V_{S30}, but there are no clear guidelines to help potential end-users to select the best method for their specific application. A key issue lies in the current state of the art for V_{S30} prediction. Two primary

forms of proxy data, topography and geology, are used to estimate V_{S30}. However, there is no direct relationship between the two methods, and therefore evaluation of their relative strengths and weaknesses falls to the end user. To address this problem, this dissertation presents a Bayesian framework for model ranking that can be used by practitioners who are interested in a mathematical approach to guide model selection. In addition to being a powerful technique for definite model ranking, this method can be implemented using any spreadsheet software that has a built in solver.

Another motivation for this research is the degree of uncertainty that is frequently associated with measurement and design when dealing with subsurface material. There is inherent variability in soils due to the natural processes that led to its formation, as well as error associated with measuring soil properties. In traditional civil engineering practice, a factor of safety was used to mitigate uncertainties in design values. It is more effective, though, to explicitly consider uncertainties directly, and doing so gives greater confidence in the obtained solutions. Furthermore, different measurement techniques and proxy-based modeling strategies will all introduce unique forms of uncertainty, and it is not effective to simply assign a single factor of safety (or equivalent) to account for those uncertainties when evaluating model performance. Instead the Bayesian framework for model ranking is adjusted to allow for thorough characterization of uncertainties that may manifest in the candidate model predictions or benchmark data against which the model performance is verified.

An additional strength of the Bayesian framework is its ability to resolve situations in which multiple models perform well by combining their outputs. In this way, users are

given additional confidence that their results will account for all pertinent information while minimizing the potential bias that could be introduced with less sophisticated techniques (e.g. simple averaging).

1.4 OVERVIEW OF THE RESEARCH METHODOLOGY

A Bayesian framework for V_{S30} model ranking is developed and presented in this dissertation, and is presented in a form that can be used with uncertainty information or without it. In this way, engineers and other users are given multiple means of utilization of the proposed methods based on familiarity with the underlying probabilistic concepts as well as the availability of the requisite data for analysis. The methodology is based on utilizing the Maximum Likelihood Method to evaluate candidate model performance, and then utilizes the maximized likelihood of a model's performance to compute its relative probability (with reference to the other candidate models) of being correct.

IN CHAPTER 2:

Fundamental background information is presented. This information is included in the dissertation to help the reader get up to speed on relevant information that is necessary to understand the rest of the work. This includes calculation of V_{S30} and its formulation as a parameter for estimating site response, the Maximum Likelihood Method, and liquefaction hazard quantification concepts.

IN CHAPTER 3:

The methodology for ranking V_{S30} models using a Bayesian framework to assist in development of a new, synthetic site condition database is presented. The chapter includes

the requisite information for derivation of the likelihood function as well as how the likelihood function can be utilized to perform a model ranking. Maximum likelihood estimation is used to find the optimal parameters of the likelihood function, and a procedure that can be implemented in spreadsheet based software is included. The method is demonstrated to provide improved ranking information when the model ranking is refined by geologic unit. Guidance is also provided for users interested in developing an independent site condition database, and the results of the study to create the state-of-the-art synthetic site conditions database for California are presented.

IN CHAPTER 4:

The Bayesian V_{S30} model ranking procedure is applied to other regions in the United States. These additional regions provide a lens through which critical consideration can be applied to the method. The degree to which the new method can provide meaningful results to users is discussed.

IN CHAPTER 5:

The Bayesian method for ranking V_{S30} models is revisited, but with application of uncertainty considerations to the model ranking formulation. The effects of uncertainty on the method and the sensitivity of the results to uncertainty are also explored, and the uncertainties that exist in both the benchmark data and the model predictions are quantified. Options for users who have incomplete uncertainty information are also presented.

IN CHAPTER 6:

A liquefaction hazard quantification is performed in Alameda, CA. The new V_{S30} site condition database developed in Chapter 3 is used to inform the hazard data sets that are

obtained from the USGS hazard tools, and probabilistic estimations of liquefaction hazard are obtained.

CHAPTER 2

OVERVIEW OF BACKGROUND CONCEPTS

2.1 V_{S30}

The time averaged velocity in the top 30 meters of subsurface material is commonly used in earthquake engineering as a means of characterizing the site conditions, such as potential for amplification (e.g., FEMA 2015). The general form of the equation to calculate the time-averaged shear wave velocity to a specified depth, z, is presented as Equation (2.1):

$$V_{Sz} = \frac{z}{\sum_{i=1}^{n} \frac{\Delta z_i}{V_{S,i}}} \tag{2.1}$$

where, V_{Sz} is the time averaged shear wave velocity to depth z, Δz_i is the thickness of layer i, V_{Si} is the shear wave velocity of layer i, and n is the number of layers that exist between the surface and depth z. It is important to note how this equation differs from a simple weighted average, in which the proportion of the depth of the ith layer is multiplied by $V_{S,i}$. Using the time averaged approach is based on the travel time of shear waves as they travel through the 30 meters of soil below the ground surface explicitly. This formulation better preserves the behavior of slow layers, which tend to be the most likely to demonstrate amplification during an earthquake.

However, despite its correlation to seismic amplification, there are known limitations to using V_{S30} as a means to quantify site response as well. A clear limitation is that it only quantifies soil behavior to a depth of 30 meters. Conditions further from the ground surface

also affect the site response, and those effects are implicitly lost if only characterizing the site response using V_{S30}. Additionally, V_{S30} is unable to account for frequency dependence and lacks the ability to distinguish between the response of velocity gradients and sharp contrasts for which V_{S30} may be similar (Wald et al. 2011).

Furthermore, it is unclear whether V_{S30} is truly a reasonable parameter to inform seismic site response. Recent studies (e.g. Aboye et al. 2015) have demonstrated that there in considerable uncertainty introduced into GMPEs due to the use of simple site classes (which are based on V_{S30}) as the decision criteria for amplification factor choice.

2.2 DEVELOPMENT OF V_{S30} AS A PARAMETER FOR ESTIMATING SEISMIC SITE CONDITIONS

In 1991 (Martin, 1994) and 1992 (Martin and Dobry, 1994), a pair of workshop was hosted to evaluate the current state of the art in ground motion prediction. One of the primary results of the workshops was a new site condition classification system that was based primarily on V_{S30} (i.e. V_S to 100 feet), but with additional constraints that consider local geology. The workshop participants considered this solution to be a good balance between over simplification and complexity, and their site class categories were recommended for inclusion into the 1994 NEHRP seismic design provisions.

Because V_{S30} is now consistently included in NEHRP seismic design provisions (although the provisions have been updated slightly since 1994) and GMPEs, researchers continue to study its effects and limitations (e.g. Lee et al. 1995, Castellaro et al. 2008, Lee and Trifunac 2010). It can be assumed that, unless a new standard parameter for

characterizing site condition is accepted by the seismological community, V_{S30} will continue to be used (Boore et al. 2011, Gregor et al. 2014).

Due to its continued use in GMPEs and site condition classification, in addition to the scrutiny placed on V_{S30} as a viable parameter, researchers have worked to develop new techniques to measure V_{S30} as well as predict it using proxy data when measurement data are not available (e.g. Wald and Allen, 2007, Wills et al. 2015, Thompson et al. 2014). Proxy-based methods, methods based on estimating V_{S30} using related information, have become popular for their ability to utilize vast amounts of readily available data. The two most common proxies, geology and topography, are discussed below.

Park and Elrick (1998) developed a V_{S30} map for southern California that grouped similar geologic units based on age, grain size, and depth. Their work was actually preceded by Fumal and Tinsley (1985), who used the Joyner et al. (1981) suggestion of characterizing site response with the velocity to a depth of one quarter wavelength of the period of interest, and combined that with the Tinsley and Fumal (1985) mapping of Quaternary sedimentary units. However, Park and Elrick (1998) concluded that using V_{S30} was more effective due to its lower level of complexity, thereby expanding the amount of usable data. Wills et al. (2000) expanded the work of Park and Elrick (1998) and applied their general method to the state of California, but with the end product being a statewide map of NEHRP site class recommendations instead of V_{S30} values. Wills and Clahan (2006) then refined the work of Wills et al. (2000) by dividing the state into simplified geologic units and providing V_{S30} predictions for each simplified geologic unit group. Wills and Gutierrez (2011) studied the effects of different groupings of geologic units and

introduced the concept of subdividing young alluvium based on slope. Wills et al. (2015) developed a new V_{S30} site conditions map of California based on the work of Wills and Gutierrez (2011) that featured fewer simplified geologic units than the Wills and Clahan (2006) map, but which demonstrated enhanced performance.

Wald and Allen (2007) developed a methodology that can be referred to as a topography-based V_{S30} estimation. They used data from the shuttle radar topography mission (SRTM) (Farr et al. 2007) to investigate correlations between topography and V_{S30}. They found that a correlation does exist between slope and V_{S30}, with higher slopes correlating to higher values of V_{S30}. The researchers postulated that higher quality material will be more likely to be able to hold a steeper slope than weaker material, and that V_{S30} will be spatially distributed accordingly. The final product of the Wald and Allen (2007) research was a method for globally estimating V_{S30} based on topographic gradient at 30 arcsecond resolution. Allen and Wald (2009) investigated whether a higher resolution data set would provide improved estimates, but found that there was little improvement and sometimes poorer performance at higher resolutions (i.e., 9 arcseconds).

Recently, a hybrid model (Thompson et al., 2014) has been developed to combine the strengths of geology-based methods with those of topography-based methods. The basis of this hybrid method is a geology-based estimation of V_{S30}, and that data are then refined with topography-based information to generate an updated V_{S30} prediction. This new method has promise as a strong union of multiple sources of proxy data for enhancing V_{S30} estimates.

2.3 MAXIMUM LIKELIHOOD METHOD

The Maximum Likelihood Method (MLM) is a technique that can be used to estimate the parameters for a set of data. If θ represents the unknown statistical parameters of the data, **D**, then the MLM can be used to maximize $l(\theta|\mathbf{D})$, a function that describes the parameters θ given the data **D**. The function $l(\theta|\mathbf{D})$ is the likelihood function, and a maximization of the likelihood function will result in an estimation of the true value of θ (Givens and Hoeting, 2005).

The MLM is applicable under most regular conditions and for most normally used distributions. Under the assumption that normal conditions are being met, the estimate derived from the MLM will demonstrate consistency, invariance, and normality (Barnett 1999; Gentle 2002). Consistency refers to the maximum likelihood estimator approaching the true value as the number of observations in **D** increase. Invariance is the property that if the maximum likelihood estimate (θ^*) is found, then a function $\gamma=g(\theta)$ has the maximum likelihood estimate $\gamma^*=g(\theta^*)$. And normalcy denotes that as the number of observations in **D** increase, the maximum likelihood estimate θ^* tends towards a normal distribution with a mean of θ and covariance matrix $\mathbf{H}^{-1}$ with $\mathbf{H}_{ij} = E(-\delta^2 L(\theta|\mathbf{D})/\delta\theta_i \delta\theta_j)$. **H** can be estimated with the negative Hessian matrix of the log-likelihood function evaluated at θ^*. (Givens and Hoeting, 2005).

Although there are times when the MLM will not provide good results (e.g., Cam, 1990; Cheng and Traylor, 1995), those conditions are rare and involve situations that are unlikely to be encountered in normal engineering practice. The main challenges in

successful utilization of the MLM tend to be the development of the likelihood function itself or in maximizing it. To illustrate the MLM and its ability to develop an estimation of a statistical distribution's parameters, MLM is applied to the normal distribution to derive the mean and standard deviation.

In a general sense, the likelihood function can be expressed as (e.g. Juang et al. 2015):

$$l(\theta \mid \mathbf{D}) = \prod_{i=1}^{n} f\left(\mathbf{d}_i \mid \theta\right) \tag{2.2}$$

where $f(\mathbf{d}_i|\theta)$ is the probability density function of the distribution in question. For a normal distribution (e.g. Haldar and Mahadevan 2000), the likelihood function is as follows:

$$l\left(\mu, \sigma^2 \mid \mathbf{D}\right) = \prod_{i=1}^{n} \frac{1}{\sigma\sqrt{2\pi}} \exp\left[-\frac{\left(x_n - \mu\right)^2}{2\sigma^2}\right] \tag{2.3}$$

where μ and σ^2 are the parameters of the normal distribution to be estimated. It may be of interest to the reader that the BIC method, presented in Chapter 3, can be used along with the maximum likelihood estimators (as derived here for the normal distribution) as a means to evaluate various distributions and which one best fits a set of data. This would allow users to select between, for example, a normal and a lognormal distribution to describe a set of data.

It is commonly known that the two parameters used to describe a normal distribution are the mean and standard deviation, and the formulae used for their computation are similarly well known. However, this example can be treated as a proof of the skills necessary to perform a maximum likelihood estimation. Expanding the product in Equation (2.3):

$$l\left(\mu,\sigma^2 \mid \mathbf{D}\right)=\left(\sigma^2\right)^{\frac{-n}{2}}\left(2\pi\right)^{\frac{-n}{2}}\exp\left[\frac{1}{2\sigma^2}\sum_{i=1}^{n}\left(x_i-\mu\right)^2\right] \tag{2.4}$$

From Calculus, it is known that a function reaches a maximum (or minimum) at the location where the derivative of the function has a value of zero. Therefore, the derivative of the likelihood function can be set to zero to maximize its value. Often, it is desirable to use the natural logarithm of the likelihood for maximization due to the simplification of the mathematics that it offers. This is an acceptable choice because the natural logarithm is a monotonically increasing function, and a maximization of the log of the likelihood function (referred to as the log-likelihood function) is therefore a maximization of the likelihood function. Doing so in this example yields Equation (2.5):

$$L\left(\mu,\sigma^2 \mid \mathbf{D}\right)=-\frac{n}{2}\ln\left(\sigma^2\right)-\frac{n}{2}\ln\left(2\pi\right)-\frac{\sum_{i=1}^{n}\left(x_i-\mu\right)^2}{2\sigma^2} \tag{2.5}$$

As mentioned previously, it is desirable to take the derivative to find the maxima. Because there are two variables in this equation, a partial derivative must be taken. The partial derivative with respect to μ is as follows:

$$\frac{\partial L\left(\mu,\sigma^2 \mid \mathbf{D}\right)}{\partial\mu}=-\frac{\left(-2\right)\sum\left(x_i-\mu\right)}{2\sigma^2} \tag{2.6}$$

Setting Equation (2.6) equal to zero, reducing, and multiplying by σ^2 yields:

$$\sum x_i-n\mu=0 \tag{2.7}$$

Rearranging:

$$\mu = \frac{\sum x_i}{n} \tag{2.8}$$

which is known to be the mean of a normal distribution.

The same procedure can be repeated for the second parameter, σ^2. The partial derivative of Equation (2.5) is:

$$\frac{\partial L\left(\mu, \sigma^2 \mid \mathbf{D}\right)}{\partial \sigma^2} = -\frac{n}{2\sigma^2} + \frac{\sum\left(x_i - \mu\right)^2}{2\left(\sigma^2\right)^2} = 0 \tag{2.9}$$

$$-n\sigma^2 + \sum\left(x_i - \mu\right)^2 = 0 \tag{2.10}$$

$$\sigma^2 = \frac{1}{n}\sum\left(x_i - \mu\right)^2 \tag{2.11}$$

As Equation (2.8) is the equation for the mean, Equation (2.11) is the equation for calculating the variance of a standard deviation. With proper understanding, the MLM is an effective tool for calculating the unknown parameters of an assumed distribution for a set of data.

2.4 OVERVIEW OF LIQUEFACTION QUANTIFICATION METHODS

Earthquake-induced liquefaction is a phenomenon that has received considerable attention from researchers. The hazards associated with liquefaction include settlement, lateral spreading, and sand boils. When liquefaction occurs, it can cause damage to structures and infrastructure, potentially leading to loss of life or functionality. Many efforts have been undertaken to predict the occurrence of and damage associated with liquefaction triggering.

The term liquefaction refers to a specific soil phenomenon that can manifest when saturated granular soils experience a sudden loading. When liquefaction occurs, the sudden increase in stresses cause the pore water pressure to rise. The granular soil particles become temporarily suspended by the pore water, losing contact with one-another in the process. This suspension of the soil particles causes a loss of strength and stiffness, and the soil can begin to behave like a liquid (e.g., Fiegel and Kutter 1994, National Academies of Sciences, Engineering, and Medicine, 2016).

In 1964, two devastating earthquakes in Niigata, Japan and Alaska prompted development of methods for assessment of liquefaction potential, including Whitman (1971) and Seed and Idriss (1971), the latter of which has been termed the "simplified procedure."

The simplified procedure specified that, essentially, liquefaction triggering could be roughly assessed by a ratio of a soil's seismic resistance, the cyclic resistance ratio (CRR), to the seismic loading applied to the soil, the cyclic stress ratio (CSR). The ratio, expressed in Equation (2.12), is the factor of safety against liquefaction.

$$FS = \frac{CRR}{CSR} \tag{2.12}$$

The CSR, adjusted for magnitude 7.5 events, is defined in Equation (2) (Youd et al., 2001):

$$CSR_{7.5} = 0.65\left(\frac{PGA}{g}\right)\left(\frac{\sigma_v}{\sigma'_{vo}}\right) r_d \left(\frac{1}{MSF}\right)\left(\frac{1}{K_\sigma}\right) \tag{2.13}$$

where *PGA* is the horizontal peak ground acceleration at the study site in term of *g*, *g* is the acceleration due to gravity, σ_v is the total vertical stress, σ'_{vo} is the is the initial vertical effective stress, r_d is a stress reduction coefficient, *MSF* is the magnitude scaling factor, and K_σ is a correlation factor to adjust for overburden pressure.

Significant effort has been dedicated to assessing the CRR of soils, and since the seminal Seed and Idriss (1971) work, procedures based on multiple testing methods have been developed. The simplified procedure was developed based on standard penetration test (SPT) data, and revisions were made to improve its estimation of CRR (e.g. Seed 1979; Seed and Idriss, 1982; Seed et al., 1985; Youd et al., 2001; Idriss and Boulanger, 2010). Other in-situ testing methods include cone penetration test (CPT) (e.g., Robertson and Campanella, 1985; Robertson and Wride, 1998), shear wave velocity test (Andrus and Stokoe, 2000), and others. The three formulations for CRR based on each of the three previously mentioned methods are reproduced below. For the sake of brevity, the variables within each equation are explained, but calculations for each are not included. This section is primarily included to inform the reader of the various methods that exist for formulation of CRR. It is intended to be useful primarily as a comparative indicator of the general approaches that can be considered for use when CRR is to be evaluated at a site.

The SPT-based CRR calculation is based on a clean-sand equivalent, corrected blow count (Idriss and Boulanger, 2010).

$$CRR_{7.5} = \exp\left[\frac{(N_1)_{60,cs}}{14.1} + \left(\frac{(N_1)_{60,cs}}{126}\right)^2 - \left(\frac{(N_1)_{60,cs}}{23.6}\right)^3 + \left(\frac{(N_1)_{60,cs}}{25.4}\right)^4 - 2.8\right] \quad (2.14)$$

where $(N_1)_{60,cs}$ is the energy corrected blow count clean sand equivalent.

The CPT-based CRR calculations are based on the calculated normalized tip resistance (Robertson and Wride, 1998)

$$CRR_{7.5} = \begin{cases} 0.833\left[\dfrac{(q_{c1N})_{cs}}{1000}\right] + 0.05; & \text{if } (q_{c1N})_{cs} < 50 \\ 93\left[\dfrac{(q_{c1N})_{cs}}{1000}\right]^3 + 0.08; & \text{if } 50 \le (q_{c1N})_{cs} < 160 \end{cases} \tag{2.15}$$

where $(q_{c1N})_{cs}$ is the normalized clean sand tip resistance, with normalization to 1 atm. The normalization procedure is presented in Robertson and Wride (1998).

The shear wave velocity-based CRR can be calculated as follows (Andrus and Stokoe, 2000):

$$CRR = a\left(\frac{V_{S1}}{100}\right)^2 + b\left(\frac{1}{V_{S1}^{*} - V_{S1}} - \frac{1}{V_{S1}^{*}}\right)MSF \tag{2.16}$$

where V_{S1} is shear wave velocity corrected for overburden-stress, V^*_{S1} is the limiting upper value of V_{S1} for liquefaction triggering, and a and b are curve fitting parameters. An alternative shear wave velocity-based method, including probabilistic assessment using V_S can be found in Kayen et al. (2013).

Although the methods mentioned up to this point have been deterministic in nature, Ku et al. (2012) used a maximum likelihood based approach to develop a probabilistic method for assessment of liquefaction potential based on the Robertson and Wride (1998) method and its updates (Robertson 2009a, 2009b). Juang et al. (2013) applied the Robertson (2009a, 2009b) method and Ku et al. (2012) methods to develop a simplified procedure for estimating liquefaction induced settlement and settlement exceedance curves based on CPT

testing. Probabilistic methods are an attractive alternative to conventional deterministic methods due to their capacity to allow engineers to more readily express uncertainty as a probability of liquefaction.

CHAPTER 3

PROBABILISTIC METHODS FOR EVALUATING V_{S30} MODELS - FOCUSING ON THE CALIFORNIA DATABASE*

3.1 INTRODUCTION

Accurate estimation of earthquake damage potential, from site-specific analysis to regional predictions, is a field that has been studied for years and continues to draw interest from researchers. Practically, a model that can accurately estimate earthquake-induced hazard potential at a regional scale can lead to cost savings and better planning for professionals involved in hazard planning and mitigation fields.

One commonly used parameter when estimating the potential for amplification of seismic waves is the time-averaged shear wave velocity in the top 30 meters of subsurface material, or V_{S30}. The National Earthquake Hazards Reduction Program (NEHRP) publishes codes that are used in seismic hazard design, and V_{S30} values are used to classify soils for design purposes. That soil classification is then used to predict the amount of amplification that can be expected for a selected site. When performing site-specific analysis, measurements at a site can provide sufficient information for hazard mitigation. However, when hazard potential estimation becomes necessary at scales larger than site-specific analysis, such as at the city or state-wide scales, measurement of subsurface conditions becomes cost prohibitive, and interested parties must turn to proxies that use

A similar form of this chapter is under review for publication in *Earthquake Spectra*:
Brownlow, A. W., Chen, Q.; Khoshnevisan, S., Shahjouei, A., Javanbarg, J., Zhang, J., and Juang, C. H., 2017. Probabilistic methods for evaluating V_{S30} models - focusing on the California database, *Earthquake Spectra*, Under Review.

what little information is already available, e.g., surficial geology (Wills and Silva 1998; Wills and Clahan 2006; Scasserra et al. 2009; Wills et al. 2015), topography and slope (Wald and Allen 2007; Allen and Wald 2009), terrain features (Yong et al. 2012), and geology-topography hybrid data (Scasserra et al. 2009; Wills and Gutierrez 2011; Parker et al. 2017), to provide estimates of the parameters used to estimate seismic hazard potential. In addition, various interpolation or kriging-based methods have been developed and applied in recent mapping studies of various quantities of interest for earthquake hazards, e.g., (Lee and Tsai 2008; Thompson et al. 2007; Thompson et al. 2014; Chen et al. 2016*a*; Chen et al. 2016*b*; Liu et al. 2017a&b), and correlations between shear-wave velocity and other comment geotechnical in situ tests (e.g., cone penetration test) have been proposed, e.g., (Andrus et al. 2007, Stuedlein 2010). Large-scale estimations of V_{S30} can aid decision-makers in their selection of a proper proxy for the region of interest.

In any situation where a design V_{S30} value is to be chosen based on one of multiple available V_{S30} models, there is no clear method to assist in the validation and comparison of the available methods. Any such decision would be based on the decision maker's judgment instead of a definable procedure, or, barring sufficient information to make a decision, some combination of the available models, also dependent on judgment, could be used. However, statistical methods do exist to assist decision makers in model selection (e.g. Buckland et al. 1997; Schwarz 1978; Zhang et al. 2014; Juang et al. 2015).

A Bayesian method for model evaluation and ranking is developed and implemented in this study. This methodology utilizes Maximum Likelihood Estimation (MLE), a technique that can be used to compute statistical parameters of interest for a set of data

(Juang et al. 2015). Alternatively, as it is used herein, MLE can be used to evaluate how well a model (or set of models) will fit a set of data when the data's distribution is known or can be assumed. This is used to calculate a value known as the likelihood, which refers to how well the model is able to predict the sample data against which it is being evaluated. The likelihood can then be used to compute the Bayesian Information Criterion (BIC) (Schwarz 1978), which is a value that allows for comparison of candidate models' likelihoods. The reader is referred to Juang et al. (2015) and Juang et al. (2017) for examples of geotechnical applications of the principle of maximum likelihood.

Utilizing MLE and BIC, this paper proposes a methodology for assessing the relative probability that a proxy-based V_{S30} model, among multiple candidate V_{S30} models, will provide the correct value for V_{S30} when evaluated against benchmark data. The proposed method can be used with any number of available models, and, as will be demonstrated, provides the model ranking for situations when one model is deemed superior as well as when multiple models show comparable levels of performance. The methodology is then applied to assess candidate V_{S30} models and to develop an optimal recommended V_{S30} database for the state of California. This database can be considered a synthetic database, as it will be comprised of V_{S30} predictions from other models and combinations of V_{S30} predictions when multiple models show competitive performance. This method does not seek to develop its own V_{S30} predictions but to capitalize on the best predictions available.

3.2 METHODOLOGY

When performing a regional analysis of the potential for amplification of seismic waves, there tend to be multiple models available to obtain an estimation of V_{S30}. In these

situations, a need arises to evaluate the relative performance of each model in order to obtain the best estimation of site condition. The method proposed in this work is intended to easily allow users to rank available models by evaluating their ability to accurately predict V_{S30} values at benchmark locations, and if necessary, to combine non-dominate models to obtain an optimal V_{S30} model. The principle of maximum likelihood is used to evaluate the ability of each model to predict the benchmark data. The methodology builds on the principle of maximum likelihood and utilizes the concept of Bayesian Information Criterion. A general outline of the procedure is described in Figure 3.1.

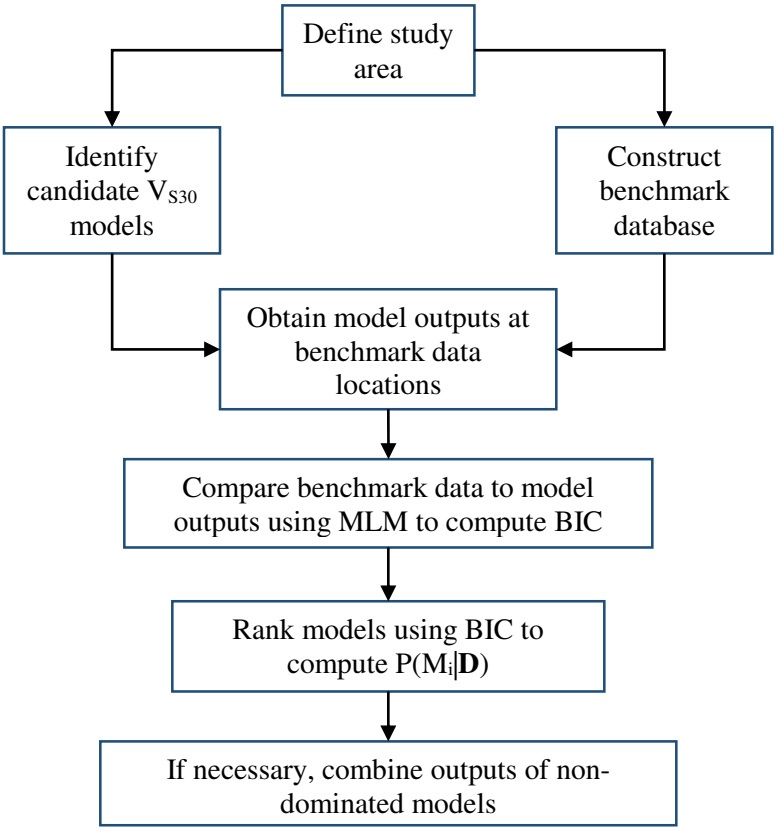

Figure 3.1: Flowchart of the steps involved when performing a BIC-based model ranking

PRINCIPLE OF MAXIMUM LIKELIHOOD ESTIMATION

The principle of maximum likelihood estimation (MLE), can be used to estimate statistical parameters for a sample of data where those parameters are unknown. The obtained parameters represent the best fit of the assumed distribution of the population to the sample data. The following sections will include a brief discussion of MLE, as well as a discussion of its applicability to V_{S30} models.

For a model with parameter(s), $\boldsymbol{\theta}$, to be estimated, and observed data set, $\mathbf{D}$, there exists a joint probability density function (PDF), $f(\mathbf{D}|\boldsymbol{\theta})$, that represents the chance of observing $\mathbf{D}$ given $\boldsymbol{\theta}$. In the context of this paper, $\mathbf{D}$ is the benchmark database of V_{S30} values against which a V_{S30} model will be compared. The equation of the PDF, if viewed as a function of $\boldsymbol{\theta}$, can be written as $l(\boldsymbol{\theta}|\mathbf{D})$, and is referred to herein as the likelihood function. Assuming that the observations of a data set $\mathbf{D}$ are statistically independent, the likelihood function can be evaluated using (e.g. Juang et al. 2015):

$$l(\boldsymbol{\theta} \mid \mathbf{D}) = \prod_{i=1}^{n} f(\mathbf{d}_i \mid \boldsymbol{\theta}) \tag{3.1}$$

where $\prod f(\mathbf{d}_i \mid \boldsymbol{\theta})$ is the joint probability of observing the data $\mathbf{D}$ given the unknown parameters $\boldsymbol{\theta}$, $\boldsymbol{d}_i$ is an individual observation within $\mathbf{D}$, and n is the total number of data in $\mathbf{D}$. Equation (1) is a generalized form of the equation used for MLE. In this study, it is assumed that the data are log-normally distributed. Therefore, Equation (1) becomes (e.g. Haldar and Mahadevan 2000):

$$l(\theta_1, \theta_2|\mathbf{D}) = \prod_{i=1}^{n} \frac{1}{x_i \theta_2 \sqrt{2\pi}} e^{\frac{-(\ln x_i - \theta_1)^2}{2\theta_2^2}} \tag{3.2}$$

where θ_1 and θ_2 are the parameters of the lognormal distribution.

The objective of the MLE analysis is to maximize the value of the likelihood function, which will yield an optimal value of $\boldsymbol{\theta}$ (Givens and Hoeting 2005). In this context, the maximized likelihood function represents the assumed model's best fit of the data. It is known that a maximum or minimum value of a function is obtained when the first derivative of the function has a value of zero. Therefore, the likelihood function must be differentiated with respect to $\boldsymbol{\theta}$. For ease of evaluation, it is often desirable to take the natural logarithm of the likelihood function and the resulting general and study specific forms of the log-likelihood function are written as

$$\ln\left[l\left(\boldsymbol{\theta}\,|\,\mathbf{D}\right)\right]=\sum_{i=1}^{n}\ln\left[f\left(\mathbf{d}_i\,|\,\boldsymbol{\theta}\right)\right] \tag{3.3}$$

$$\ln\left[l\left(\theta_1,\theta_2\,|\,\mathbf{D}\right)\right]=\left(2\pi\theta_2{}^2\right)^{-\frac{n}{2}}\cdot\sum_{i=1}^{n}x_i^{-n}-\frac{1}{2\theta_2{}^2}\sum_{i=1}^{n}\left(\ln x_i-\theta_1\right) \tag{3.4}$$

Since the natural logarithm is a monotonically increasing function, a maximization of the log-likelihood function is also a maximization of the likelihood function. In this work, the log-likelihood function in the form of Equation (4) is used.

RANKING OF COMPETING V_{S30} MODELS

While MLE is indeed useful for estimation of model parameters, in reality, it is possible to have several competing models for a given problem. To justify which model is the best based on geotechnical knowledge, the Bayesian Information Criterion (BIC) (Schwarz 1978) is often used for comparing and ranking these models. The BIC, defined in Equation (5), can be computed for each model in a set with models M_1, M_2, …, M_r (Ku et al. 2012):

$$\mathrm{BIC}_i = -2 \cdot \ln\left[l\left(\theta^* \mid M_i, \mathbf{D}\right)\right] + k \ln(n) \tag{3.5}$$

where θ^* is the maximized parameter of the likelihood function, $\ln[\, l(\theta^* | M_i|\mathbf{D})\,]$ is the value of the log-likelihood function for model M_i at point θ^* for data set **D**, k is the number of parameters of the model (e.g. $k = 2$ for a lognormal distribution), and n is the number of data values in **D**. The BIC is considered an appropriate means for selecting model fit due to its design to account for both model fit and complexity. The model with the lowest BIC value is considered to be best supported by the data. The first term in Equation (5) accounts for a model's goodness of fit, while the second term accounts for model complexity, negatively affecting the model's BIC ranking for higher degrees of complexity (i.e., having more parameters).

Once the BIC is calculated for each model, the competing models can be compared using Equation (6) (Burnham and Anderson 2004), which gives the probability that a certain model, M_i, is a good predictor of the data **D** relative to the other models included in the analysis (Ku et al. 2012; Juang et al. 2015).

$$P(M_i \mid \mathbf{D}) = \frac{\exp\left[-\frac{\Delta_i(\mathrm{BIC})}{2}\right]}{\sum_{j=1}^{r} \exp\left[-\frac{\Delta_j(\mathrm{BIC})}{2}\right]} \tag{3.6}$$

where Δ_i(BIC) is the difference between the BIC of model M_i and the minimum BIC of the models included in the analysis and r is the number of models included in the analysis. The values of $P(M_i|\mathbf{D})$ for all investigated models can be used to rank their relative

performance, with higher probabilities corresponding to better performance of the model with respect to the benchmark data **D**.

NON-DOMINATED MODEL PERFORMANCE

When performing the analysis, the ideal outcome is to find one V_{S30} model that exhibits superior performance relative to the other models, as evidenced by the lowest BIC value (Equation 5) or the highest probability value (Equation 6). However, it is possible for more than one model to perform well enough at predicting the benchmark data that each model that has shown sufficient performance should be considered when making a final model output selection. In the cases where more than one model performs well, the models' outputs can be combined using the total probability theorem (after Zhang et al. 2014):

$$p^*\left(Vs_{30} \mid \mathbf{D}\right) = \sum_{k=1}^{r} p^*\left(Vs_{30,k} \mid M_i, \mathbf{D}\right) P\left(M_i \mid \mathbf{D}\right) \tag{3.7}$$

where $p^*\left(Vs_{30} \mid \mathbf{D}\right)$ is the final, predicted value of V_{S30}, and $p^*\left(Vs_{30,k} \mid M_i, \mathbf{D}\right)$ is the predicted V_{S30} given by model M_i. For a pair (or group) of models to be considered non-dominated, the value of $P(M_i|\mathbf{D})$ for a given model must be greater than $1/20^{th}$ of the next-highest model. In this case, the values of each qualifying model should contribute to the final accepted value of the parameter being investigated. It has been extensively studied and proven that combining model outputs using a general form of Equation (7) will result in a superior set of predictions based on known information when compared to single model results (e.g. Raftery et al. 1997).

3.3 CANDIDATE V_{S30} PREDICTION MODELS

The criteria for selecting V_{S30} models for this study are based on the desired outcomes. Namely, it is desirable for a given model to be able to predict V_{S30} at any location in the study area. Therefore, the model needs to take location data as inputs (e.g. a latitude and longitude pair) and gives an estimated V_{S30} value as an output. For the region of interest (California), three models are available for this evaluation, the USGS global V_{S30} model (Wald and Allen 2007), which is based on a correlation between topography and V_{S30}; a California Geological Survey (CGS) geology-based V_{S30} model by Wills et al. (2015), and a second USGS model that combines slope and geologic inputs to create a refined estimation of V_{S30} (Thompson et al. 2014).

TOPOLOGY-BASED V_{S30} MODEL

Wald and Allen (2007) developed a model capable of predicting V_{S30} based on an empirical relationship between topographic slope and V_{S30}. With the availability of topographic data gathered by a space shuttle mission in 2000, Wald and Allen developed a global map of V_{S30} values. A notable strength of this method, when compared to geology-based methods, is that it provides a high-resolution grid of individual estimates instead of a single-value estimate for large areas. Figure 3.2 illustrates the data available in the model and the extent to which it is available. A limitation of this model is that the maximum value

predicted by the model is 760 m/s. The model's output should be interpreted as 760 m/s or greater at locations where 760 m/s is predicted.

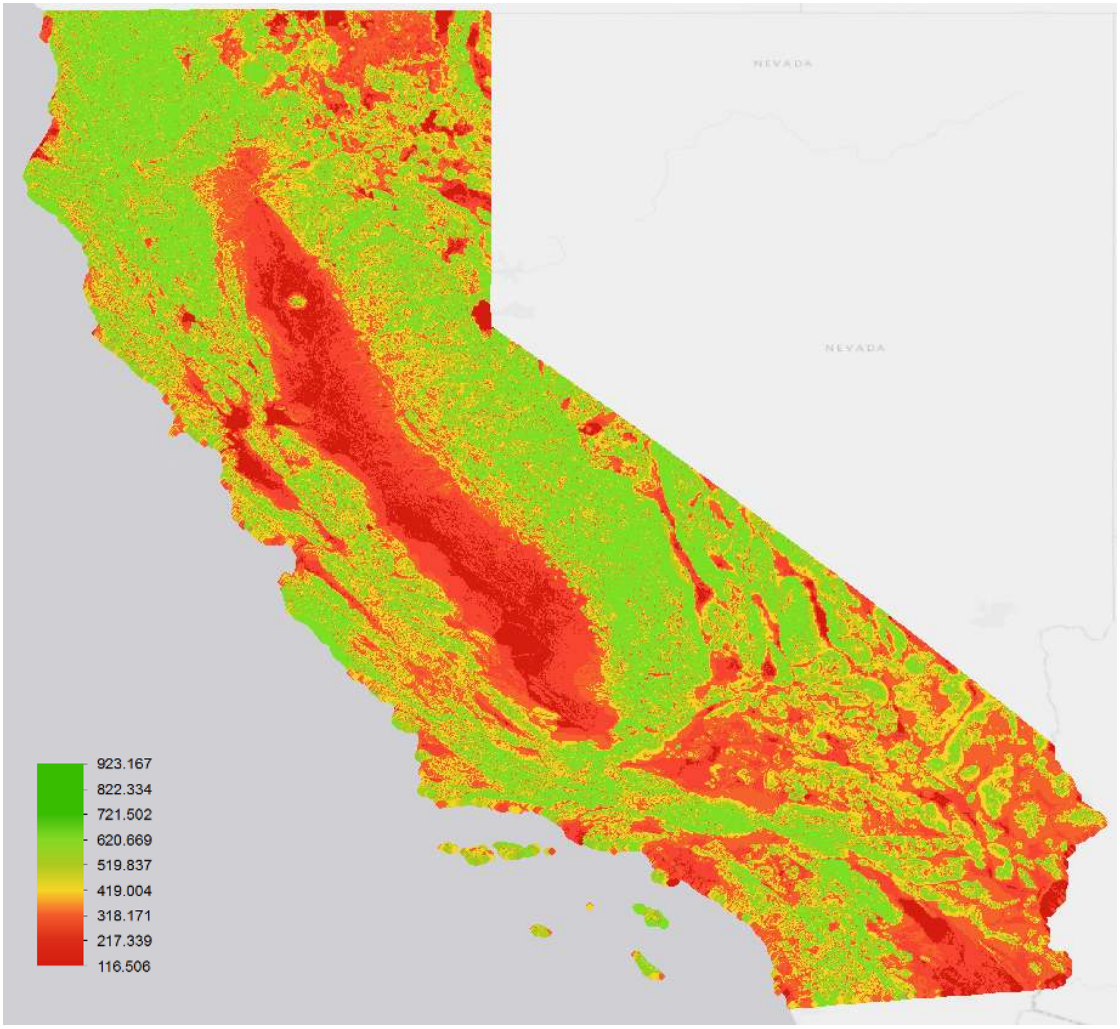

Figure 3.2: Graphical representation of the Wald and Allen (2007) topology and slope based V_{S30} model. The colors in the figure represent a gradient of V_{S30} values, with green being high V_{S30} and red being low V_{S30}.

SURFICIAL GEOLOGY-BASED V_{S30} MODEL

Classification of site conditions based on geology has been used extensively and consistently as a reliable methodology. Recent work (e.g. Wills et al 2015) combines multiple surficial geologic units which possess similar characteristics into so-called

simplified geologic units. Site condition information (i.e., V_{S30} values) is then averaged within each simplified geologic unit. Because input data are averaged when developing site condition maps using this methodology, only a single V_{S30} value is available for each simplified geologic unit. This results in large areas of consistent geology being assigned a constant V_{S30} value. Figure 3.3 illustrates this phenomenon well, with large areas of consistent surficial geology clearly evident in the figure.

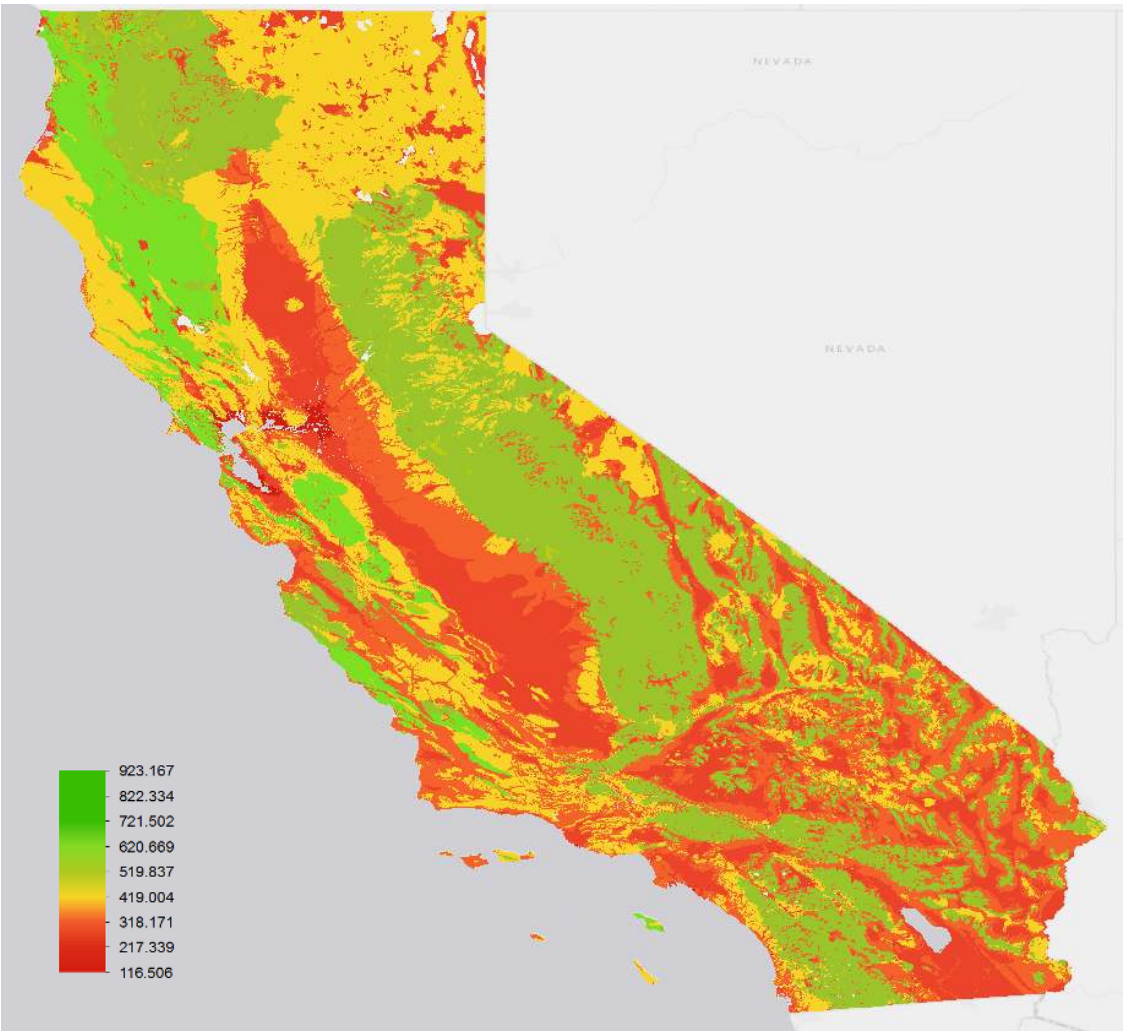

Figure 3.3: Graphical representation of the Wills et al. (2015) model in ArcMap. Each color represents a surficial geologic unit that has a unique V_{S30} value assigned to it.

HYBRID V_{S30} MODEL

Thompson et al. (2014) have developed a model that utilizes both geologic and topographic constraints in estimating V_{S30}. Using regression kriging, this methodology combines topology-based estimations with geologic unit-based estimations while also considering site-specific measurement data to produce updated site condition estimations. This method derives its strength from the ability to combine topographic data with geologic data, and is still capable of producing unique V_{S30} estimations for each location instead of only producing a set of single value estimations, as is the case with the geology-based method. Figure 3.4 shows a rendering of the model's outputs of V_{S30} values in California.

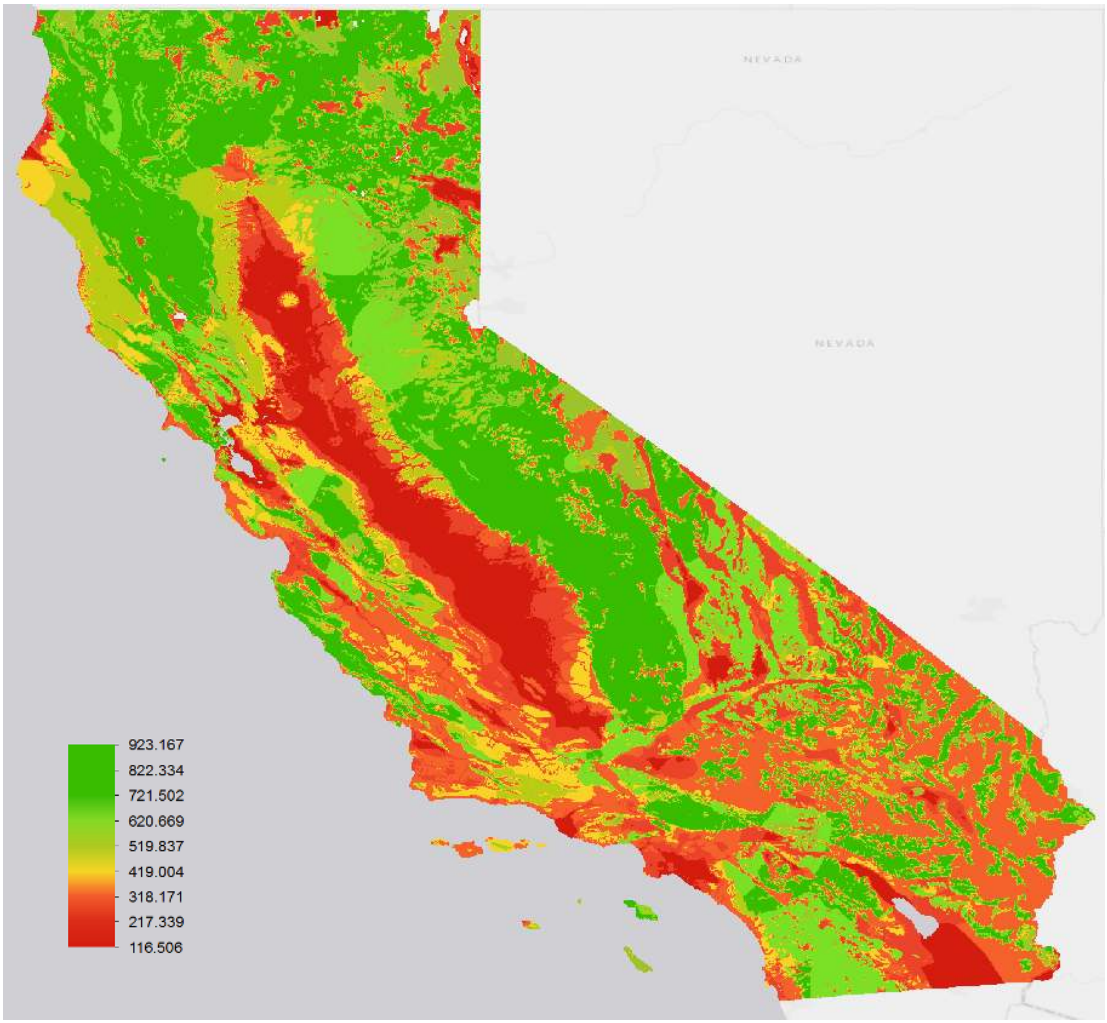

Figure 3.4: Graphic representation of the Thompson et al. (2014) model, rendered in ArcMap. Red areas correspond to areas of lower V_{S30}.

Obtaining V_{S30} Model Outputs

The V_{S30} model outputs are available in geographic information system (GIS) file format from each source. These files are manually uploaded into ArcMap, a commercial GIS package developed and distributed by ESRI (www.esri.com). This software package contains a tool that allows separate sets of data to be joined together based on spatial location. After converting the files to an appropriate format, the spatial join tool is used to

join the output files from different models into one comprehensive file containing all model outputs. This step can be computationally intensive if the models provide high-resolution spatial data across a large area, but once completed, it allows for very rapid comparison of the models throughout the rest of the procedure.

The Wald and Allen (2007) and Thompson et al. (2014) models are both obtained in the form of .grd files and are then converted to point data in ArcMap. Each point in the file consists of a V_{S30} value and spatial data to correspond to a specified location. These point estimations are available on a global grid with 30-arcsecond spacing. By contrast, the Wills et al. 2015 paper separates simplified geologic units into polygons, and each unit's polygon stores a V_{S30} value to represent the area covered by that polygon. The spatial join tool in ArcMap is capable of joining points to points and points to polygons, and both methods are utilized to join the three model's outputs to the benchmark data for location-based comparison. The point-to-point join tool is set to join data points that are closest to one another, and the point-to-polygon tool joins the points falling within any polygon to the values of that polygon.

3.4 BENCHMARK V_{S30} DATA

To evaluate multiple V_{S30} models, it is assumed that the "best" model will be the one that most accurately predicts the benchmark V_{S30} data. Therefore, obtaining high-quality benchmark data are of paramount importance for this methodology to produce high-quality results. However, the eventual model ranking, discussed below, is based on a comparison between each model's relative ability to predict the benchmark data. As such, the

methodology is merely an indication of which model shows the best performance relative to the other models; it does not evaluate the accuracy of the model itself.

OBTAINING BENCHMARK V_{S30} DATA

Two databases are identified for use as benchmarks for this study. One is the USGS V_{S30} measurement database (Yong et al. 2015), which provides V_{S30} data and associated spatial location information for locations throughout the United States. The other is the NGA-West2 database (Ancheta et al. 2013; Seyhan et al. 2014), developed by the Pacific Earthquake Engineering Research Center (PEER) for the NGA project. The Next Generation Attenuation (NGA) project is an ongoing research effort to improve the state of seismic hazard research and knowledge and to develop new, more accurate earthquake attenuation equations. This database is selected for its ongoing utilization in state-of-the-art earthquake-related research. The NGA project has been divided into West and East study areas corresponding to portions of the United States (i.e., eastern and western United States), though the NGA-West2 project database also includes data from other areas of the world. However, only data corresponding to locations in California is selected for inclusion in the benchmark database in this study. The spatial distribution of data in the benchmark database can be seen in Figure 3.5. The unfiltered benchmark database consists of 3412 data points.

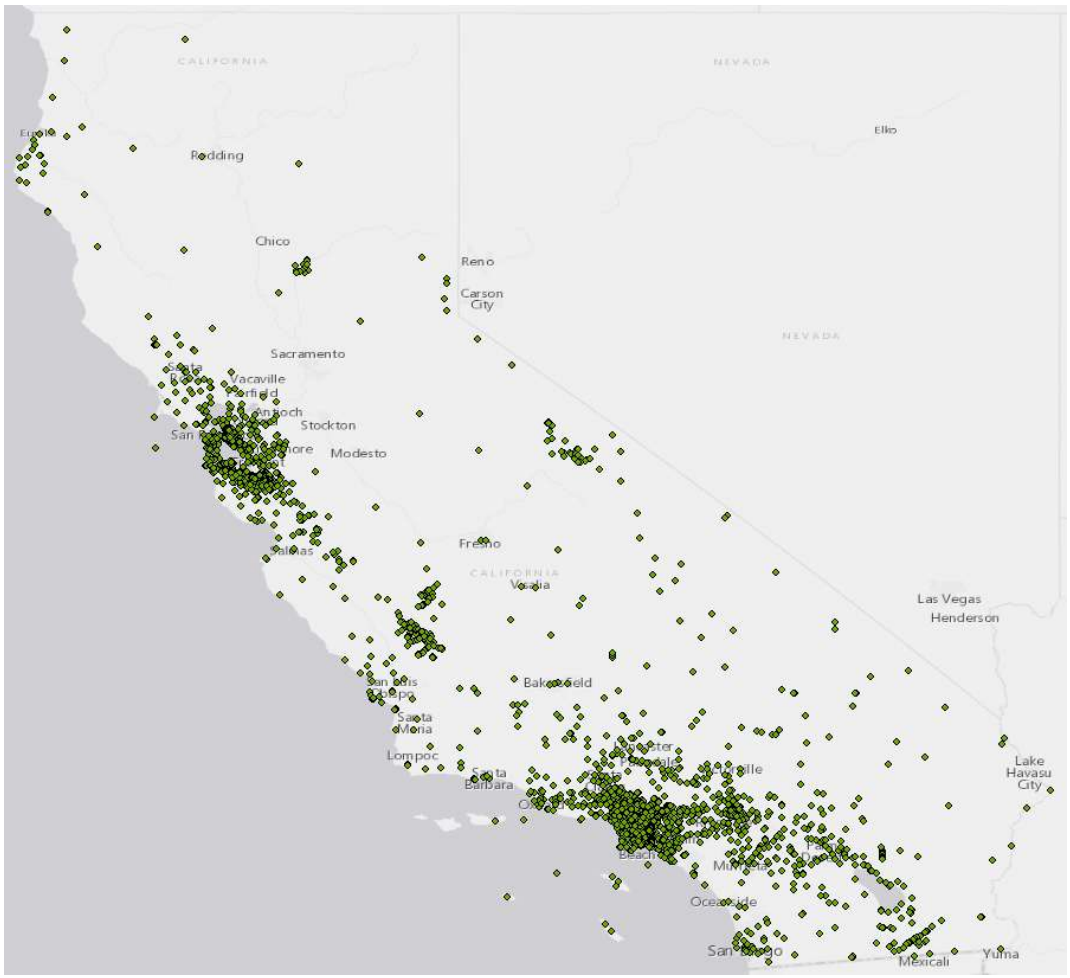

Figure 3.5: Spatial distribution of benchmark data in California

It can be seen in Figure 3.5 that much of the available data are concentrated in two areas: the San Francisco Bay area in the northern portion of the state, and the Los Angeles area to the south. The distribution of the benchmark database's V_{S30} values is plotted in Figure 3.6.

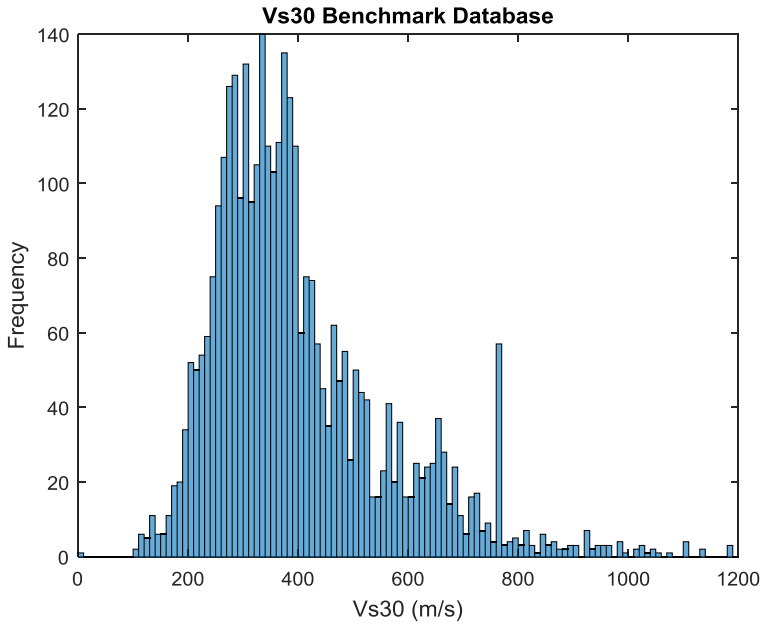

Figure 3.6: Distribution of V_{S30} values in the benchmark database

3.5 EXAMPLE APPLICATION AND DEVELOPMENT OF A V_{S30} DATABASE FOR CALIFORNIA

In this section, the proposed methodology is applied to evaluate the performance of multiple V_{S30} models and, using the results of the model evaluation, to develop a V_{S30} database for California. The three V_{S30} models' outputs are combined with the benchmark data using ArcMap's spatial join tool, which allowed efficient location-based pairing of benchmark data points to appropriate model outputs.

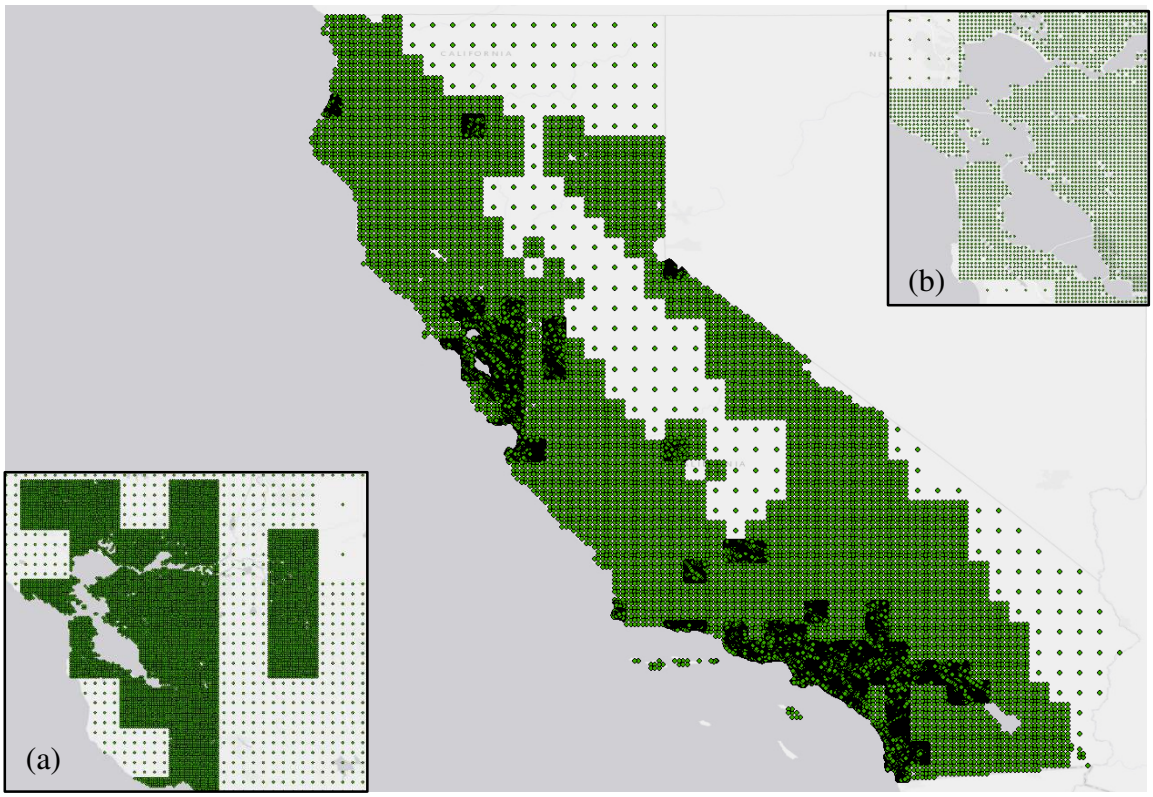

Figure 3.7. Grid used for California, shown with a varying resolution of model data. Inset (a) shows the San Francisco Bay and surrounding area, with all three resolutions used in the study visible in the image. Inset (b) shows a closer shot of the San Francisco Bay, with only the finest two resolutions of data visible.

In order to reduce the computational load when performing the analysis, a grid of varying resolution is used. A higher resolution grid is used in higher population areas, such as in the San Francisco Bay and Los Angeles areas. A lower resolution is distributed in areas with lower populations, such as the Sierra Nevada mountain range in the middle of the state. The grids used in this study are shown in Figure 3.7.

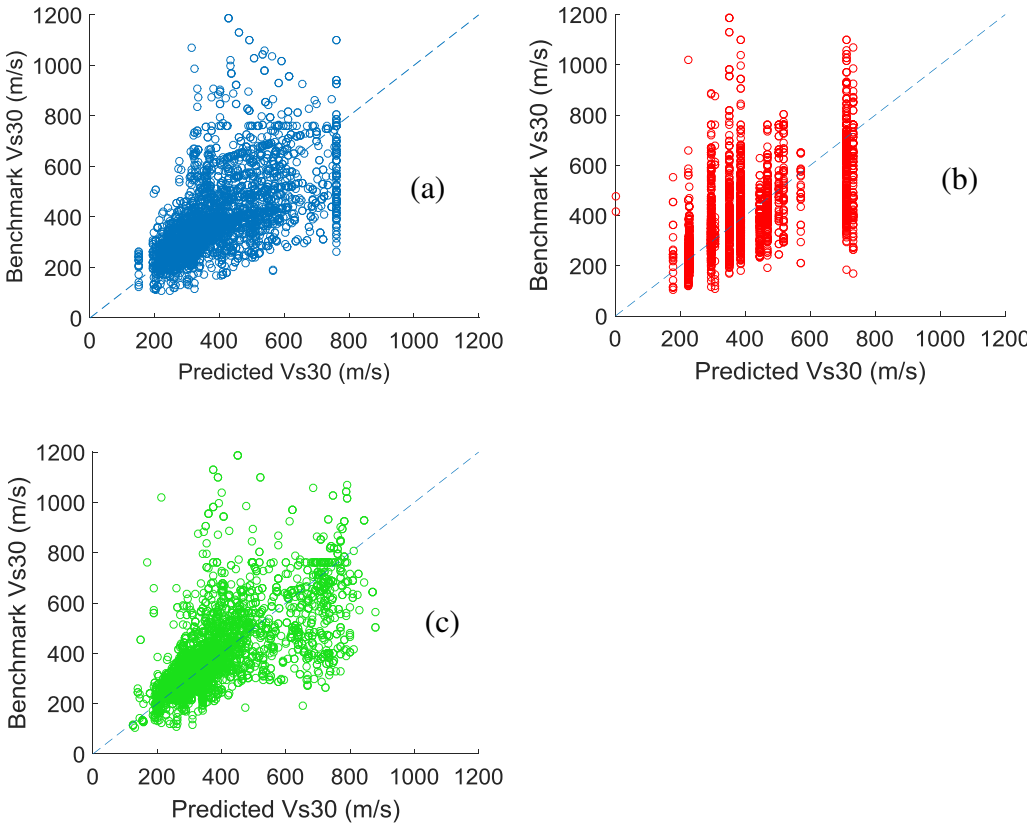

Figure 3.8: Scatter plots of model performance in predicting benchmark V_{S30} values by the (a) Wald and Allen (2007) topography-based, (b) Wills et al. (2015) geology-based, and (c) Thompson et al. (2014) hybrid models. The dashed line is a 1:1 (45 degree) line indicating a perfect match between predicted and benchmark V_{S30} values.

Figure 3.8 plots the benchmark V_{S30} values and the values predicted by each V_{S30} model at the benchmark locations. Although not sufficient for determining the relative performance of each model, Figure 3.8 does provide some insights into the behavior of each model and general performance. First, in Figure 3.8(a), it can be seen immediately that there appears to be a hard limit of 760 m/s imposed on the upper bounds of the model. Therefore, the model has limited capacity to correctly characterize sites with V_{S30} greater than 760 m/s. Velocities greater than 760 m/s tend to be observed at sites with

predominantly rocky subsurface conditions. Therefore, it can be expected that the Wald and Allen topology-based model will perform poorly in any locations with rocky subsurface conditions. A similar limit can be observed for values that fall below 150 m/s. Figure 3.8(b), which corresponds to the Wills et al, geology-based model, shows a distinct banking behavior at various values of V_{S30}. This illustrates the limitation of the approach used to develop the model, whereby the model assigns a constant V_{S30} value to all locations characterized with a given geologic classification. However, as is seen in the figure, this method can result in some poor characterizations of data points from time to time. Figure 3.8(a) and Figure 3.8(c) do not demonstrate the same banding behavior witnessed in Figure 3.8(b), but rather show a scatter of data clustered around the 1:1 line.

Quantitative performance evaluation of the three V_{S30} models in term of the probability (Equation 4) is shown in Figure 3.9. The probabilities are evaluated using all benchmark data in California. It can be seen in the figure that the Thompson et al. model is superior in its prediction of V_{S30} values based on the benchmark data. Therefore, any entity wishing to select the best model based on a simple analysis of their relative performance would be able to quickly determine that the Thompson et al. (2014) model should be used.

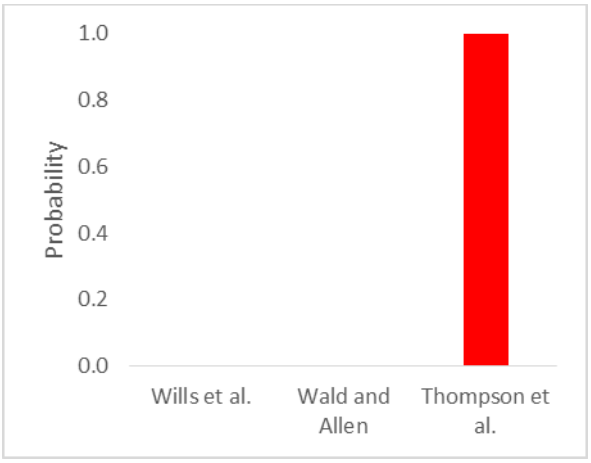

Figure 3.9. Ranking of V_{S30} model performance (i.e. $P(M_i|D)$) for the state of California

Refining Rankings with Respect to Common Properties

The Bayesian Method for the model ranking procedure (described previously) is used to rank various models and their ability to accurately predict benchmark data. It is common knowledge that subsurface conditions differ on a site-by-site basis. Therefore, a performance analysis of predictive models that evaluates their accuracy over large areas that include different site conditions runs the risk of masking an individual model's strengths. To mitigate the potential loss of model performance in this study, the data are separated by surficial geology using the maps of simplified surficial geologic units defined in Wills et al. (2015) and summarized in Table 3.1.

Table 3.1: Representation of Simplified Geologic Units in Benchmark Database

Geologic Unit	Number of Benchmark Data Points
af/Qi	125
crystalline	341
KJf	124
Kss	39

Qal1	364
Qal2	745
Qal3	563
Qi	19
Qoa	501
Qs	33
QT	115
sp	26
Tsh	159
Tss	169
Tv	74
Total	3397

The results of the model ranking in term of the probability (Equation 4), when divided by geologic unit, have been tabulated in Table 3.2. Recall that any models that show performance 20 times greater than the next best model are said to be dominant, and the models with worse performance are disregarded.

Table 3.2: Tabulated results of model ranking in terms of $P(M_i|D)$ for California

Geologic Unit	Wills et al.	Wald and Allen	Thompson et al.	No. Benchmark
af/Qi	0.75	0	0.25	125
Crystalline	0	0	1.00	341
KJf	1.00	0	0	124
Kss	0.89	0	0.11	39
Qal1	0	0	1.00	364
Qal2	0	0	1.00	745
Qal3	0	0	1.00	563
Qi	0	0	1.00	19
Qoa	0	0	1.00	501
Qs	0.06	0.06	0.88	33
QT	1.00	0	0	115
sp	0.99	0	0.01	26
Tsh	0.73	0	0.27	159
Tss	0	0	1.00	169
Tv	0	0	1.00	74

As can be seen in Table 3.2, the Thompson et al. (2014) model tends to have the best performance for a majority of the geologic units in California, indicated by a higher probability number. However, it should be noted that the Wills et al. (2015) model also performs best in some geologic units. It is clear, then, that choosing to refine the study by geologic units has improved the end user's ability to select an appropriate model for their use when geologic information is known. It is also worth noting that the Wald and Allen (2007) model does not perform as well as the other two. In fact, the model only contributes to the prediction of one geologic unit: Qs. In Table 3.2, the number of benchmark data points available to assess each geologic unit is also shown.

In four units (af/Qi, Kss, Qs, and Tsh), none of the models' relative performance is sufficient to be considered dominant. For those four units, the outputs of the Wills et al. (2015) model and the Thompson et al. (2014) model must be combined to give the most confident estimation of V_{S30}.

DATABASE OF V_{S30} FOR CALIFORNIA

Using the model combination methodology discussed previously and the results of the model ranking from the previous section, a new statewide database of V_{S30} predictions for the state of California is created. This new database is generated by selecting the model output that shows the best performance for each location in the state, and can be considered a synthetic database as a result. The new database provides V_{S30} estimates at the variable resolution grid locations displayed in Figure 3.7. The entire database, in comma delimited (.csv) file format, is provided as an electronic supplement to this paper. It should be noted,

however, that this methodology can be used to produce a database for any defined grid of locations at which model outputs can be obtained.

For reference, Table 3.3 contains the simplified geologic units in the state and the models which should be used for prediction in areas with that geology.

Table 3.3: Geologic Units and Contributing Models for Updated California Database

Geologic Unit	Wills et al. 2015	Wald and Allen 2007	Thompson et al. 2014
af/Qi	x		x
Crystalline			x
KJf	x		
Kss	x		x
Qal1			x
Qal2			x
Qal3			x
Qi			x
Qoa			x
Qs	x	x	x
QT	x		
sp	x		
Tsh	x		x
Tss			x
Tv			x

As seen in Table 3.3, in many instances, only one model's output is to be used. To generate the final database, the values of $P(M_i|\mathbf{D})$, reported previously, are used to determine the relative weight of each model. However, in instances where only one model is to be used, the model's output is given a weight of 1.0, and not the value of $P(M_i|\mathbf{D})$. This is in contrast to situations in which more than one model's outputs contribute to the final output, where the relative weighting is based on $P(M_i|\mathbf{D})$.

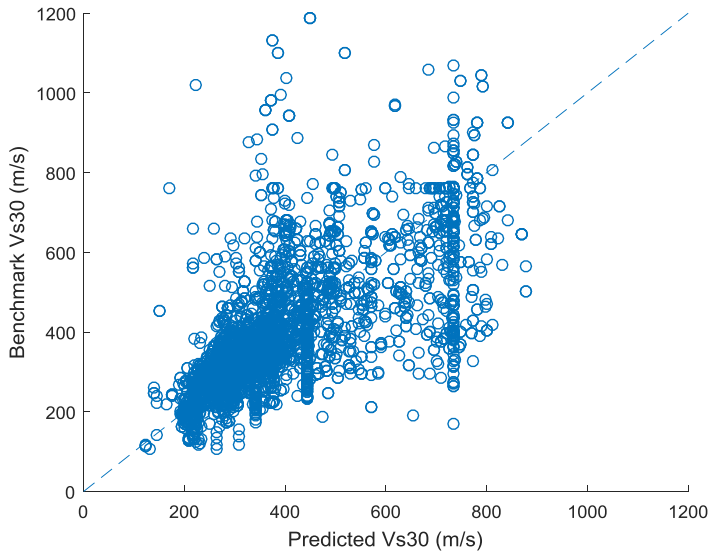

Figure 3.10. Comparison of new V_{S30} database to benchmark data

Figure 3.10 plots the new V_{S30} database at benchmark locations. As seen in Figure 3.10, there is a good performance of the model to fit the 1:1 line when comparing the new database to the benchmark data.

Figure 3.11 shows the mapped V_{S30} values in the new V_{S30} database. The inset in the figure shows the distribution of V_{S30} values within the database. The various resolutions of the data can be clearly observed in the figure.

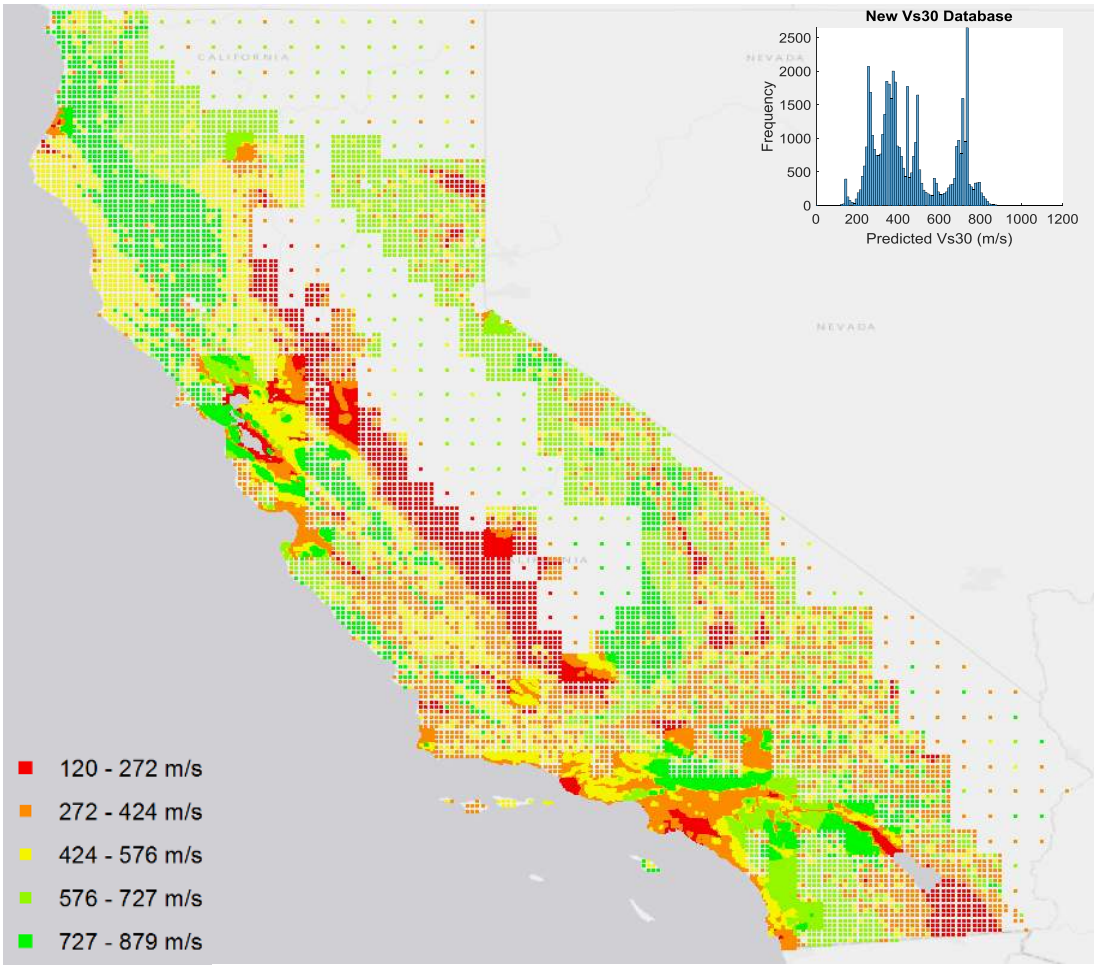

Figure 3.11: V_{S30} Map of California based on new database with histogram of prediction data (inset)

3.6 APPLICATION OF THE V_{S30} DATABASE

V_{S30} is an important indicator of site response in many earthquake engineering applications and is used by ground-motion prediction equations and building codes. To demonstrate the application of the new V_{S30} database (shown in Figure 3.11), the recommended V_{S30} values are used to calculate site amplification factors. As an example, the long-period site amplification factor F_v is calculated following the recommendations given in FEMA (2015) (Table 11.4.2 in the referred document). For the spectral

acceleration parameter at a period of 1 second, denoted as S_1, the 2014 USGS National Seismic Hazard Maps (Petersen et al. 2014) are used to obtain its values at the grid locations. The resulting map of site amplification factor F_v in California is shown in Figure 3.12.

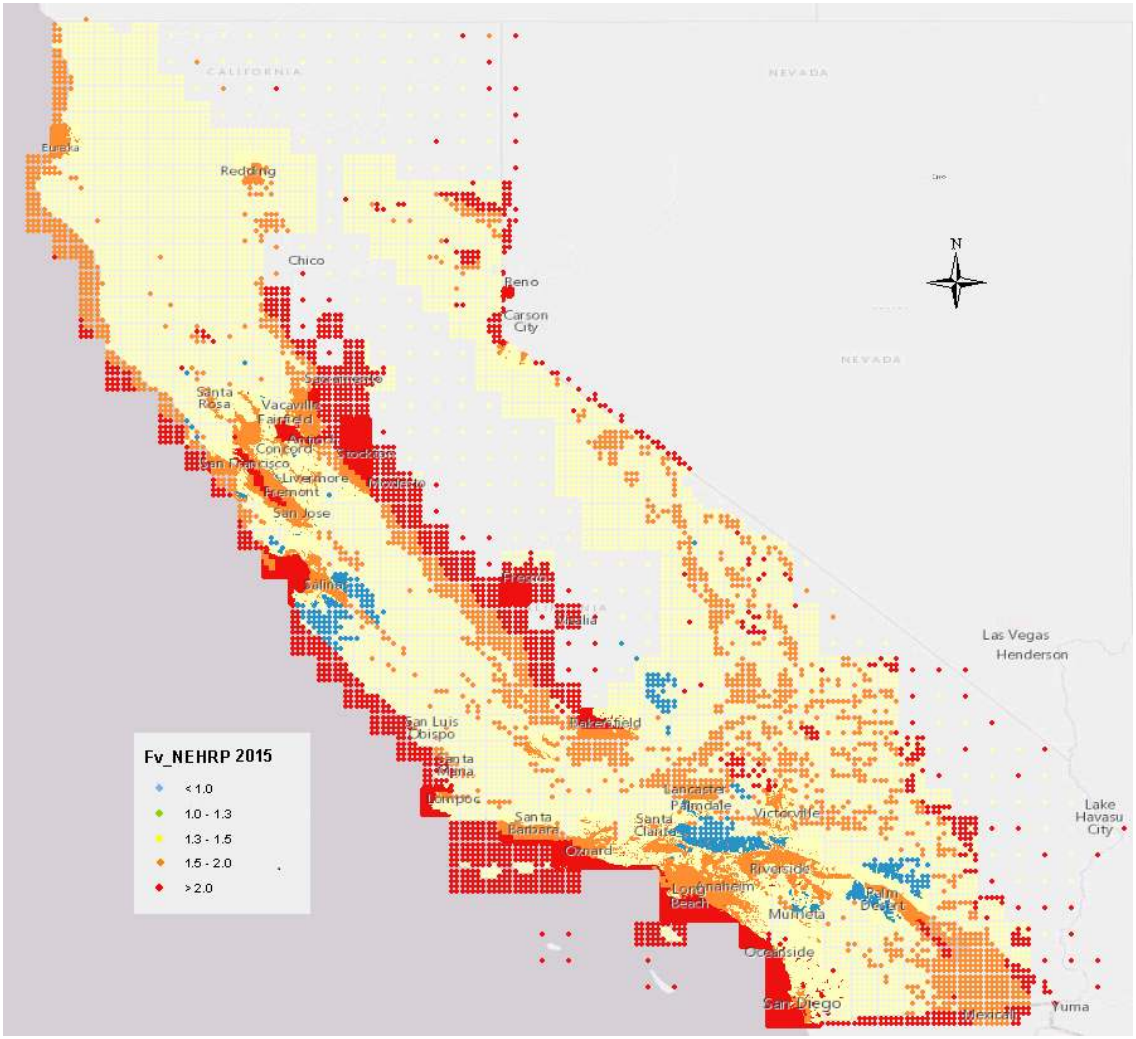

Figure 3.12: Site amplification factor F_v map of California based on new V_{S30} database.

3.7 DISCUSSION

Although the methodology presented in this paper is demonstrated for use in evaluating V_{S30} models and their predictive capacity, it can be used in any situation in which multiple geotechnical models must be compared and evaluated against one another. This procedure has been documented for such general application by Zhang et al. (2014). In addition, it is possible to modify the methodology to account for uncertainties in both benchmark database and outputs from evaluated models, provided that information on the uncertainties is available or can be estimated. While quantifying and evaluating uncertainties would enhance the validity of the results demonstrated above, that procedure is beyond the scope of this paper.

The BIC-based methodology presented herein has also been verified independently using Laplace's Approximation (Carlin and Louis, 2009), which is a highly accurate but much more computationally intensive method. Figure 3.12 shows a plot to demonstrate the convergence of ranking results between the BIC method and Laplace's approximation. This figure is generated using random sampling from the benchmark database in California to create a new, temporary database for which the model ranking is performed. This procedure was repeated multiple times for each number of data points to generate the convergence curve shown. Although good agreement can be achieved as early as the threshold of 15 data points, it is recommended that users choose approximately 20 data points as their threshold for using BIC method whenever possible, and to use results obtained with fewer than 20 data points with caution.

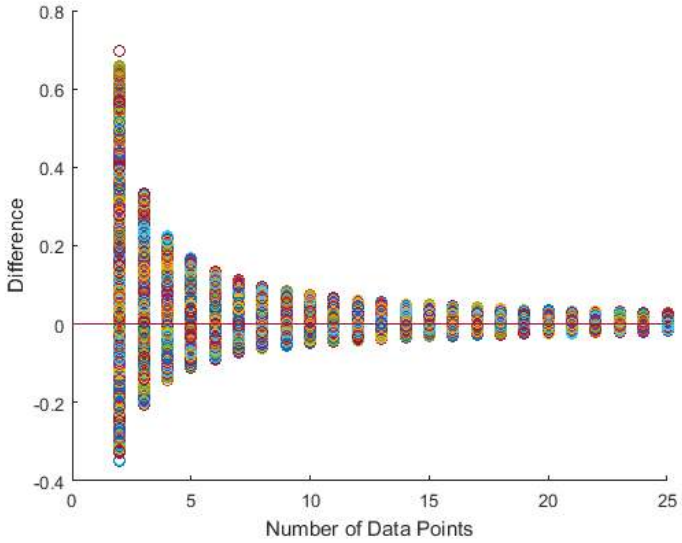

Figure 3.13: Convergence of BIC and Laplace Approximation ranking results expressed as a difference

With this convergent performance, the BIC-based Bayesian model ranking is a viable and computationally more efficient option for spatial ranking of V_{S30} models, especially when there are a sufficient number of benchmark data points. The V_{S30} ranking results of this study, using the BIC-based methodology, have been verified with Laplace's approximation, and the two methods are found to have a very good agreement.

In the analysis of V_{S30} models presented in previous sections, the V_{S30} models and benchmark database have also been refined based on common properties, such as surficial geologic units. In cases where there were fewer than 20 benchmark data points within a geologic unit, two options are considered: either assign the global ranking to those units with insufficient information or group all remaining units into one special category and assign a ranking to that new group which would apply to all included units. Both options suffer from essentially the same limitation, i.e., all individual units' performance will not be explicitly considered in the ranking. However, when considering the ways in which bias

might manifest itself using each option, the primary consideration is that units grouped into a special category will be more likely to experience an extreme bias towards one unit's performance, especially in situations where there is considerably more benchmark data for one unit than the others. Therefore, in this work, the first option is used, i.e., geologic units with insufficient benchmark data points were assigned the same ranking as that of the global model analysis.

Finally, while this new methodology is effective at identifying the strongest model for use in regional-level analysis, it should be noted that this method does not claim to improve upon the limitations of individual V_{S30} models chosen for the analysis nor does it improve any model's ability to predict site-specific conditions. Any site-specific design should be based on investigations performed at that site and is beyond the scope of this paper.

3.8 CONCLUSIONS

In this work, probabilistic methods are developed and implemented to assess the relative probability that a proxy-based V_{S30} model, among multiple candidate V_{S30} models, will provide the correct value for V_{S30} when evaluated against benchmark data. The methodology utilizes the maximum likelihood principle to evaluate how well a candidate V_{S30} model can predict the sample data and uses the Bayesian Information Criterion to quantify and rank the relative performance of multiple V_{S30} models. The methodology is computationally efficient and can be easily implemented using spreadsheet-based software that has basic probability tools. Analyses of this work show that, for California, the hybrid V_{S30} model has the best overall performance and is the superior model for the majority of the geologic units, when evaluated against the compiled benchmark database. With the

ranking results, a new synthetic V_{S30} database for California is developed, which contains a superior set of V_{S30} predictions when compared to any single V_{S30} model. The methodology developed in this work, though demonstrated only in evaluating and developing a V_{S30} database, can be used in any situation in which multiple models must be compared and evaluated against one another, which will be explored in future studies.

ACKNOWLEDGEMENTS

This work is partially supported by the AIG PC Global Services, Inc. All results and findings presented in this paper are the opinion of the authors and do not reflect the views of AIG.

CHAPTER 4

SITE CONDITION EVAULATION AND V_{S30} RECOMMENDATIONS FOR SELECTED U.S. REGIONS

In this chapter, the methodology presented in Chapter 3 is applied to two additional US regions: the Seattle and Puget Sound area and the Salt Lake City, Ogden, and Provo area. These two regions each had two models available for evaluation, the topography-based Wald and Allen (2007) model and the geology-topography hybrid model (Thompson et al., 2014), both which were evaluated previously for California. Also similar to the previous chapter, the benchmark database was primarily constructed from the NGA-West2 and USGS V_{S30} measurement databases. However, 12 additional V_{S30} measurements were added to the Seattle database (Stuedlein, 2010).

4.1 SEATTLE AND THE PUGET SOUND

GEOLOGY INFORMATION

In Chapter 3, the geologic information used to refine the model results for ranking was obtained from the Wills et al. (2015) model. However, because the Wills et al. model is constrained to the state of California, it is unusable in other parts of the country. The Washington State Department of Natural Resources (WA-DNR) and the Utah Geologic Survey have published geology information for their respective state online, and that information can be downloaded for use in GIS programs. The WA-DNR website can be accessed at http://www.dnr.wa.gov/programs-and-services/geology/geologic-maps. The

geologic resources from the Utah Geological Survey website can be accessed at http://geology.utah.gov/resources/data-databases/.

MODELS

Two models were identified as available for use in the Seattle and Puget Sound area. The Thompson et al. (2014) hybrid model and the Wald and Allen (2007) topography-based model both provide global estimates of V_{S30} and are therefore suited for use here.

DATA AND RANKING RESULTS

The Seattle and Puget Sound area had a total of 87 benchmark data points available, but after adjusting for points classified as plotting on water, the final benchmark database was constrained to 82 benchmark data points. Using the geology data obtained from the Washington State Department of Natural Resources, the data were assigned a geologic unit classification. It should be noted, however, that the same rigor was not taken to group the data by simplified geologic unit as was done by Wills et al. (2015). This step was not considered necessary because there were sufficiently fewer geologic units in the study area as to avoid the need for grouping of units with like characteristics. However, this opportunity for enhanced classification of geologic units in the Seattle and the Puget Sound region represents an additional avenue for research and offers the potential for development of a new geology-based V_{S30} model.

Of the 84 data points in the database, 65 data points, or approximately 77%, plotted within three geologic units, as summarized in Table 4.1.

Table 4.1: Summary of Geologic Units and Associated Benchmark Data in the Puget Sound Area

Geologic Unit	Count
Qa	15
Qg1o	16
Qg1t	34
Other	19
Total	**84**

The "Other" category in Table 4.1 contains the data of 4 additional geologic units, and represents 23% of the benchmark data. Because a significant portion of the benchmark data could not be evaluated in the respective geologic units, a model ranking was performed for each of the three appropriately represented units individually as well as for the entire region (i.e., all 84 data points), and the regional evaluation results were assigned to the "Other" category.

Table 4.2 shows the ranking results for the Seattle and Puget Sound area. Note that the table actually refers to two separate runs of the model ranking, once to obtain the ranking results within the individual geologic units, and once more to perform a regional ranking. The regional ranking results indicate the relative performance of both models and can be used to guide decisions if geologic unit information is not present. In addition, the regional results indicate the model that should be used for any unit defined under the "Other" category, in this case the Thompson et al. (2014) hybrid model.

Table 4.2: Results of the Model Ranking for the Seattle and Puget Sound area

	Wald and Allen Topography	Thompson et al. Hybrid
Qa	0.06	0.94
Qg1o	0.06	0.94
Qg1t	0	1.0
Regional	0	1.0

It can be seen in the table that the hybrid model performed best overall, but that the topography-based model contributed in two of the three geologic units in the area, if only slightly.

SEATTLE SITE CONDITIONS MAP

Using the ranking results for the Seattle area, a new site conditions map was generated. As was done in Chapter 3, a variable resolution grid was used to place emphasis in areas that are projected to be of higher interest, such as highly developed urban areas (e.g. downtown Seattle). The site conditions map is shown in Figure 4.1.

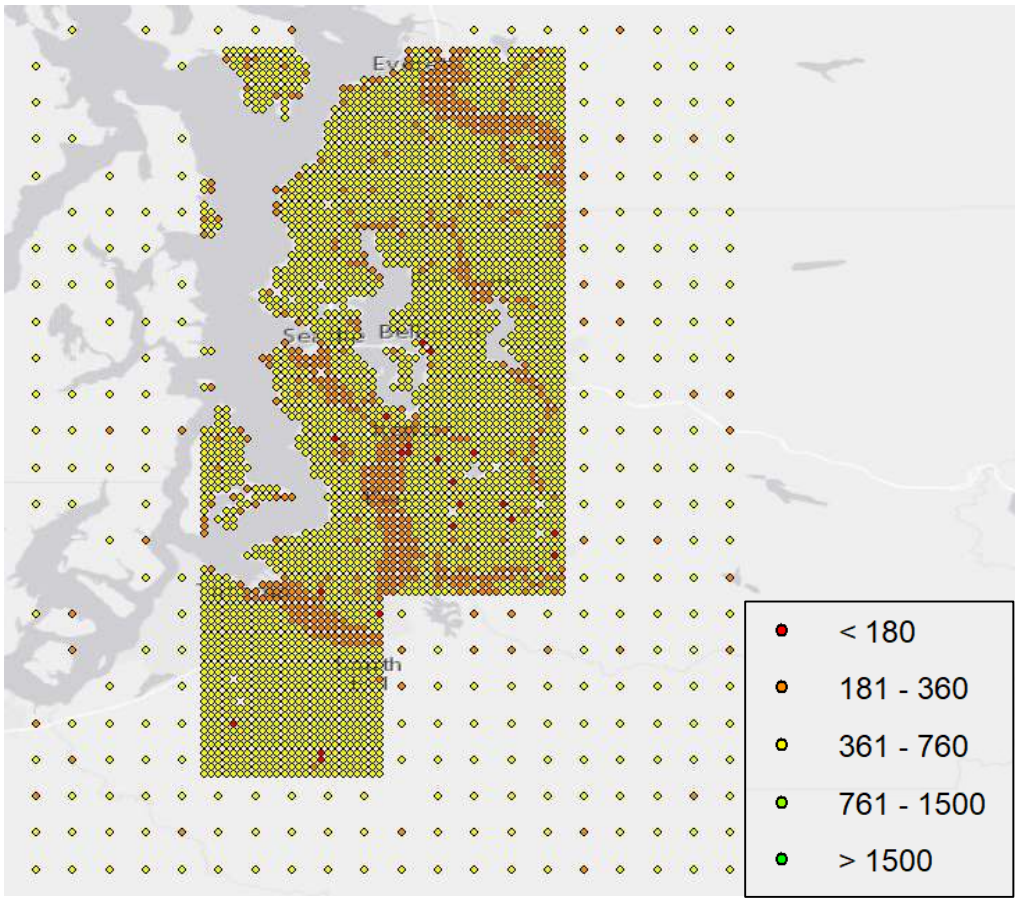

Figure 4.1: Site conditions map of Seattle and the Puget Sound

It can be seen in the figure that although most of the greater Seattle area has a relatively high V_{S30}, there are some areas of weaker material that designers and stakeholders should be aware of when making decisions. Based on the ranking results in which the Thompson et al. 2014 model was dominant, however, there is little deviation from the Hybrid model, even when refining the rankings by geologic units. Therefore, the Bayesian method for model ranking provides little improvement over the hybrid model. However, as will be discussed later in this chapter, it is still useful as a model selection tool. Figure 4.2 is included to illustrate the amount of improvement that can be expected between using the

hybrid model predictions and the synthetic, updated V_{S30} database based on the model rankings. It is clear that there is only a small change in V_{S30} predictions, up to approximately 30 m/s at the largest.

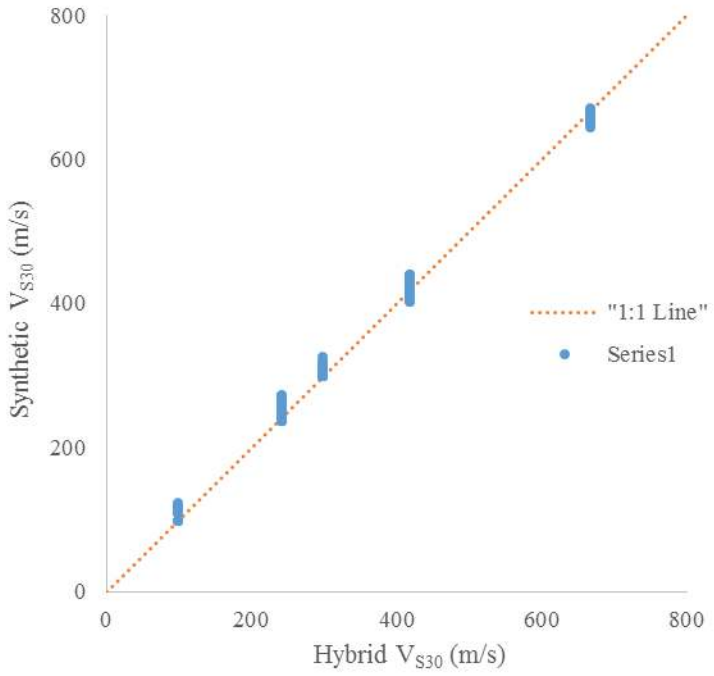

Figure 4.2: Illustration of the difference between the (dominant) hybrid model prediction and the updated site condition database

4.2 SALT LAKE CITY, OGDEN, AND PROVO

GEOLOGY INFORMATION

Geology information was obtained from the Utah Geologic Survey. Upon inspection of the benchmark data and how it was classified by geology, it was found that a significant majority of the data (95%) fell into one of two categories of geologic unit, while only 12 data points (5% of the database) described the other 6 units in the region. Therefore, the same strategy of grouping the geologic units with insufficient data for model ranking was

adopted. The breakdown of data dispersion and model ranking results can be seen in Table 4.3 and Table 4.4, respectively.

Table 4.3: Geologic Units and Number of Benchmark Data in the Salt Lake City Area

Geologic Unit	**Count**
Qa	90
Ql	133
Other	12
Total	**235**

Table 4.4: Results of the Model Ranking for Salt Lake City, Ogden, and Provo

	Wald and Allen Topography	Thompson et al. Hybrid
Qa	0	1.0
Ql	1.0	0
Regional	1.0	0

Using the ranking results, a site condition map for the Salt Lake City area was developed. The map and VRG of this region can be seen in Figure 4.3.

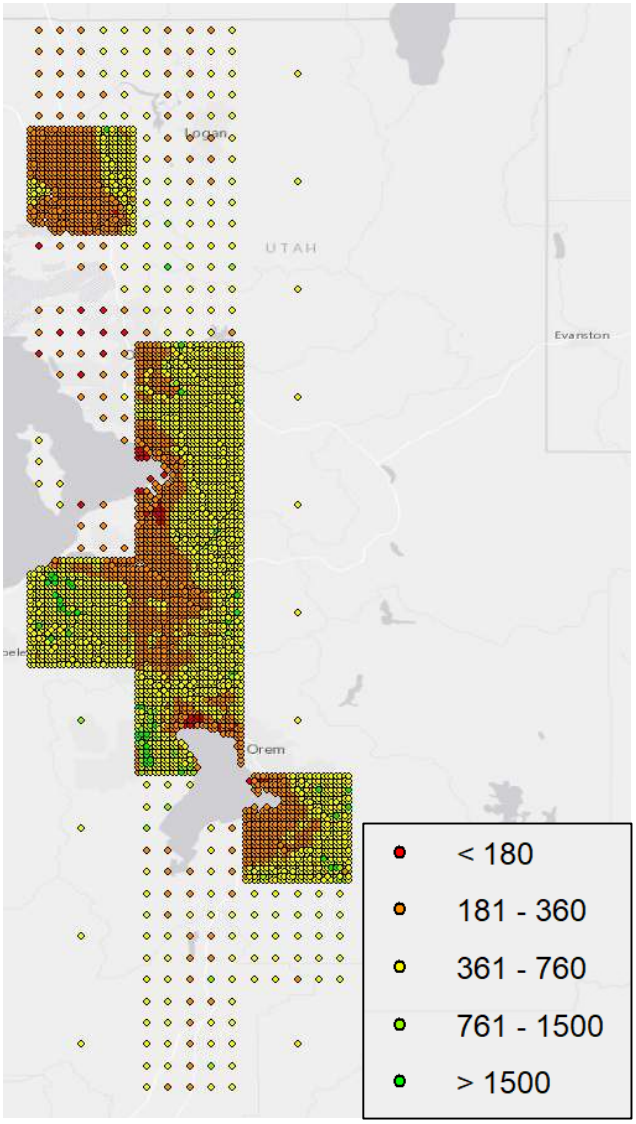

Figure 4.3: Site conditions map of the Salt Lake City area

It is interesting to note that the topography-based model exhibits greater performance in this region in one of the two geologic units that were used for ranking, and is also the dominant model for the regional analysis. This result is surprising when considered in light of the results for other regions, especially California, in which the topography-based model was never the dominant model during the analysis. A possible explanation is that this result

is due to relatively low quality geology-based V_{S30} estimation information that is being used to inform the Hybrid model. Intuitively, it is logical that a poor characterization of geology-based V_{S30} estimates would negatively affect the predictive capacity of the hybrid model, which uses both geology and slope-based information.

4.3 DISCUSSION

The results obtained from the studies of the above two areas reveals some interesting properties regarding the Bayesian method for model ranking and its applicability to site condition characterization. First, it should be noted that additional areas were investigated as part of this research. However, only one publicly available model, the Wald and Allen (2007) topography model was identified for study. The regions investigated and the available models are shown in Table 4.5.

Table 4.5: Regions investigated for potential model ranking analysis and the candidate models available

	Candidate Models		
Region	*Wald and Allen Topography*	*Wills et al. Geology*	*Thompson et al. Hybrid*
California	x	x	x
Seattle and Puget Sound	x		x
Salt Lake City, Ogden, and Provo	x		x
Charleston, SC	x		
New York, NY	x		
New Madrid Seismic Zone	x		

It becomes immediately apparent then, that the Bayesian method for model ranking is only applicable when multiple candidate models exist. In the case where only one model exists, that model must be chosen by potential users.

In other situations, even when only two model choices exist, the Bayesian model ranking framework provides useful information to users. First, at its most basic level, the framework provides users with a simple evaluation of the better model for site condition selection. This analysis can be seen in the regional ranking results for the Seattle and Salt Lake City areas. Although only two models were available for comparison, the regional ranking provides a concrete selection of the overall better method.

As discussed in the Salt Lake City, Ogden, and Provo section, the topography-based model, which has shown poor relative performance in California and Seattle, was identified as the superior model. Because the hybrid model is newer and has previously shown superior performance, it is possible that potential V_{S30} model users would be inclined to select the Hybrid model. However, application of the Bayesian framework identified that doing so would result in relatively poor ranking results.

4.4 SUMMARY

The Bayesian model ranking framework developed in Chapter 3 was applied to two regions to develop new, synthetic V_{S30} site conditions databases from available models. In both regions, two models, the Wald and Allen (2007) topography-based model and the Thompson et al. (2014) hybrid model were chosen as the candidate models, and their performance was evaluated. It was found that the Thompson et al. (2014) model showed superior performance at the regional level in the Seattle and Puget Sound area, while the Wald and Allen (2007) model demonstrated superior performance in the Salt Lake City, Ogden, and Provo region. The model rankings were also refined for analysis within the

individual geologic units where sufficient benchmark information was present, and the synthetic V_{S30} site condition database was developed from those results.

After consideration of the results of model rankings in two additional regions, it can be seen that there is still merit to using the Bayesian framework for V_{S30} model ranking if at least two candidate V_{S30} models are present. Although there is potentially only small benefit to generating a new, synthetic V_{S30} database, it is useful to have confirmation that a selected model is most appropriate among the candidate models.

CHAPTER 5

QUANTIFYING UNCERTAINTIES IN BAYESIAN FRAMEWORK-BASED V_{S30} MODEL EVALUATIONS

5.1 INTRODUCTION

The devastation caused by earthquakes throughout human history has been a driving force behind the efforts that scientists and engineers have devoted to their study. An area of significant research in earthquake engineering has been the potential for amplification at a site (e.g., Gilbert, 1907). The time-averaged shear wave velocity to a depth of 30 meters (V_{S30}) has been identified as a parameter that can be used to estimate the seismic site condition and can be used for estimation of site amplification (e.g., Borchdert, 1994, Boore et al., 1994) and in ground motion prediction equations (GMPEs) (e.g. Boore and Atkinson, 2008). Although V_{S30} is not capable of fully characterizing site amplification, it is still widely used in building codes (e.g. ASCE 2010; FEMA, 2015), and therefore, an important need exists to develop accurate, reliable strategies to predict the parameter.

While V_{S30} can easily be calculated if the appropriate geotechnical measurement data exists to 30 meters, it is often desirable to have large-scale estimates of V_{S30}. Measurement for V_{S30} can be expensive, time consuming, or otherwise challenging, so methods to estimate V_{S30} without measurement are attractive alternatives. As V_{S30} has become more widely utilized, multiple methods for estimating its value based on proxy information have emerged. Proxy-based methods are popular due to the relative ease of acquiring the proxy information, such as topographic slope (Wald and Allen, 2007; Allen and Wald, 2009),

surficial geology (Wills et al., 2000; Wills and Clahan, 2006; Scasserra et al., 2009; Wills et al. 2015), terrain features (Yong et al. 2012), or hybrid methods that combine proxies (Thompson et al. 2014). However, users of proxy-based methods, from researchers to insurers, have no clear guidelines for which proxy-based method is best for their specific application, despite the existence of statistical methods that could be used to aid their decisions (e.g. Buckland et al, 1997; Schwarz, 1978; Zhang et al., 2014; Juang et al., 2015). In Chapter 3, Brownlow et al. (2017) presented a Bayesian framework for ranking and selection of V_{S30} models, and that methodology is adopted and enhanced in this paper. Specifically, this paper focuses on methods to account for uncertainties that exist in both the proxy-based models that are used to predict V_{S30} and the uncertainties in benchmark data used to evaluate candidate model performance.

Using the Bayesian framework developed in Chapter 3, the new method updates the likelihood function to contain uncertainty terms for both model uncertainties and benchmark data uncertainties. An example calculation using the updated methodology is performed and compared to the results that do not account for uncertainties. A sensitivity study is also included to illustrate the effects of changing uncertainty values and how the ranking results can be influenced.

5.2 METHODOLOGY

To adequately quantify the uncertainties present in a V_{S30} model, the potential sources of uncertainties in the model must first be identified. Because the purpose of a model is to predict reality, it is important that the set of data used to represent reality is of sufficient quality to be of use. However, even high quality benchmark databases will contain

observational errors that affect their ability to effectively calibrate a model. Uncertainties can also arise from a model's inability to fully account for the complexity of a geotechnical system, a limitation referred to as model uncertainties.

In this paper, the assumed relationship between a predictive model and reality is expressed in Equation (5.1) (e.g., Ronold and Bjerager, 1992).

$$\left(V_{S30}\right)_d = N \cdot \left(V_{S30}\right)_p \tag{5.1}$$

where $(V_{S30})_d$ is observed V_{S30} data, such as that in a benchmark database for model calibration purposes; $(V_{S30})_p$ is the predicted V_{S30} value from a model, and N is a model bias factor that relates the two values. If each term in Equation (5.1) is assumed to have some uncertainty, then those terms can be characterized as random variables. Furthermore, because none of the terms can have a zero value, it can also be assumed that each term in Equation (5.1) is lognormally distributed. For ease of communication throughout the text, the following properties of the lognormal distribution are presented (e.g. Haldar and Mahadevan 2000):

$$\lambda = \ln\left(\frac{\mu}{\sqrt{1+\left(\sigma/\mu\right)^2}}\right) \tag{5.2}$$

$$\xi = \sqrt{\ln\left[1+\left(\frac{\sigma}{\mu}\right)^2\right]} \tag{5.3}$$

where μ and σ are the mean and standard deviation and λ and ξ are the parameters that describe the lognormal distribution.

V_{S30} Model Likelihood Function

Often, a decision maker such as a design engineer is required to make decisions regarding model selection with limited information. In the case of V_{S30} models, the Brownlow et al. (2017) study in Chapter 3 proposed a Bayesian method for model ranking to assist with model selection. The framework of that study is used herein, though modifications are suggested in this text to better accommodate uncertainty calculations.

The Bayesian method for model ranking is based on identifying the likelihood function for a distribution and maximizing it for the parameters of the distribution. Considering a general version of Equation (5.1) in which all three terms are random variables, a mean and standard deviation and therefore the parameters of a lognormal distribution exist for each term—λ_d and ξ_d for $(V_{S30})_d$, λ_N and ξ_N for N, and λ_p and ξ_p for $(V_{S30})_p$. Maximum likelihood estimation (MLE) is used to maximize the likelihood function for each V_{S30} model under consideration.

From Equation (5.1), Equations (5.4) and (5.5) can be written.

$$\ln\left(V_{S30}\right)_d = \ln N + \ln\left(V_{S30}\right)_p \tag{5.4}$$

$$0 = \ln N + \ln\left(V_{S30}\right)_p - \ln\left(V_{S30}\right)_d \tag{5.5}$$

Let $y = \ln N + \ln (V_{S30})_p - \ln (V_{S30})_d$. The variable y is normally distributed with a mean of $\lambda_N + \lambda_p - \lambda_d$ and a standard deviation of $\sqrt{\left(\xi_N{}^2 + \xi_p{}^2 + \xi_d{}^2\right)}$. The above equation indicates that the chance to observe $(V_{S30})_d$ is equal to the probability to observe a value of zero when the random variable is y, i.e.,

$$P\left[\left(V_{S30}\right)_d \mid \lambda_N, \xi_N\right] = \Phi\left(\frac{0-\lambda_N-\lambda_p+\lambda_d}{\sqrt{\left(\xi_N{}^2+\xi_p{}^2+\xi_d{}^2\right)}}\right) \tag{5.6}$$

where Φ is the probability density function (PDF) of the standard normal random variable (e.g., Ang and Tang 2007).

Assuming there are *n* observations about $(V_{S30})_d$ and that these observations are statistically independent, the chance to observe these *n* observations are as follows

$$P\left(V_{S30,d1}, V_{S30,d2}, ..., V_{S30,dn} \mid \lambda_N, \xi_N\right) = \prod_{i=1}^{n} \Phi\left(\frac{0-\lambda_N-\lambda_{p,i}+\lambda_{d,i}}{\sqrt{\left(\xi_N{}^2+\xi_{p,i}{}^2+\xi_{d,i}{}^2\right)}}\right) \tag{5.7}$$

where $\lambda_{p,i}$, $\lambda_{d,i}$, $\xi_{p,i}$, and $\xi_{d,i}$ are the values of λ_p, λ_d, ξ_p, and ξ_d for the *i*th observation, and $V_{S30,\,di}$ is the *i*th observation.

Equation (5.7) is indeed the likelihood function of λ_N and ξ_N. To maximize the likelihood function, the derivative of the likelihood function is used to identify maximum and minimum values. The natural logarithm can be used to simplify the likelihood function, producing the so-called log-likelihood function:

$$L\left(V_{S30,d1}, V_{S30,d2}, ..., V_{S30,dn} \mid \lambda_N, \xi_N\right) = \sum_{i=1}^{n} \Phi\left(\frac{0-\lambda_N-\lambda_{p,i}+\lambda_{d,i}}{\sqrt{\left(\xi_N{}^2+\xi_{p,i}{}^2+\xi_{d,i}{}^2\right)}}\right) \tag{5.8}$$

Because the natural logarithm is monotonically increasing, maximizing the log-likelihood function is equivalent to maximizing the likelihood function. It is common practice to use a log-likelihood function to reduce the computational complexity of the

maximization. In this application, the terms λ and ξ are the parameters of the likelihood function to be maximized.

RANKING RELATIVE PERFORMANCE OF V_{S30} MODELS

The methodology presented in Chapter 3 can be used to evaluate competing V_{S30} models and determine which model demonstrates the best performance using a Bayesian method for model ranking. However, instead of computing the Bayesian Information Criterion (BIC) to determine $P(M_i|\mathbf{D})$, the analysis in this paper is based on results obtained using Laplace's Approximation (Zhang et al. 2014) to compute a value termed the Laplace Information Criterion (LIC). The LIC and BIC can both be used to compute $P(M_i|\mathbf{D})$, which indicates the probability that model *i* is able to correctly predict the benchmark data **D**. The deviation from the Bayesian method for model evaluation presented in Chapter 3 is due to the higher degree of accuracy achieved using the LIC.

To identify a superior model, the models' predictions are compared to benchmark data. In Chapter 3, Brownlow et al. (2017) propose a Bayesian method for evaluating each model's performance by evaluating their ability to accurately predict the benchmark data in a set of models $M_1, M_2, \ldots, M_r$:

$$\mathrm{P}(M_i \mid \mathbf{D}) = \frac{\exp\left[-\frac{\Delta_i(\mathrm{BIC})}{2}\right]}{\sum_{j=1}^{r}\exp\left[-\frac{\Delta_j(\mathrm{BIC})}{2}\right]} \tag{5.9}$$

$$\mathrm{BIC} = -2\cdot\ln\left[l\left(\theta^* \mid M_i, \mathbf{D}\right)\right] + k\ln(n) \tag{5.10}$$

where, M_i is one of the models being evaluated, **D** is the benchmark data, Δ_i(BIC) is the difference between model M_i's BIC value and the minimum BIC of the set of models being evaluated, P(M_i|**D**) is the probability that model M_i's prediction is the true value of V_{S30} given the benchmark data, $\ln[l(\theta^*|M_i,\mathbf{D})]$ is the value of the optimized log-likelihood function at θ^*, θ^* is the optimized value of the parameter(s) evaluated using maximum likelihood estimation, k is the number of parameters in the likelihood function (e.g. $k = 2$ for a lognormal distribution), and n is the number of data points in **D**.

The LIC, used instead of the BIC, can be calculated using the following equation:

$$\mathrm{LIC} \approx \frac{(2\pi)^{\frac{r_i}{2}} l\left(\beta_i^* \mid \mathbf{D}\right)}{\sqrt{\left|\mathbf{A}\left(\beta_i^* \mid \mathbf{D}\right)\right|}} \tag{5.11}$$

where β_i^* is the point where the likelihood function is maximized, r_i is the dimension of β_i^*, and $\mathbf{A}(\beta_i^*|\mathbf{D})$ is the Hessian matrix of the logarithm of the likelihood function evaluated at β_i^*. The variables β_i^* and r_i in Equation (5.11) are equivalent to the variables θ^* and k, respectively, in Equation (5.10). It should be noted that the natural log of Equation (5.11) should be used if the log-likelihood function is used to evaluate β_i^*.

Therefore, P(M_i|**D**) can be calculated as follows:

$$\mathrm{P}(M_i \mid \mathbf{D}) \approx \frac{\exp\left[-\frac{\Delta_i(\mathrm{LIC})}{2}\right]}{\sum_{j=1}^{r} \exp\left[-\frac{\Delta_j(\mathrm{LIC})}{2}\right]} \tag{5.12}$$

The value of P(M_i | **D**), obtained for an individual model, denotes the probability, relative to all models in the study, that the model in question, M_i, represents the true value

of V_{S30}. Therefore, a ranking of each models' predictive performance can be established, and the best model can be chosen.

Dominant and Non-dominant Model Performance

As denoted by Equation (5.12), the final result of this methodology is a probability value that indicates each model's relative performance, allowing the user to identify the best predictor of the benchmark data. In some cases, as will be shown later in this report, one model dominates the others. In a situation where one model shows superior performance, the result indicates that the dominant model's predictions are always the best choice for areas that are well represented by the benchmark data. However, in some cases, more than one model can demonstrate sufficient performance to warrant consideration. A model is considered non-dominated if $P(M_i \mid \mathbf{D})$ is at least $1/20^{th}$ of the next largest model's probability. In the case that there is not a single dominant model, Equation (5.13), based on total probability, can be used to resolve each model's predictions into a single value for end use.

$$p^*\left(Vs_{30} \mid \mathbf{D}\right) = \frac{\sum_{k=1}^{t} p^*\left(Vs_{30,k} \mid M_k, \mathbf{D}\right) P\left(M_k \mid \mathbf{D}\right)}{\sum_{k=1}^{t} P\left(M_k \mid \mathbf{D}\right)} \tag{5.13}$$

In Equation (5.13), $p^*(V_{S30} \mid \mathbf{D})$ is the final predicted value of V_{S30} to be used by the investigator, $p^*(V_{S30,k} \mid M_k, \mathbf{D})$ is the predicted V_{S30} by model M_k, $P(M_k \mid \mathbf{D})$ is the probability that model M_k is correct, as evaluated in Equation (5.12), and t is the number of non-dominated models to be included in the final prediction.

INCOMPLETE UNCERTAINTY INFORMATION

In many cases, it is unlikely that uncertainty information will be available for both the database and each model included in the study. Depending on the nature of the available data, Equation (5.8) can be reduced to only account for those uncertainties that can be quantified. Because measurement error tends to be well understood, it is common for benchmark data to either possess uncertainty distribution information or to easily establish uncertainty distribution values based on the information that is known about how the benchmark data were developed. Model prediction data, by contrast, is not nearly as easily evaluated for uncertainties. Each model will be developed using unique methods, and those methods will include assumptions, each of which possess their own uncertainty, and which will likely need to be evaluated individually. In the event that uncertainty information cannot be determined for the model predictions, the following equation applies.

$$L\left(V_{S30,d1}, V_{S30,d2}, ..., V_{S30,dn} \mid \lambda_N, \xi_N\right) = \sum_{i=1}^{n} \Phi\left(\frac{0 - \lambda_N - \left(V_{S30}\right)_{p,i} + \lambda_{d,i}}{\sqrt{\left(\xi_N{}^2 + \xi_{d,i}{}^2\right)}}\right) \tag{5.14}$$

Similarly, in the event that the model uncertainty is known and the benchmark data uncertainty is unknown, the log-likelihood function can be expressed as Equation (5.15).

$$L\left(V_{S30,d1}, V_{S30,d2}, ..., V_{S30,dn} \mid \lambda_N, \xi_N\right) = \sum_{i=1}^{n} \Phi\left(\frac{\left(V_{S30}\right)_{d,i} - \lambda_N - \lambda_{p,i}}{\sqrt{\left(\xi_N{}^2 + \xi_{p,i}{}^2\right)}}\right) \tag{5.15}$$

In the event that neither the model prediction uncertainty nor the benchmark data uncertainty can be quantified, Equation (5.16) can be used as the log-likelihood function.

$$L\left(V_{S30,d1}, V_{S30,d2}, ..., V_{S30,dn} \mid \lambda_N, \xi_N\right) = \sum_{i=1}^{n} \Phi\left(\frac{\left(V_{S30}\right)_{d,i} - \lambda_N - \left(V_{S30}\right)_{p,i}}{\xi_N}\right) \qquad (5.16)$$

It is important to note that, if uncertainty is to be considered in the analysis (i.e., through use of Equations (5.8), (5.14), or (5.15)) each uncertainty term must be evaluated in its entirety. It is critical that, if incomplete uncertainty information exists for a particular uncertainty term, the uncertainty is not considered in the analysis. The reason for this is the nature by which the uncertainty is considered, and is best illustrated with a simple theoretical example.

Consider a situation in which only the uncertainty in the model predictions is to be used to evaluate three V_{S30} models, but for which only one model, A, has uncertainty information available, while the other two models, B and C, have no uncertainty information available. Because the uncertainties in the model predictions will weaken their performance, it is very unlikely that model A will be able to show competitive performance relative to models B and C, regardless of its actual performance. It is likely that model A could have shown dominant performance in a comparison in which no uncertainty was considered, but that performance would be lost if it was evaluated with uncertainties against models where no uncertainty information was included.

The same tenet holds for the benchmark data. Unless all benchmark data can have uncertainty information included, it should not be included in the analysis.

5.3 APPLICATION OF METHODOLOGY

To illustrate the methodology presented within this paper, three publicly available V_{S30} models are evaluated and compared. Furthermore, a database of high quality V_{S30} data, complete with uncertainty information, was compiled to assist with the comparison.

V_{S30} MODELS

Current V_{S30} prediction techniques utilize topography, geology, or a combination to inform their predictions. These techniques are commonly referred to as proxy-based methods. Proxy-based methods are useful for spatial prediction of V_{S30} because they utilize information that is more readily available than subsurface exploration data, which is frequently cost-prohibitively expensive to obtain for regional studies. Two sources of information that can be used for V_{S30} proxy-based estimates are topography and geology. Topographic information is available for the entire globe thanks to the Shuttle Topography Radar Mission (STRM) (Farr and Kobrick, 2000; Farr et al., 2007), which provided digital elevation data for the globe at resolutions up to 1 arcsecond (approximately 30 meters) per measurement. Some geologic information is available through state-specific geologic societies, the United States Geologic Survey (USGS), or various state-sponsored departments of natural resources. However, detailed geologic information is not always available, or is not available digitally, which can be challenging for researchers working with geology-based proxies.

The models used in this analysis are the same as those included in Brownlow et al. (2017). As mentioned in Brownlow et al. (2017), appropriate V_{S30} models would need to possess a few baseline criteria to be included in the analysis. Specifically, appropriate V_{S30}

models would be able to provide a predicted V_{S30} value with only location as an end-user input with sufficient resolution. No specific resolution was determined as a decision-making criterion, but it was desirable for predictions to be densely-packed enough to be reasonably representative of any benchmark data locations. The study was limited to the state of California due to the relative abundance of data available for benchmarking applications and the number of publicly available V_{S30} models (three, total) available for comparison. Two of the models, developed by Wald and Allen (2007) and Thompson et al. (2014), are available at 30 arcsecond resolution. The third, Wills et al. (2015), gives predictions at any location.

TOPOGRAPHY-BASED MODEL

A topography-based V_{S30} model was developed to take advantage of the STRM data collected in 2000 by the space shuttle Endeavor (Wald and Allen 2007). The model uses a correlation between the slope measurements and observed V_{S30} values to create global predictions of V_{S30}. The model was developed for a 30 arcsecond resolution, which is detailed enough to allow for good characterization of small scale geologic features that are important for proper site characterization. The predictions are generated at the same 30 arcsecond resolution for which the topography was evaluated. The data could be obtained from the USGS global V_{S30} website for either a predefined area or for a user-defined area with ease. However, between the time of this study and the time of writing, the tool for obtaining these model outputs has been removed from the USGS website.

One of the strengths of the topography-based model is its ability to spatially interpret specific topography characteristics and give an appropriate characterization. The result of

that characteristic is a map of predictions in a 30 arcsecond grid with individual values at each prediction location. However, a limitation of this model is that its maximum predicted V_{S30} is 760 m/s, which is lower than the V_{S30} observed in predominantly hard rock subsurface conditions. Therefore, model outputs that are 760 m/s should be interpreted as being at least 760 m/s. Figure 5.1 is a graphical representation of the Wald and Allen (2007) model with scale included. However, the scale included in the next few figures uses a consistent color gradient, and therefore the maximum and minimum values on the scale are not necessarily indicative of the maximum and minimum V_{S30} values displayed in a given figure.

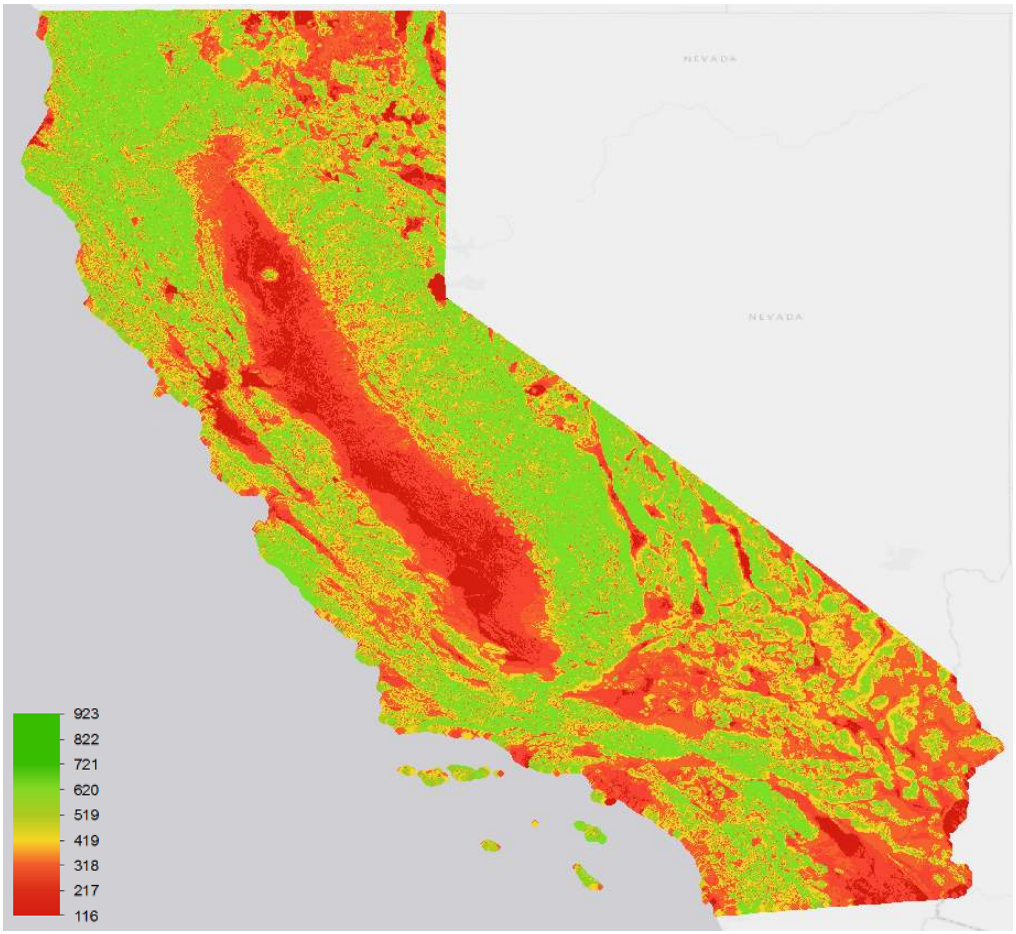

Figure 5.1: Visual representation of the Wald and Allen (2007) topography-based V_{S30} model. Velocity shown in m/s. Note that the maximum value in the scale does not necessarily correspond to the maximum V_{S30} displayed in the figure.

SURFICIAL GEOLOGY-BASED MODEL

Geology-based models utilize the extensive degree of geologic investigation and characterization that has been performed across the country. Geologic maps show soil and rock classification information, including physical properties, and tend to be widely available. Wills et al. (2015) have refined a geology-based model that implements a correlation between simplified geologic units and V_{S30}. Park and Elrick (1998) and Wills et al. (2000) initially performed studies correlating geology to V_{S30}, the former being confined to the Los Angeles area and the latter applying to the entirety of California. Wills

et al. (2000) grouped geologic units of similar age and physical properties for the sake of relating the relatively scarce number of V_{S30} values in the state to each geologic unit, though that was not always possible, and the final result was a map of California that classified areas by their NEHRP V_s category or intermediate category. Wills and Clahan (2006) updated the model by regrouping misclassified units, increasing the amount of V_{S30} measurements used for classification, and reporting V_{S30} values for each simplified geologic unit in the map. Wills and Gutierrez (2011) identified a slope-based correlation to subdivide young alluvium units to improve V_{S30} predictions in those areas. The Wills et al. (2015) work applies the Wills and Gutierrez (2011) slope-based correlation to the V_{S30} map of California and utilizes a more detailed set of geologic maps to improve the accuracy of the surficial geology classifications.

The Wills et al. (2015) model was developed based on the notion that surficial geology provides an indication of the V_{S30} that can be expected in a given area. Therefore, the model is built with geology as its primary means of predicting V_{S30}. However, geologic maps, even at their most detailed, are still incapable of displaying the minute variations in subsurface conditions. Furthermore, although the volume of available V_{S30} measurement data has improved in recent years, there is still a significant lack of data, so geologic units need to be combined to effectively use the available information. Finally, an averaged V_{S30} value must be recommended for each geologic unit in this method. As a result of both the relatively coarse characterization of local effects and the combination of geologic units, when V_{S30} values are assigned to each map unit, the resulting map contains large areas that are all rated to have the same V_{S30} value. This is a weakness of the model, since there are

many local effects that can also control V_{S30} (and site response). Figure 5.2 provides a visual representation of the V_{S30} values that are predicted by the model. As mentioned previously, because a consistent scale was shared between each of Figure 5.1 through Figure 5.3, the maximum and minimum values are not necessarily representative of the maximum and minimum values predicted by the model.

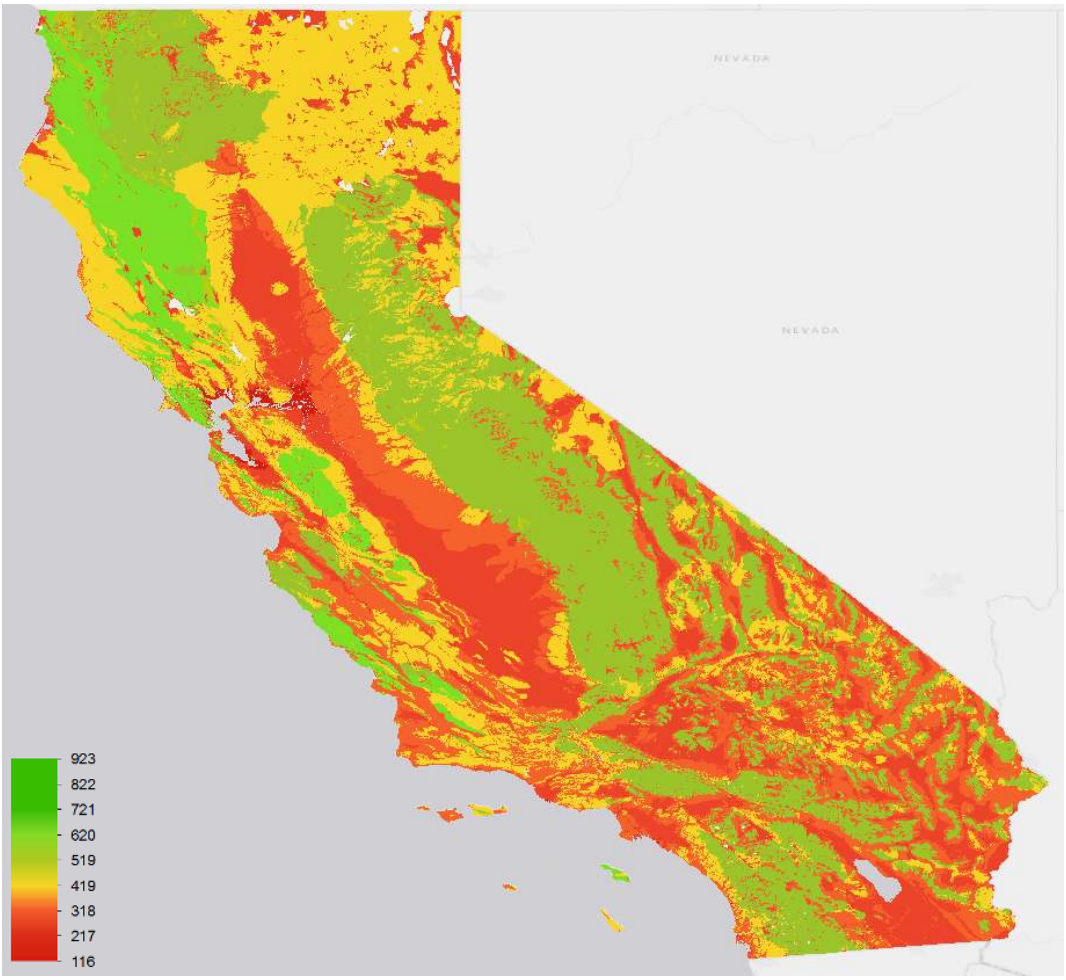

Figure 5.2: Visual representation of the Wills et al. (2015) geology-based V_{S30} model. Velocity in m/s.

HYBRID MODEL

Wills and Gutierrez (2011) and Thompson et al. (2014) presented a method for combining predictions from both geology-based and topography-based V_{S30} predictions.

The model attempts to capitalize on the strength of each individual model by utilizing the local information available at high resolution from the topography-based method and combining it with the strong predictability available from geology-based methods. Furthermore, the method implements the geostatistical method known as regression kriging (RK) to refine the model locally for known V_{S30} values.

The Thompson et al. (2014) model uses the Wills and Clahan (2006) geology-based model as a baseline for V_{S30} estimates, and establishes a scaling function that utilizes the Wald and Allen (2007) for predicting local deviations in V_{S30} based on topography. The code to generate a map containing the hybrid model predictions is available as a Linux-based repository on the file hosting site Github (github.com/usgs/earthquake-global_v_{S30}). Figure 5.3 illustrates the V_{S30} estimates from the Thompson et al. (2014) model for California.

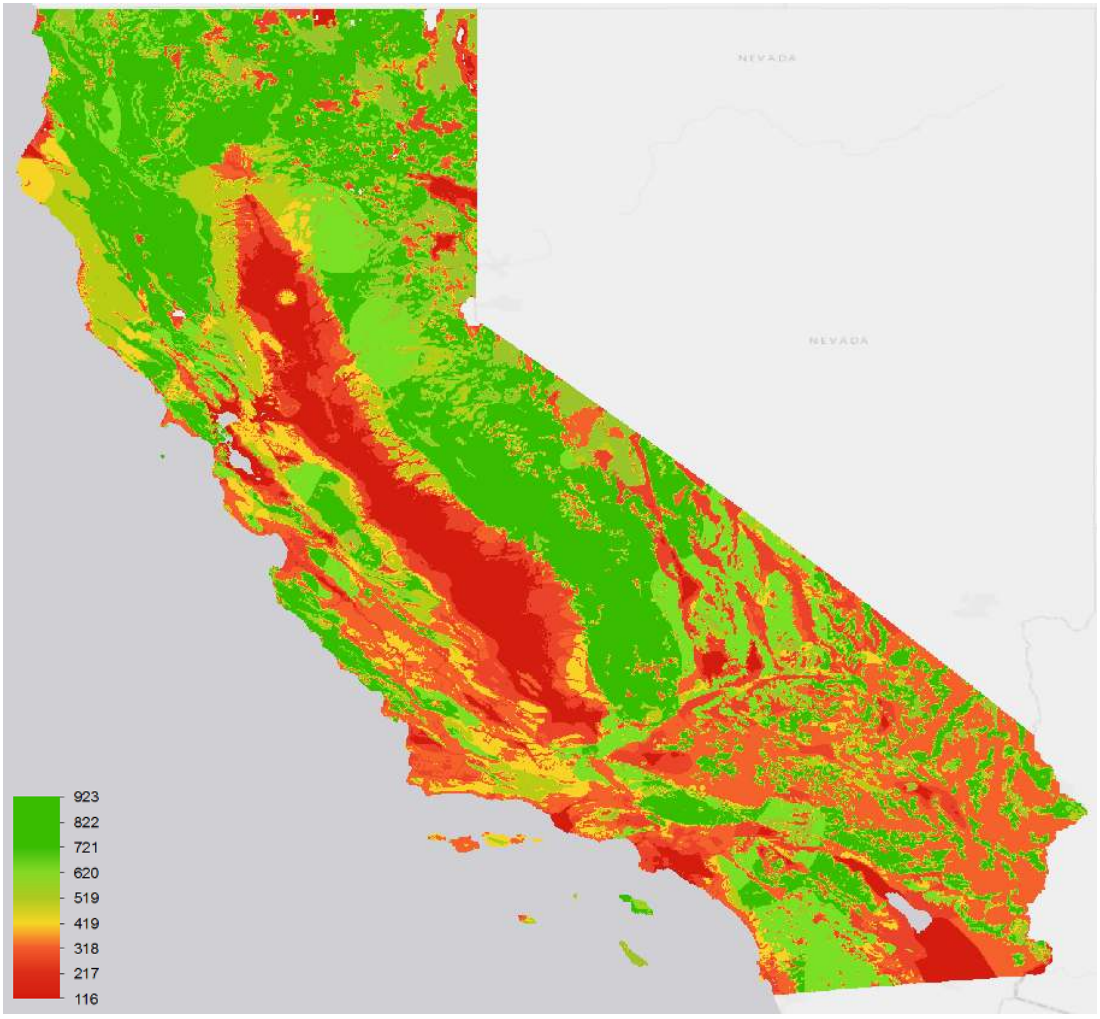

Figure 5.3: Visual representation of the Thompson et al. (2014) hybrid V_{S30} model. Velocity in m/s.

V_{S30} Model Outputs

For comparison of the spatial V_{S30} prediction capabilities of each model to be possible, the V_{S30} models needed to provide some form of location data for each V_{S30} prediction location. The Wald and Allen (2007) and Thompson et al. (2014) model data were obtained in raster file format with predictions in a 30 arcsecond grid. The Wills et al. (2015) model is available as an electronic supplement to their study, and is available as one of two file types that can be imported into ArcGIS for analysis.

ArcMap, a program that is part of the ArcGIS software suite by ESRI, is a geographic information system (GIS) program that allows users to easily view and manipulate spatial data. The program was utilized to convert the source files from each model into usable formats for comparison when necessary. Additionally, ArcMap contains functionality that allows users to easily combine data based on spatial position, referred to as a "spatial join" operation in the program, and that tool was used to relate the models to the benchmark data, which is discussed below.

5.4 BENCHMARK DATABASE

In order to properly evaluate each model's capacity for accurate prediction of site conditions, a high quality database of V_{S30} data was compiled for this study. In addition to providing location information and V_{S30} information, the source databases also needed to either provide uncertainty information or give enough additional information to allow for estimation of uncertainties associated with each V_{S30} value provided. The two databases used by this study are the NGA-West2 ground motion database (Ancheta et al., 2013) and the USGS V_{S30} measurement database (Yong et al., 2015).

The NGA-West2 database was compiled as part of the Next Generation Attenuation Project, and was developed to create a consistent, state of the art source of ground motion data for use in developing ground motion prediction equations (GMPE's). The NGA-West2 database is the database used in the second and most recent iteration of the NGA project. Although the database's intended purpose is not to provide V_{S30} data, significant care was put into accurate characterization of the V_{S30} data. The V_{S30} data provided by the database is a combination of measured V_{S30}, extrapolated V_{S30} when measurements do not

extend to 30 meters, and proxy-based estimates when the other data are not available. Furthermore, the database contains a value for the natural logarithm of the standard deviation for each V_{S30} measurement-based value or estimate provided by the database. Ancheta et al. (2013) describe the entirety of the data available in the database.

The USGS V_{S30} database consists of various sources of measurement data used to provide V_{S30} values for locations across the United States. The database's characteristics are summarized in Yong et al. (2015). The database is comprised of data that were obtained using multiple measurement techniques. Table 5.1 summarizes (and simplifies) the data from Yong et al. (2015) and shows the various methods used to obtain the data. Because the database does not include uncertainty information, that information was assumed based on the measurement technique(s) used. The specifics of the process used to estimate the uncertainty of each method in Table 5.1 is provided with a list of assumed values is presented in the Benchmark Database Uncertainty section of this paper.

Table 5.1: Summary of data available from Yong et al. (2015)

Measurement Technique	**Number of Test Sites**
AM	13
Downhole	318
Downhole-Crosshole	1
iMASW	31
MASW	153
ReMi	731
SASW	307
SCPT	984
Seismic Refraction	61
Seismic Refraction/Reflection	28
CXW	27
Multi-method	99
Total	**2753**

It can be seen in Table 5.1 that the majority of measurements originate from only a few measurement techniques. It is notable that nearly half of the database consists of invasive methods, with the majority of those measurements originating from SCPT soundings. The other half of the database consists of measurements from various noninvasive techniques, though 99 of the total reported V_{S30} values in the database are reported as originating from multiple methods. It should be noted that the information in Table 5.1 is condensed, and a single technique listed in the table may represent multiple methods of performing the same general technique.

Figure 5.4 shows the spatial dispersion of data in the combined database for this report. It can clearly be seen that the majority of benchmark data are clustered around the San Francisco Bay area to the north and Los Angeles and Orange County area to the south. Therefore, it is reasonable to assume that the results reported later in this report will be most applicable for those regions.

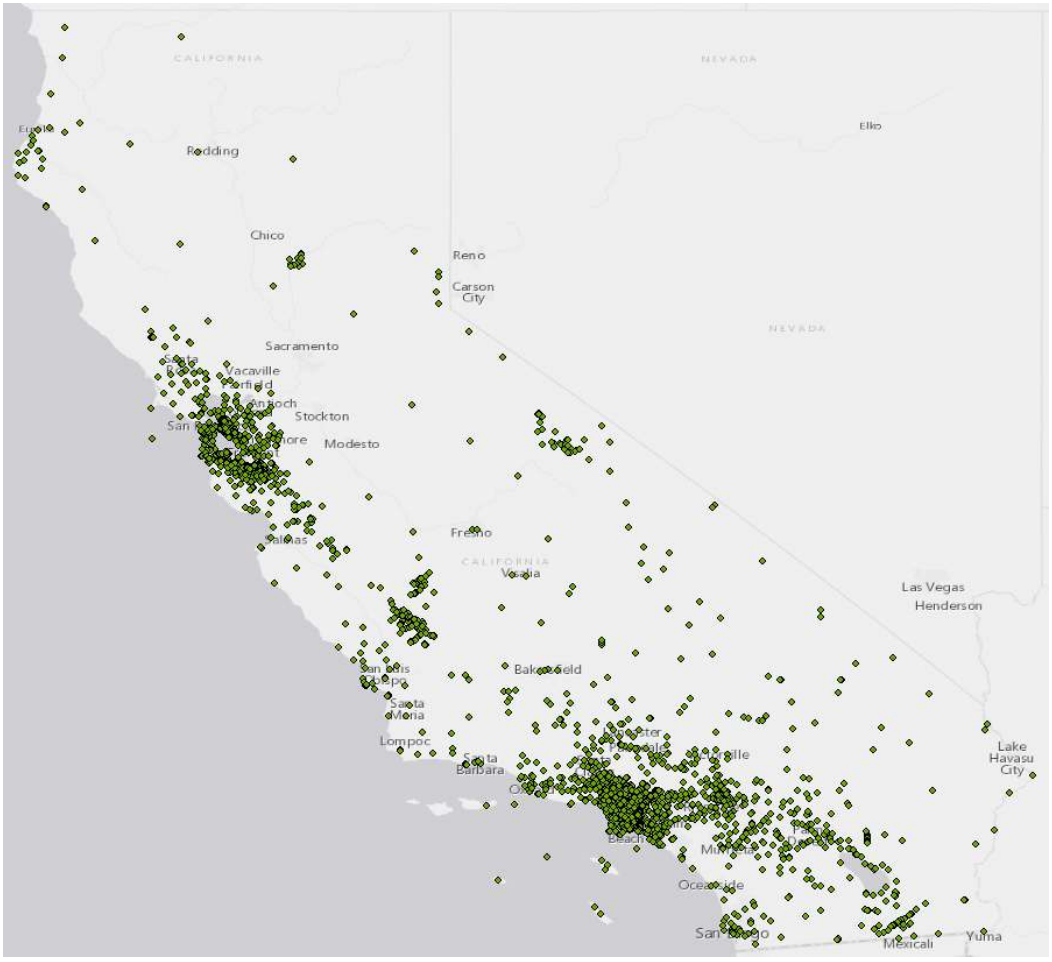

Figure 5.4: Distribution of benchmark data in California

BENCHMARK DATABASE UNCERTAINTY

To implement the new methodology, uncertainty information for the benchmark database is needed. In a perfect theoretical environment, there would be no uncertainty in the benchmark data, and the benchmark would be a perfect representation of reality. However, much of geotechnical engineering involves uncertainty, including the evaluation of geotechnical parameters. Geotechnical subsurface exploration techniques can be divided into two general categories: invasive and noninvasive techniques. Invasive techniques

involve penetration of the ground surface for the purpose of measuring the soil properties. They are considered to be a good source of data because the soil properties are being measured as directly as possible, which leaves less room for misrepresentation of the measurement data due to nearby subsurface features (Moss, 2008). A limitation of invasive methods is that they disturb the soil that they intend to measure, potentially altering the soil's properties in the process. Additionally, invasive techniques tend to be relatively expensive. Noninvasive techniques avoid the problem of disturbing the soil structure, and tend to be less expensive than invasive methods due to lower equipment costs. Invasive methods involve creating a known vibratory ground motion, referred to as an active source, and interpreting how that source varies between the input location and the receiver location. Noninvasive techniques, on the other hand, can use either an active source or passive sources (e.g. cars on a highway or waves on a beach) and a series of receivers to measure the way that seismic energy propagates beneath the surface.

The invasive tests included in the Yong et al. (2015) database are the downhole, suspension logging, crosshole, and seismic cone penetration test (SCPT) methods. The noninvasive methods include the microtremor array method (AM), controlled-source measurement of surface wave dispersion (CXW), horizontal-to-vertical-spectral-ratio (HVSR), refraction mictrotremor (ReMi), spectral analysis of surface waves (SASW), Multi-channel analysis of surface waves (MASW), interferometric multi-channel analysis of surface waves (iMASW), seismic reflection and refraction, and spatial autocorrelation (SPAC).

Moss (2008) studied measurement uncertainty in V_{S30} techniques. Although not all of the techniques listed in Table 5.1 were addressed in the Moss (2008) report, it serves as a good baseline for establishing additional uncertainty information for the other methods. Moss (2008) found that uncertainty in V_{S30} measurements tends to increase with increasing velocity, and therefore uses coefficient of variation (COV), defined as the standard deviation divided by the mean, to report measurement uncertainty for various techniques. For SASW and MASW, a COV of 5-6% was reported, and invasive techniques were reported to have a COV of 1-3% with an associated bias correlation to account for soil disturbance. Although other noninvasive techniques were investigated as part of the Moss (2008) study, insufficient data were available for drawing meaningful conclusions. However, the baseline COV of 5-6% for SASW and MASW as noninvasive techniques is useful for calibrating expectations for the expected COV of other techniques. Because of the results of the Moss (2008) study, downhole measurements in the database were assigned a COV of 1% and SCPT measurements were assigned a COV of 2%. A value of 5.5% was assigned to the COV for SASW and MASW techniques.

Pancha et al. (2008) studied the ReMi technique, including its uncertainty. They found that the maximum variation in V_{S30} was slightly over 9%, and a COV of approximately 5% can be obtained from their data. The researchers theorized that some variations in their results could be explained by variations in the passive source.

Although not a study on uncertainty, the viability of the seismic reflection and refraction methods were investigated by Odum et al. (2013). They compared seismic reflection and refraction V_{S30} measurements to those obtained using ReMi and found an

average difference of 12% between the two methods, though the differences were generally evenly split between being higher and lower than one-another at each measurement location. A COV of 6% was assumed for this method.

The iMASW method was evaluated by O'Connell and Turner (2011), and was compared to downhole measurements. It was found to have very good agreement to downhole predictions to within 1% accuracy. A COV of 3% was adopted for this technique due to its impressively similar performance to an invasive technique.

Liu et al. (2000) performed a comparison between the AM method and borehole measurements, finding that the AM V_{S30} measurements were within 11% of the measured borehole data. The assumed COV for AM V_{S30} measurements was chosen to be 5.5%.

In the case of the CXW method, a COV of 5.5% was a sufficient assumption. This assumption was made by observing the initial study data by Poran et al. (1996) and a lack of additional literature addressing uncertainties in the CXW method.

When the database lists more than one method that was used to generate V_{S30} data, it was decided that a COV of 5.5% was a sufficient assumption. This assumption was based on the lack of information regarding how the data from multiple methods was resolved into a single V_{S30} value in the Yong et al. (2015) database. A relatively small number of data points (127 in a combined database of 3000+ individual values) were affected by this assumption, so its veracity is relatively minimized. Furthermore, this assumption is almost certainly conservative for the 100 multi-method measurements, since multimethod analysis is believed to improve confidence in measured V_{S30} (Odum et al., 2013).

5.5 V_{S30} MODEL RANKING RESULTS FOR CALIFORNIA

To illustrate the methodology described in this paper, the state of California is used as an example case. The results from this paper will be compared to those produced by Brownlow et al. (2017), as it is an extension of the methodology in that paper. Comparison with the results from Brownlow et al. (2017) will help highlight the importance of explicit consideration of uncertainties when performing a model comparison.

DATA PREPARATION

As mentioned previously, ArcMap was used to handle the spatial prediction data from each model. Using the spatial join tool in ArcMap, each benchmark data point had the closest V_{S30} prediction from each of the 3 candidate models joined to it. Therefore, the finalized spatial view of the data is identical to that of the benchmark database itself. This procedure was selected as an acceptable way to relate model data to the benchmark database due to the nature of the model data and how it is presented. The Wald and Allen (2007) and the Thompson et al. (2014) models both provide V_{S30} estimates as an image consisting of boxes (similar to pixels but with 30 arcsecond center-to-center spacing) that contain stored V_{S30} and location information. Therefore, it is reasonable to interpret the model as assigning the V_{S30} value from each box to the entire area covered by that box. Although the ArcMap program needs to convert the image file to point data before the spatial join tool can be used, picking a model estimate for each benchmark data point preserves the logic of assigning V_{S30} to the corresponding area of interest for both models. Figure 5.5 shows the model as viewed in ArcMap for illustration of this point. In the figure, both the point data estimate and the area which each point data represents are shown. The

point data markers are not colored to show VS30 so that they will remain easily distinguishable in the figure. By contrast the Wills et al. (2015) model provides its V_{S30} predictions in the form of a series of polygons that define geologic units and their boundaries. The benchmark data were assigned the V_{S30} value of whichever Wills et al. (2015) polygon it resided within.

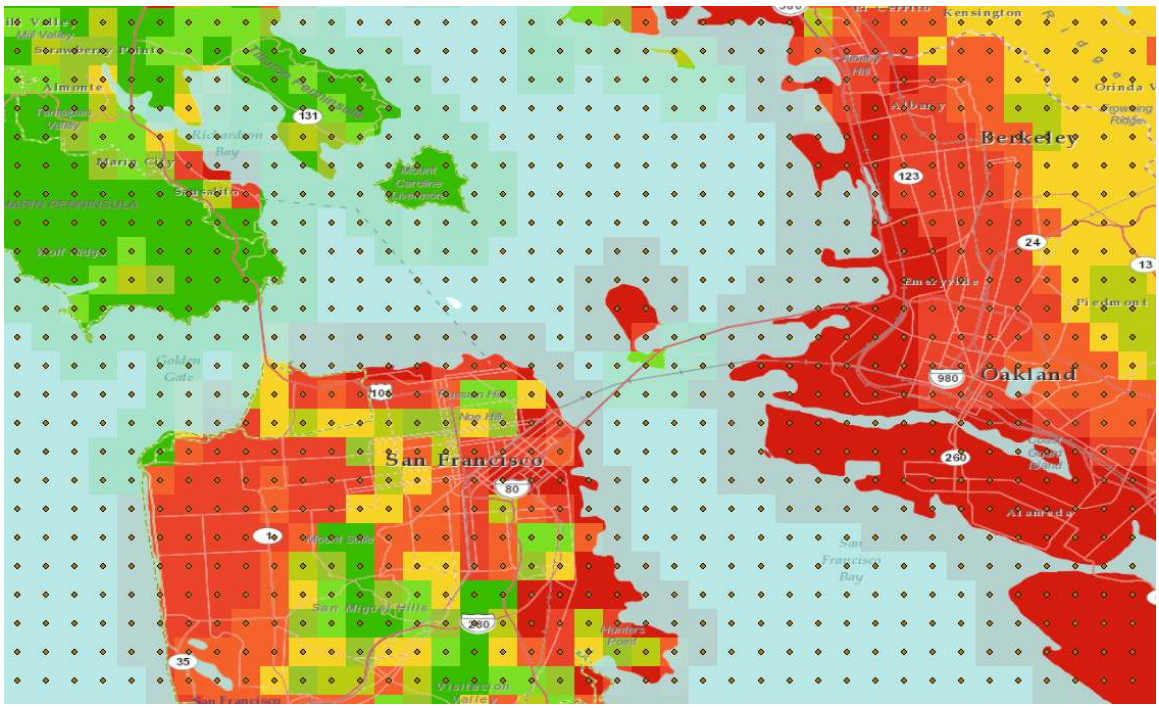

Figure 5.5: San Francisco Bay area with the Thompson et al. (2014) model resolution rendered in ArcMap. Each colored box and point of data in the figure represents one V_{S30} prediction.

To further improve the amount of information obtained from the analysis, the models were ranked based on their performance within each simplified geologic unit identified in Wills et al. (2015). The simplified geologic unit classification for each benchmark database value was assigned during the spatial join operation of the Wills et al. (2015) model.

The benchmark database uncertainty was discussed in a previous section. It was used in addition to the reported measurements to calculate the corresponding values of λ and ξ using Equations (5.2) and (5.3), respectively. Because model uncertainty was not able to be easily characterized, it was assumed that each model had the same uncertainty and that uncertainties did not fluctuate with each prediction for the sake of avoiding confounding results. Thus, for each model, the COV was set to 10%, though any consistent COV value would be sufficient to avoid biased results. The potential impact of model uncertainty will be discussed in a later section as well. It should be noted that a correlation equation does exist to establish uncertainty estimates for geology-based V_{S30} predictions (Moss, 2008). However, because this was the only model uncertainty available, it was not included due to reason discussed earlier in this text.

Model Ranking With Uncertainty Considerations

The models were evaluated using a MATLAB script that handles the raw data (in Excel file format) and performs the analysis. The script uses the "fminunc" command to evaluate the objective function (Equation (5.8) in this case) and then calculates the LIC. Table 5.2 displays the ranking results obtained from this study as well as the results from the Brownlow et al. (2017) study (which does not consider uncertainty).

Table 5.2: Comparison of results including uncertainty to results obtained in Brownlow et al. (2017)

	Wald and Allen Topography		**Wills et al. Geology**		**Thompson et al. Hybrid**		Number of benchmark data points
	Brownlow et al.	This Study	Brownlow et al.	This Study	Brownlow et al.	This Study	
af/Qi	0	0	0.75	1.00	0.25	0	125
Crystalline	0	0	0	0	1.00	1.00	341
KJf	0	0	1.00	1.00	0	0	124

Kss	0	0	0.89	0	0.11	1.00	39
Qal1	0	0	0	0	1.00	1.00	364
Qal2	0	0	0	0	1.00	1.00	745
Qal3	0	0	0	0	1.00	1.00	563
Qi	0	0	0	0	1.00	1.00	19
Qoa	0	0	0	0	1.00	1.00	501
Qs	0.06	0.33	0.06	0.16	0.88	0.51	33
QT	0	0	1.00	0.99	0	0.01	115
sp	0	0	0.99	0.86	0.01	0.14	26
Tsh	0	0	0.73	0.32	0.27	0.68	159
Tss	0	0	0	0	1.00	1.00	169
Tv	0	0	0	0.01	1.00	0.99	74

Comparison of the results immediately shows the impact of considering the uncertainties in the analysis. The af/Qi, Kss, Qs, sp, and Tsh simplified geologic units showed notable changes in relative model performance once uncertainty was considered. The significance of this result lies in the potential for application, in which model selection must be considered not only on the basis of the most advanced model, but also on the validity of the data that are used to verify its predictions. It can also be observed that in most geologic units, the Thompson et al. (2014) hybrid model outperforms the other models, while the Wald and Allen (2007) model only performs well enough to contribute to the estimation of one geologic unit, Qs.

Sensitivity of Ranking Results to Model Uncertainty

Although specific uncertainties could not be characterized for each model, it is still possible to test the impact of uncertainty assumptions on the ranking results. To illustrate the sensitivity of the ranking results to model uncertainty, the model ranking was performed multiple times with a varying COV for the Thompson et al. (2014) model. Because the rankings obtained from the Bayesian model ranking method are relative, the

sensitivity illustration is much more meaningful when all but one COV are fixed. For this analysis, the COV of the Wald and Allen (2007) and Wills et al. (2015) models was fixed at 10%, and the COV of the Thompson et al. (2014) model (COV_H) was varied from 5% to 60% in 5% increments, where the H subscript denotes the hybrid model. Three geologic units, KJf, Qal1, and Qs were selected for inclusion in this analysis for their illustrative capacity. KJf is a unit in which the Thompson et al. (2014) model did not perform well, Qal1 is a unit in which the Thompson et al. (2014) model demonstrated superior performance, and Qs is the only unit in which all three models contribute to the final predictions of V_{S30}. Figure 5.6 shows the results of the three geologic units chosen to represent the sensitivity study. Graphical results for the entire sensitivity study are available in the Appendix at the end of this dissertation.

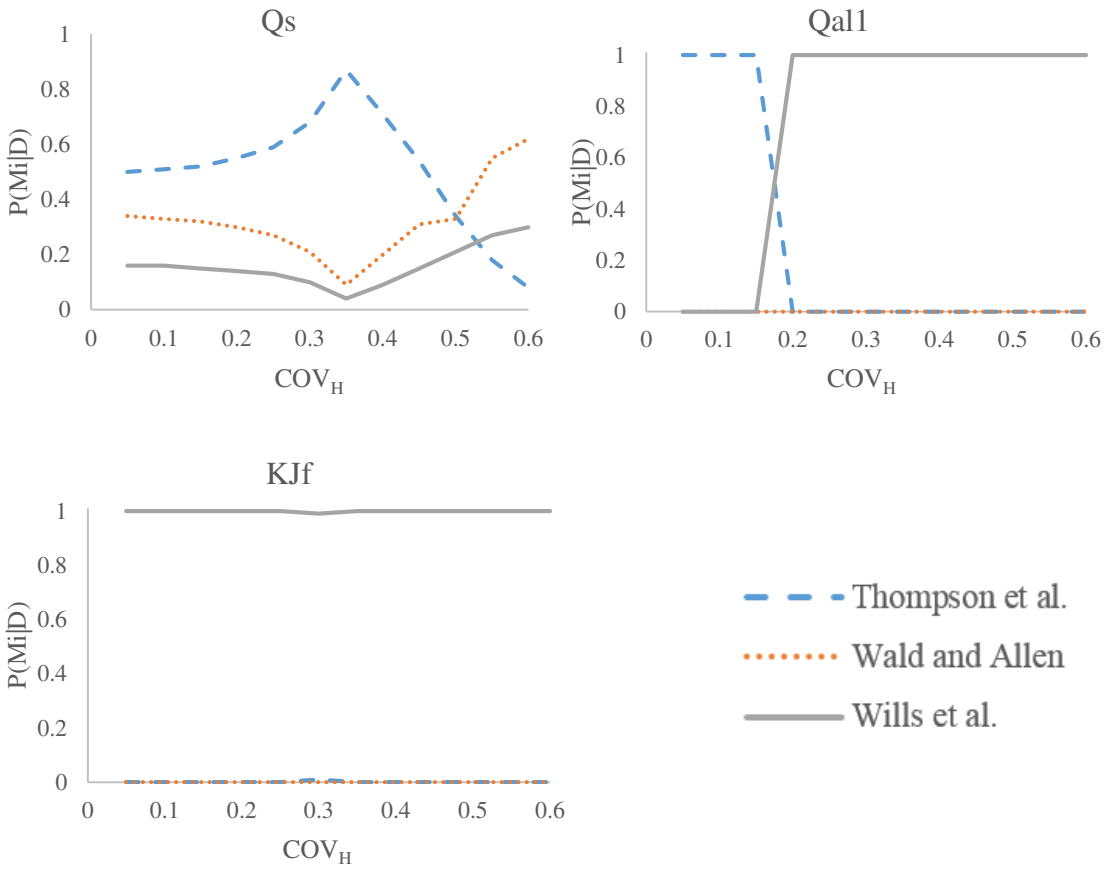

Figure 5.6: Sensitivity analysis of model based uncertainty and its effects on ranking results for three geologic units

As shown in Figure 5.6, the KJf performance of the Thompson et al. (2014) model was generally unaffected by varying COV_H. Not apparent in the figure are minute changes in the probability of $P(M_i|\mathbf{D})$ that manifested as COV_H was adjusted, reaching a maximum of 1% when COV_H = 30%. The performance of the hybrid model in Qal1 units followed an intuitive, if abrupt, trend. The value of $P(M_i|\mathbf{D})$ dropped from 100% to 0% between COV_H = 15% and 20% for the Thompson et al. (2014) model, while the Wills et al. (2015) model showed the reverse trend and the Wald and Allen (2007) model did not contribute. In the Qs geologic unit, a different trend was observed. As COV_H, and, therefore, the uncertainty

in the model predictions increased, the relative performance of the Thompson et al. (2014) model similarly increased until COV_H exceeded 35%, after which its performance deteriorated rapidly. This is a counterintuitive result because of the tendency to expect performance to decrease as standard deviation, used here to represent uncertainty, increases. However, in this case, it is likely that the increased standard deviation of the model uncertainties helps to explain some variation in the scatter of the data between benchmark and model prediction values. In this case, the method interprets the scatter of data, which is now partially understood as a part of the model uncertainty, as less impactful than a purely incorrect prediction by the model that falls outside of its distribution. In other words, to a certain extent, increasing the standard deviation decreases the performance ranking penalty associated with wrong guesses. This phenomenon was also observed by Zhang et al. (2009) and Zhang et al. (2012) in their work regarding model uncertainty.

5.6 DISCUSSION AND CONCLUSIONS

The results of this study highlight the importance of explicit consideration of uncertainty when performing model rankings. The methodology presented in this paper will not only allow users to evaluate competing V_{S30} models and select the model best suited for their application, but they can do so with confidence that their results account for uncertainty information that would otherwise be a potential cause for concern or reason to mistrust their results. Although the results presented herein are impactful, there are also many ways in which the analysis could be improved.

The benchmark database was compiled from publicly available sources, and there is definite overlap between the benchmark database and the databases used to verify each

model. This overlap can cause a candidate model to appear to demonstrate better performance than it would otherwise because it has been partially calibrated to the benchmark data. The uncertainty quantification for the benchmark data were performed with a considerable degree of judgement exercised in the interpretation and uncertainty selection. Therefore, one clear opportunity for improvement would be to construct a high quality database of independent measurements and evaluate the model performance against that data. Furthermore, additional studies targeting the uncertainty associated with V_{S30} measurement techniques would significantly improve the veracity of the results.

As stated earlier in the text, the model uncertainty was not quantified individually, and an assumption of uniform COV for each model was used to avoid biased results. The results from this report could be enhanced by quantification of the uncertainty associated with each model's predictions. Moss (2008) provides a method for determining the uncertainty for geology-based methods, and a similar relationship for topography and hybrid models would allow for further evaluation of relative performance.

This text can be considered a follow-up to the Brownlow et al. (2017) study, and is intended to illustrate an enhancement to the methodology presented therein. It is important for users to understand the limitations of Bayesian model ranking to avoid over-reliance on the results. As clearly demonstrated in this paper, although the results of Brownlow et al. (2017) are generally good, the analysis presented in this paper illustrates that the results are still imperfect. However, due to the ease of use of the Brownlow et al. (2017) method and its viability for implementation in spreadsheet software, it remains an attractive option for engineers and decision makers who rely on proxy-based V_{S30} models.

CHAPTER 6

PROBABILISTIC LIQUEFACTION HAZARD QUANTIFICATION, WITH HAZARD INFORMATION INFORMED BY THE UPDATED V_{S30} SITE CONDITION DATABASE

6.1 INTRODUCTION

Liquefaction is a devastating phenomenon that can result in massive damages to infrastructure and potentially lead to loss of life. Liquefaction is a result of a sudden applied stress to saturated, granular soils, causing pore pressures in the soil to increase, and resulting in suspension of the soil particles in the pore water and loss of strength and stiffness. When liquefaction occurs, soils tend to temporarily exhibit liquid-like behavior and have been observed to lose bearing capacity, flow down shallow gradients, and rise to the surface. Liquefaction-induced damages include settlement, lateral spreading, and sand boils, which each pose their own unique challenges for prediction and quantification.

Multiple, separate methods for liquefaction hazard potential evaluation exist. These methods tend to be based on one of several in situ geotechnical subsurface investigations which can be used to evaluate soil properties. The most commonly used methods are standard penetration test-based (SPT) (e.g. Idriss and Boulanger, 2010), cone penetration test-based (CPT) (e.g. Robertson and Wride 1998), and shear wave velocity-based (e.g. Andrus and Stokoe 2000) methods.

This chapter will focus on CPT-based liquefaction hazard quantification, and will utilize the USGS CPT-measurement database for the computation of cyclic resistance. Cyclic loading data will be obtained from the USGS hazard tools, and this hazard data will be informed by the new synthetic site database developed in Chapter 3, which will in turn affect the predicted seismic loading. This section utilizes the procedure by Juang et al. (2008) to construct a joint probability distribution of $a_{\max}$ and M_w, both of which are derived from the hazard tool data. Furthermore, to automate the process of liquefaction hazard quantification, a MATLAB script was developed to automatically perform numerous liquefaction hazard quantification computations for multiple locations while requiring only minimal inputs.

6.2 METHODOLOGY

The CPT is a method commonly used by geotechnical engineers to evaluate the properties of soils below the ground surface. CPT testing is an invasive technique that involves pushing a cone into the ground and recording the forces, specifically the sleeve friction and tip resistance, that act upon it. (e.g. Schmertmann 1978, Robertson 1990). The USGS provides a digital database of CPT soundings for the continental United States online (https://earthquake.usgs.gov/research/cpt/data/). This data tends to be concentrated in areas of higher earthquake hazard, though that is not always the case. Figure 6.1 shows a map of the United States, including the general location and number of CPT data soundings for the continental US.

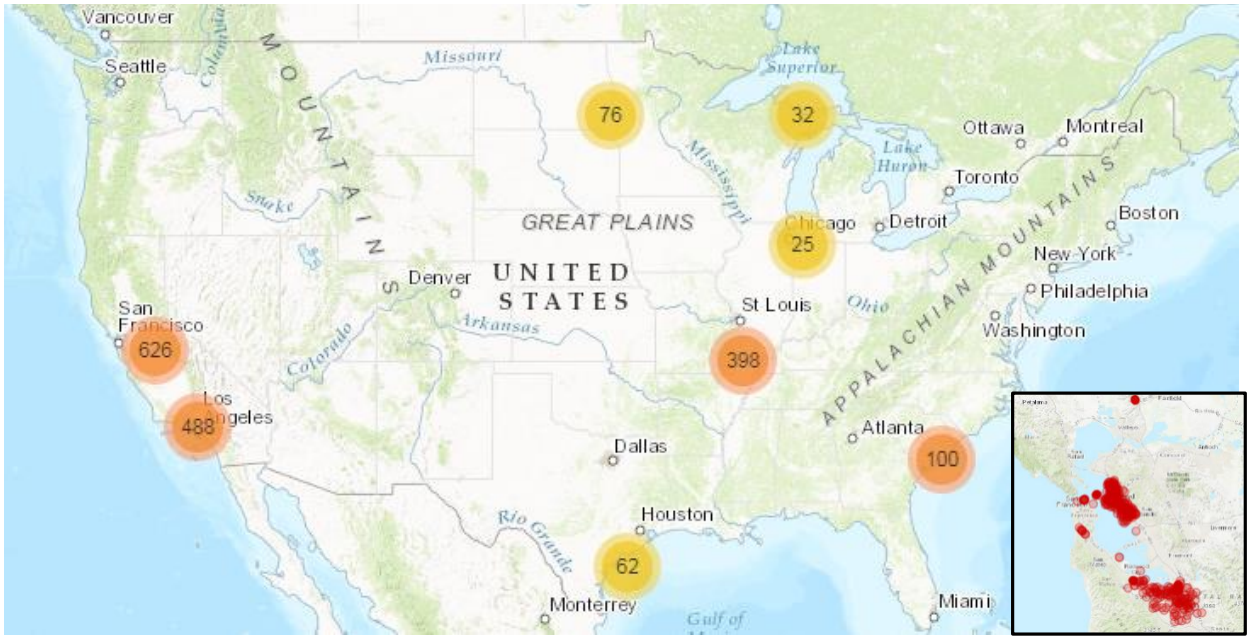

Figure 6.1: Screenshot showing approximate locations of the soundings available in the USGS CPT database. The inset shows the measurement concentration in the San Francisco Bay Area, with approximately 250 located in the center of the Bay area inset and another 180 in the south Bay area.

It can be seen in Figure 6.1 that a significant number of CPT soundings are available in California, with concentrations in the San Francisco Bay area and Los Angeles area. As shown in the inset, over 400 of the CPT soundings shown in Figure 6.1 are in the immediate Bay area.

When determining the potential for a soil to liquefy, a factor to describe the resistance of the soil to cyclic loading, or the cyclic resistance ratio (CRR), is compared to a factor describing the hypothetical cyclic loading that the soil will experience, i.e., the cyclic stress ratio (CSR). The factor of safety to resist liquefaction can be defined as (e.g. Robertson 2009*a*):

$$FS = \frac{CRR}{CSR} \tag{6.1}$$

A factor of safety of less than 1.0 is considered to be likely to liquefy, and a value greater than 1.2 is considered less likely, but still possible to experience liquefaction (Sonmez, 2003). It is important to note that these values for the factor of safety are not absolute; there is still a chance for liquefaction to occur when FS exceeds 1.2, and there is no guarantee that liquefaction will occur if FS is below 1.0.

The CRR is used to quantify the liquefaction resistance of a soil. The CPT-based CRR calculation used in this methodology was developed by Robertson and Wride (1998), and can be approximated with the following equation:

$$CRR = \begin{cases} 0.833\left[\dfrac{(q_{c1N})_{cs}}{1000}\right] + 0.05; \text{ if } (q_{c1N})_{cs} < 50 \\ 93\left[\dfrac{(q_{c1N})_{cs}}{1000}\right]^3 + 0.08; \text{ if } 50 \le (q_{c1N})_{cs} < 160 \end{cases} \tag{6.2}$$

where $(q_{c1N})_{cs}$ is the clean-sand equivalent normalized cone penetration tip resistance. The details of calculating $(q_{c1N})_{cs}$ can be found in the Youd et al. (2001) report.

The CSR represents the expected cyclic loading on a soil. It is a function of both the properties of the expected hazard and the properties of the soil. (Youd et al., 2001)

$$CSR = \left(\frac{\tau_{av}}{\sigma'_{vo}}\right) = 0.65\left(\frac{a_{\max}}{g}\right)\left(\frac{\sigma_{vo}}{\sigma'_{vo}}\right) r_d \left(\frac{1}{MSF}\right)\left(\frac{1}{K_\sigma}\right) \tag{6.3}$$

where a_{max} is the peak horizontal acceleration at the ground surface generated by the earthquake; g is the acceleration of gravity; σ_{vo} and σ'_{vo} are total and overburden stresses, respectively.

The variable r_d is the stress reduction coefficient, defined below (z is the depth in meters):

$$r_d = \frac{1.000 - 0.4113z^{0.5} 0.04052z + 0.001753z^{1.5}}{1.000 - 0.4177z^{0.5} + 0.05729z - 0.006205z^{1.5} + 0.001210z^2} \tag{6.4}$$

MSF refers to the magnitude scaling factor. The MSF value is used to normalize the intensity of the chosen design earthquake to a value that can be used with the CSR equation, which was developed for M_w 7.5 events. The MSF can be calculated as follows:

$$MSF = \frac{10^{2.24}}{M_w^{2.56}} \tag{6.5}$$

Finally, K_σ is a correction factor developed by Hynes and Olsen (1999) to account for the nonlinear effect of overburden pressure:

$$K_\sigma = \left(\frac{\sigma'_{vo}}{P_a} \right)^{(f-1)} \tag{6.6}$$

where P_a is the atmospheric pressure, and f is an exponent used to reflect site conditions. Youd et al. (2001) recommend that the exponent f be given a value of 0.7 to 0.8 for relative densities between 40 and 60%, and a value of 0.6 to 0.7 for relative densities between 60 and 80%.

6.3 LIQUEFACTION HAZARD QUANTIFICATION

To express the liquefaction hazard in the San Francisco Bay area study locations, modified forms of the liquefaction-induced settlement and the liquefaction potential index (LPI) were calculated. These two parameters were chosen because they represent different forms of quantification. The LPI is an averaged value that combines the liquefaction effects

of the top 20 meters beneath the ground surface into a single index value, while the liquefaction-induced settlement attempts to quantify the amount of settlement to be expected. The expected LPI and the expected settlement, were used in this study, and will be presented after the initial formulations for the LPI and liquefaction-induced settlement have been introduced.

6.4 LIQUEFACTION POTENTIAL INDEX

Liquefaction Potential Index (LPI) is an index that was developed by Iwasaki et al (1979, 1982) to provide a simple evaluation of the properties of the top 20 meters of soil and the potential that, given a seismic event, liquefaction induced site effects might occur. The index utilizes soil layer and FS information as its inputs as follows:

$$LPI = \int_0^{20} \left[\omega(z) \cdot F_L \right] dz \tag{6.7}$$

where z is the soil depth in meters, F_L is related to the factor of safety against liquefaction (FS) that was discussed previously as follows (Sonmez 2003):

$$F_L = \begin{cases} 0, & \text{if } FS \geq 1.2 \\ 1 - FS & \text{if } FS < 0.95 \\ 2 \times 10^6 e^{-18.427 FS} & \text{if } 0.95 \leq FS < 1.2 \end{cases} \tag{6.8}$$

The stepwise function used to calculate F_L is used to give some weight to liquefaction cases that are near 1.0, where liquefaction is possible but unlikely. More information is available in Sonmez (2003) and this relationship is represented in Figure 1 of that study.

The term ω(z) is a depth weighting factor, defined as:

$$\omega(z) = 10 - 0.5z \tag{6.9}$$

This weighting factor is included to account for the decreasing effect of liquefaction that occurs with depth. In other words, even if liquefaction does occur in a deep soil, as the depth of the liquefied layer below the ground surface increases, the chance of surface manifestation of that liquefaction decreases. Therefore, the value of $\omega(z)$ decreases with increasing depth to a value of zero when the depth reaches 20 meters.

The LPI can be used to classify the severity of liquefaction that can be expected, with higher values of LPI corresponding to greater degrees of severity.

Table 6.1: Liquefaction Potential Index and corresponding severity class (after Iwasaki 1982)

Liquefaction potential index (LPI)	Severity class of liquefaction
LPI = 0	I: Non-liquefiable
0 < LPI ≤ 2	II: Low
2 < LPI ≤ 5	III: Moderate
5 < LPI ≤ 15	IV: High
LPI > 15	V: Very high

6.5 LIQUEFACTION-INDUCED SETTLEMENT

The liquefaction-induced settlement is calculated using Equation (6.10) (Juang et al. 2013):

$$S = \sum_{i=1}^{N} \varepsilon_{vi} \Delta z_i IND_i \tag{6.10}$$

where S is the predicted liquefaction-induced settlement on level ground, Δz_i is the thickness of the ith layer, ε_{vi} is the volumetric strain of the ith layer, and IND_i is an indicator—possessing a value of either 0 or 1 to represent non-liquefied or liquefied, respectively—of whether the layer will liquefy. The utilization of the IND_i term in the formulation is used so that only the contribution of liquefied layers will be included in the

final calculated predicted settlement. The term for the volumetric strain, ε_{vi}, can be calculated using:

$$\varepsilon_v(\%) = \begin{cases} 0 & \text{if } FS \geq 2 \\ \min\left\{ \dfrac{a_0 + a_1 \ln(q)}{0.5(2-FS) - \left[a_2 + a_3 \ln(q)\right]}, b_0 + b_1 \ln(q) + b_2 \ln(q)^2 \right\} & \text{if } 2 - \dfrac{1}{a_2 + a_3 \ln(q)} < FS < 2 \\ b_0 + b_1 \ln(q) + b_2 \ln(q)^2 & \text{if } FS \leq 2 - \dfrac{1}{a_2 + a_3 \ln(q)} \end{cases} \tag{6.11}$$

where a_0, a_1, a_2, a_3, b_0, b_1, and b_2 are curve fitting parameters available in Juang et al. (2013).

6.6 EXPECTED LPI AND EXPECTED SETTLEMENT

The expected value of a parameter can be considered to be the most likely value that the parameter can be expected to assume when the probability of possible values is considered. The expected value can be expressed generally as (Ross, 2007):

$$E(x) = \sum_{i=1}^{n} x_i \cdot P(x_i) \tag{6.12}$$

where x_i is the value of the variable under investigation, and $P(x_i)$ is the probability that x has the value x_i. Juang et al. (2008) apply this concept to obtain the total probability of liquefaction in a given exposure time. The hazard terms a_{max} and M_w will be discussed below.

$$P_{LT} = \sum_{\text{All pairs of } (a_{\max}, M_w)} \left\{ P\left[L \,|\, (a_{\max}, M_w) \right] \cdot P(a_{\max}, M_w) \right\} \tag{6.13}$$

where $P[L|(a_{max}, M_w)]$ is the conditional probability of liquefaction given a pair of a_{max} and M_w and $P(a_{max}, M_w)$ is the joint probability of a_{max} and M_w. This relationship can be

considered as the expected probability of liquefaction for an event, and the framework can be applied to calculations using LPI and liquefaction-induced settlement.

The expected value concept can be applied to the LPI and settlement calculations as well.

$$LPI_E = \sum LPI \cdot P(LPI) \tag{6.14}$$

$$S_E = \sum S \cdot P(S) \tag{6.15}$$

where LPI_E and S_E are the expected LPI and expected settlement, respectively, in a given exposure time. Applying the same rationale used to develop Equation (6.13), the above equations can be rewritten as:

$$LPI_E = \sum_{\text{All pairs of } (a_{\max}, M_w)} \left\{ E\left[LPI \,|\, (a_{\max}, M_w) \right] \cdot P(a_{\max}, M_w) \right\} \tag{6.16}$$

$$S_E = \sum_{\text{All pairs of } (a_{\max}, M_w)} \left\{ E\left[S \,|\, (a_{\max}, M_w) \right] \cdot P(a_{\max}, M_w) \right\} \tag{6.17}$$

where $E[LPI|(a_{max}, M_w)]$ is the conditional expected value of LPI given a pair of a_{max} and M_w, and $E[S|(a_{max}, M_w)]$ is the conditional expected settlement given a pair of a_{max} and M_w. In other words, these two equations are expressing that a pair of a_{max} and M_w will produce a value of LPI and settlement, and by multiplying the LPI or settlement by its probability of occurrence and taking the summation for all pairs of a_{max} and M_w, the total expected value for LPI and liquefaction-induced settlement can be calculated.

6.7 HAZARD DATA AND JOINT DISTRIBUTION OF A_{MAX} AND M_W

Two sources of hazard data were used during this study, and the procedure for development of the joint probability distribution of a_{max} and M_w from those sources is available in Juang et al. (2008). That procedure is summarized in Figure 6.2.

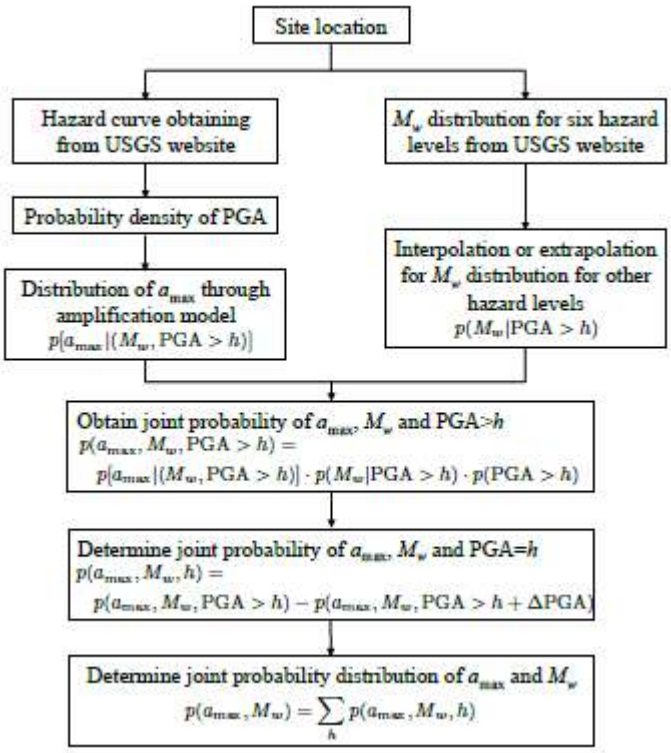

Figure 6.2: Flowchart for calculating the joint probability distribution of a_{max} and M_w

When this study was initially performed, the hazard data were obtained from the USGS deaggregation tool and the USGS hazard tool. The split in the flowchart in Figure 6.2 corresponds to obtaining data from the two tools mentioned previously. At the time of writing, the USGS has decommissioned the two tools mentioned previously and replaced them with the updated tool named the Unified Hazard Tool (UHT) (https://earthquake.usgs.gov/hazards/interactive/), from which both the hazard curves and deaggregation curve data can be obtained.

The hazard data obtained from the UHT and its manipulation are where the new synthetic V_{S30} database from Chapter 3 manifests in the liquefaction calculation. The deaggregation data requires the NEHRP site class as an input, which is based on V_{S30}. The percent contribution of the various seismic sources in the deaggregation tool are adjusted based on the site class that is assigned to the study site. The hazard curve is downloaded for the B/C boundary condition of 760 m/s, and is used to derive a_{max}. The value of a_{max} is adjusted based on NEHRP recommended site amplification factors (e.g. FEMA 2015) that can be applied to the peak ground acceleration (PGA) from the hazard curve with the following relationship:

$$a_{\max} = F_s \cdot PGA \tag{6.18}$$

where F_s is the site amplification factor for short period (0.2s) motion and PGA is the peak ground acceleration for the B/C soft rock boundary condition. The site amplification factor is obtained from the NEHRP provisions (e.g. FEMA 2015) or appropriate building codes. From this discussion it is clear that in the current state of practice, updated V_{S30} values obtained from Chapter 3 will only impact liquefaction-based calculations if there is a change in the NEHRP site classes between an old model and the current database.

6.8 IMPLEMENTATION OF MATLAB CODE

The MATLAB code, while still preliminary in some ways, was designed to be very easy for an end-user to use. Currently, the necessary inputs include CPT data (in a .txt file format downloaded from the USGS website), soil data, water table data (currently obtained from CPT-sounding files), and V_{S30} data. An important point to note is that the current state of the MATLAB code will perform the liquefaction hazard quantification calculations

automatically for any number of CPT data files in .txt format that are provided to the program.

The strength of the developed code lies in its ability to rapidly, automatically perform the liquefaction hazard quantification calculations by repeating the requisite liquefaction hazard quantification calculations for every CPT-data file that is provided as an input, collecting new hazard data based on the location provided in the CPT data file and the corresponding V_{S30} value from the provided database. However, this strength can also be a weakness due to the need to currently provide soil data to the program. If a user provides CPT-profiles for analysis that possess soil properties that are different from those entered into the code, the program will currently still provide a set of liquefaction hazard quantification results, though the results will be for incorrect soil data.

Based on the above discussion of the code in its current form, an obvious potential improvement would be to automate the assigning of soil data based on location. An option for this would be to use the geology information provided by the Wills et al. (2015) model to automatically assign soil data based on the average properties of the mapped geologic unit. This would be implemented by using the location information from the CPT data file to identify the mapped geology and assigning soil data based on the results of that location check.

6.9 RESULTS

Two locations were selected for a demonstration of the MATLAB code that was developed for automatic calculation of the expected settlement and expected LPI for a given exposure time. Additionally, settlement exceedance curves (e.g. Juang et al. 2008)

were created for the two study locations. The exceedance curves give the probability that the settlement that will be experienced at the site is greater than a certain threshold value in the given exposure time. For this study, an exposure time of 50 years was used.

The study locations can be seen in Figure 6.3. They are located on Alameda Island, on the east side of the San Francisco Bay. These study locations correspond to the locations of CPT-sounding data from the USGS CPT-database. These locations were chosen arbitrarily from among the available CPT profiles.

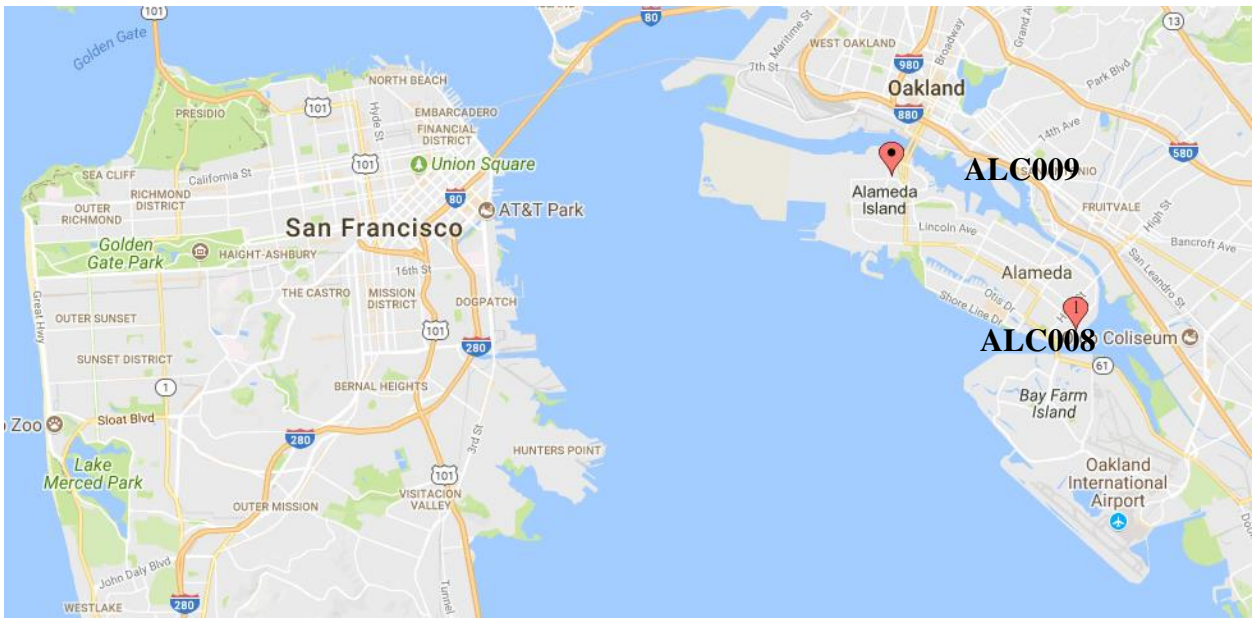

Figure 6.3: Study locations in the San Francisco Bay. ALC008 denoted by pin with "1" and ALC009 denoted by pin with a dot

Using the hazard data from the USGS tools, a joint distribution of a_{max} and M_w was prepared. The joint distribution is illustrated in Figure 6.4.

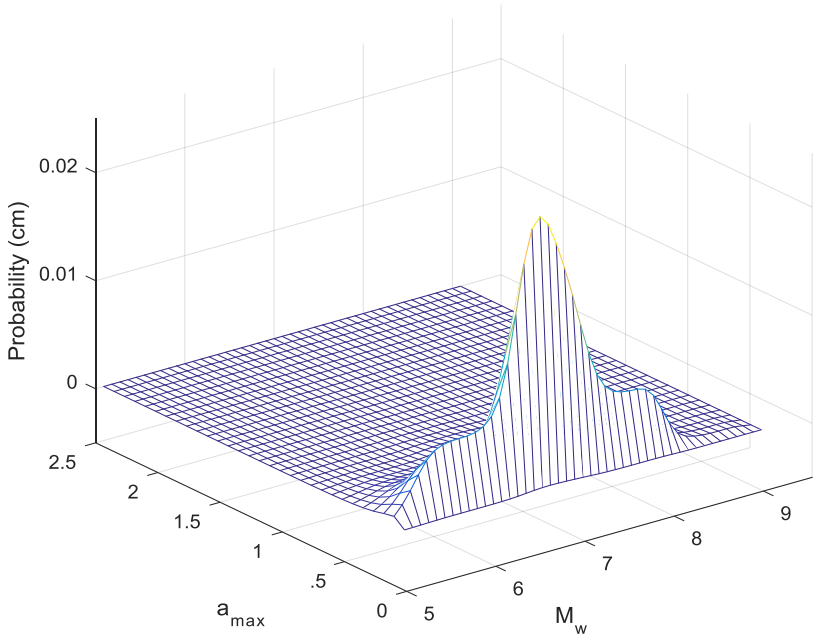

Figure 6.4: Joint distribution of amax and Mw for one site

From Equations (6.16) and (6.17), it can be seen that $E[LPI|(a_{max}, M_w)]$ and $E[S|(a_{max}, M_w)]$, respectively, are also needed. Therefore, the LPI and liquefaction-induced settlement for each pair of a_{max} and M_w was calculated as well. The results of the settlement calculation for ALC009 are shown in Figure 6.5.

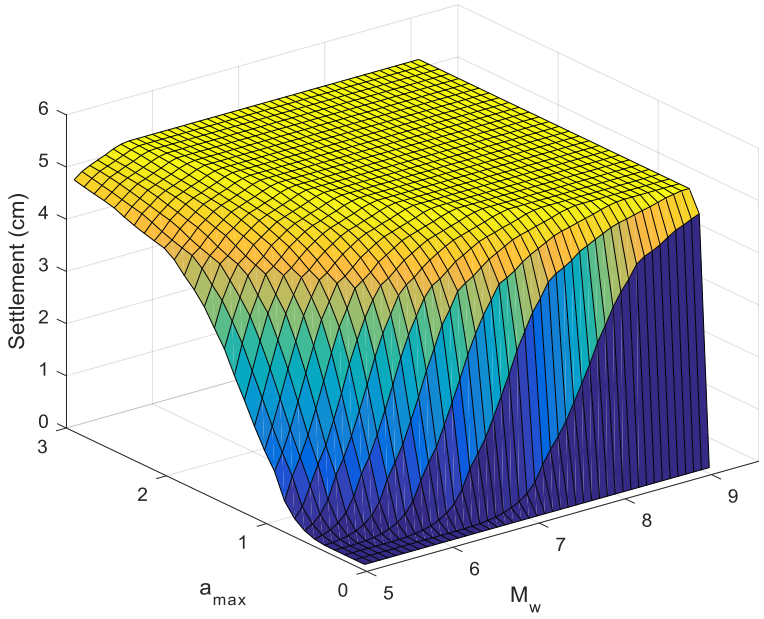

Figure 6.5: Calculated liquefaction-induced settlement for each pair of amax and Mw for ALC009

By combining the joint probability and conditional expected value calculations using Equations (6.16) and (6.17), values for the expected LPI and expected liquefaction-induced settlement for a 50 year exposure time were obtained. The results of those calculations can be seen in **Error! Reference source not found.**.

Table 6.2 Results of Expected Liquefaction Hazard Calculation

Location	Expected LPI	Expected Settlement (cm)
ALC008	4.1	5.4
ALC009	0.8	1.3

Finally, curves that illustrate the probability of exceedance for settlement threshold values for the 50 year exposure time are shown in Figure 6.6.

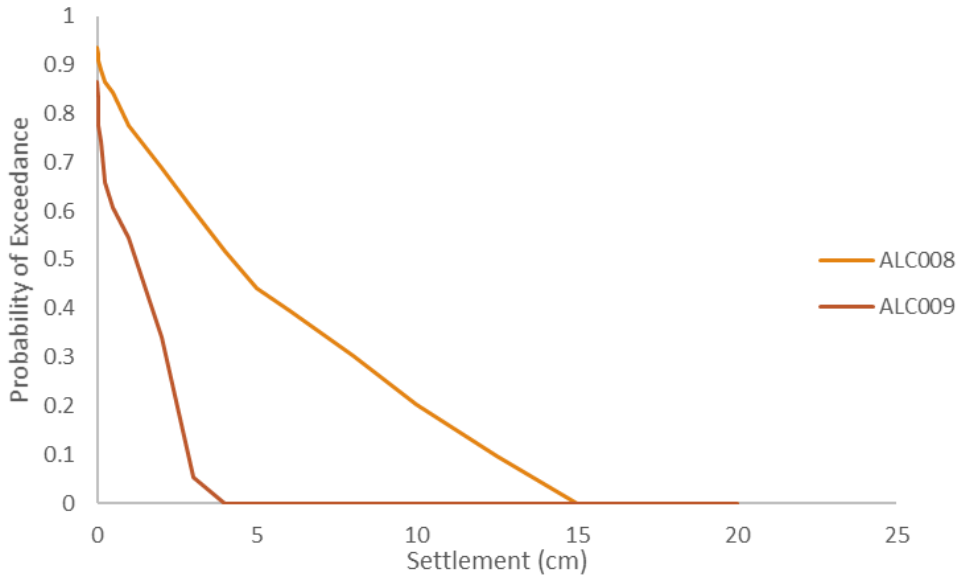

Figure 6.6: Exceedance probability curve for liquefaction-induced settlement with 50 year exposure time

It can be seen in both **Error! Reference source not found.** and Figure 6.6 that ALC008 h as a higher liquefaction risk than ALC009. It can also be seen that some degree of seismically-induced liquefaction can be expected at both locations with near certainty.

6.10 CONCLUSIONS

In this chapter, a liquefaction hazard quantification calculation was performed for two sites in Alameda, CA. The new synthetic V_{S30} site condition database, developed in Chapter 3, was used to inform the hazard data that were obtained from the USGS hazard tools. The locations and necessary soil testing data were obtained using CPT measurement files provided on the USGS CPT measurement website. Calculations were performed using MATLAB code that was developed for the purpose of automating the liquefaction hazard quantification process. The MATLAB code automatically contacts the USGS hazard tools to download the appropriate hazard data as well as performing the calculations, and is a

first step towards large-scale evaluation of CPT data for the purpose of liquefaction hazard quantification.

A finalized version of this MATLAB code will allow future researchers to easily specify the appropriate liquefaction hazard calculations they are interested in and potentially use the computed results to investigate spatial relationships between liquefaction hazards and other spatial data. An iteration of this code is available in Appendix B. Improvements to the current procedure could include incorporating other forms of soil measurement data to increase the number of locations available for liquefaction hazard quantification, creating an automatic decision-making process for the code to automatically assign appropriate soil data based on known geology, and incorporating an independent groundwater database instead of relying on CPT data to determine water table levels.

CHAPTER 7

CONCLUSIONS AND FUTURE WORK

This dissertation has presented a Bayesian method for ranking V_{S30} models, both with (Chapter 5) and without (Chapter 3) uncertainty considerations. The formulation that does not include uncertainty can easily be implemented using common spreadsheet software that includes basic statistical functions and a solver. This practical functionality makes the method ideal for utilization by engineers and persons with little training in statistical methods.

IN CHAPTER 3:

The method was shown to be effective at ranking competing V_{S30} models, and that it has the added functionality of evaluating V_{S30} models for performance within individual geologic units when sufficient information is available. The methodology was applied to data from California to rank three publicly available proxy-based models. Using the results of that analysis, a new, state of the art site conditions map for California was developed that contains V_{S30} predictions and spatial coordinate data.

IN CHAPTER 4:

The methodology that was developed in Chapter 3 was applied to two other regions in the United States: Seattle and the Puget Sound and the Salt Lake City, Ogden, and Provo area. Ranking results were obtained for the models available in those regions, and new site conditions databases are proposed for those regions as well. Furthermore, the utility and limitations of the model ranking procedure was illustrated as well. It was demonstrated that

the model ranking framework is an effective means to make informed decisions when selecting V_{S30} models, but that in some situations, there is only a small deviation from a candidate model's originally predicted values.

IN CHAPTER 5:

The Bayesian method for model ranking was revisited to add uncertainty information to the calculation. The uncertainty in the benchmark database was characterized using currently available information based on the methods used to obtain the V_{S30} values. The V_{S30} models were studied for their sensitivity to fluctuations in uncertainty estimates. It was shown that including uncertainty information in the calculation will affect the model ranking results. Furthermore, it was shown that proper characterization of uncertainty for the V_{S30} models is crucial, as their performance can be significantly affected by the uncertainty assigned.

IN CHAPTER 6:

A demonstration of a potential application of the new synthetic V_{S30} site condition database was performed. A liquefaction hazard quantification calculation was performed using a MATLAB script to automatically read CPT data files and use them appropriately. The new V_{S30} database was used to inform the hazard data that were obtained from the USGS hazard tools. Calculations of expected LPI and expected settlement were presented as well as curves representing the probability of exceedance for settlement threshold values.

DISCUSSIONS AND FUTURE WORK

Although the results presented herein represent an update to the current state of the art in proxy-based spatial V_{S30} prediction, further improvements to the research are possible. Because the new site conditions maps presented in Chapters 3 and 4 are derived from proxy-based models, the results are only as good as the best models. Therefore, it is easy to see that the results from Chapter 3 can be improved through improvement of the candidate models. Caution should be taken when using the methodology presented herein due to that inherent limitation; the method does not evaluate how well a given model performs, merely how well the candidate models perform relative to one-another.

The benchmark database is always a point of interest for users when performing model verification studies. Improvements to the benchmark database, in accuracy of measurement data, quantification of uncertainties, and/or expanded coverage of geologic units would lead to improved confidence in the results from this study. Improving the accuracy of the data in the benchmark database would lead to more robust model ranking results, as presented in Chapters 3 and 4. Improving the uncertainty quantification of the benchmark data would lead to better results if the method from Chapter 5 is used; potentially allowing for development of a new site condition database if the degree of confidence in the uncertainty quantification is high. Expanded coverage of geologic unit benchmark data would result in better results in Chapters 3, 4, and 5 due to the heightened confidence that can be placed on the ranking results. Additionally, improvements in the coverage of benchmark data would allow researchers to develop better V_{S30} models, which can then be

used to develop a new site condition database through implementation of the method in this dissertation.

Thus, the full strength of the Bayesian method for ranking V_{S30} models is demonstrated. Not only has the method been applied to ranking and synthesizing the current state-of-the-art models for proxy-based V_{S30} estimation, but it has continued application as a means to evaluate new models and to update the current site condition database appropriately.

REFERENCES

Aboye, S.A., Andrus, R.D., Ravichandran, N., Bhuiyan, A.H. and Harman, N., 2015. Seismic site factors and design response spectra based on conditions in Charleston, South Carolina. *Earthquake Spectra*, **31**(2), 723-744.

Allen, T. I., and Wald, D. J., 2009. On the use of high-resolution topographic data as a proxy for seismic site conditions (V_{S30}). *Bulletin of the Seismological Society of America* **99**, 935-943.

Ancheta, T. D., Darragh, R. B., Stewart, J. P., Seyhan, E., Silva, W. J., Chiou, B. S. J., Wooddell, K. E., Graves, R. W., Kottke, A. R., Boore, D. M., Kishida, T., and Donahue, J. L., 2013. *PEER NGA-West2 Database*, *PEER Report 2013/03*, Pacific Earthquake Engineering Research Center.

Andrus, R. D.; and Stokoe, K. H., II, 2000. Liquefaction resistance of soils from shear-wave velocity. *Journal of Geotechnical and Geoenvironmental Engineering* **126**(11), 1015-1025.

Andrus, R. D., Mohanan, N. P., Piratheepan, P., Ellis, B. S., and Holzer, T. L., 2007. Predicting shear-wave velocity from cone penetration resistance. In *Proceedings of the 4th International Conference on Earthquake Geotechnical Engineering, Thessaloniki, Greece*, paper no. 1454.

Ang, A. H-S. and Tang, W. H., 2007. *Probability Concepts in Engineering: Emphasis on Applications in Civil & Environmental Engineering*. John Wiley & Sons, Inc. New York, NY.

ASCE. 2010. *Minimum Design Loads for Buildings and Other Structures*. ASCE/SEI Standard 7-10.

Barnett, V., 1999. *Comparative statistical inference* (Vol. 522). John Wiley & Sons.

Boore, D. M.; Joyner, W. B., and Fumal, T. E., 1993. Estimation of response spectra and peak acceleration from western North America earthquakes: an interim report, *USGS Open-file Report*, 93-509, 72 p.

Boore, D. M.; Joyner, W. B., and Fumal, T. E., 1994. Estimation of response spectra and peak acceleration from western North America earthquakes: an interim report, Part 2, *USGS Open-file Report*, 94-127, 40 p.

Boore, D.M. and Atkinson, G.M., 2008. Ground-motion prediction equations for the average horizontal component of PGA, PGV, and 5%-damped PSA at spectral periods between 0.01 s and 10.0 s. *Earthquake Spectra*, **24**(1), 99-138.

Boore, D. M., Thompson, E. M., and Cadet, H., 2011. Regional correlation of V_{S30} and velocities averaged over depths less than and greater than 30 meters. *Bulletin of the Seismological Society of America* **101**(6), 3046-3059.

Borcherdt, R. D., 1994. Estimates of Site-dependent response spectra for design (methodology and justification). *Earthquake Spectra* **10**(4), 617-653.

Brownlow, A. W.; Chen, Q., Khoshnevisan, S., Shahjouei, A., Javanbarg, J., and Zhang, J., Juang, C. H., 2017. Probabilistic methods for evaluating V_{S30} models - focusing on the California database, *Earthquake Spectra*, Under Review.

Buckland, S. T., Burnham, K. P., and Augustin, N. H., 1997. Model selection: an integral part of inference. *Biometrics* **53**, 603-618.

Burnham, K. P. and Anderson, D. R., 2004. Multimodal inference: Understanding AIC and BIC in model selection. *Sociological Methods and Research* **33**, 261-304.

Cam, L.L. 1990. Maximum Likelihood: An Introduction. *International Statistical Review*, **58**(2) 153-171.

Carlin, B. P. and Louis, T. A., 2009. *Bayesian Methods for Data Analysis,* 3rd edition. Chapman & Hall/CRC Press. Boca Raton, FL.

Castellaro, S., Mulargia, F. and Rossi, P.L., 2008. VS30: Proxy for seismic amplification?. *Seismological Research Letters*, **79**(4), 540-543.

Chen, Q., Wang, C., and Juang, C. H., 2016*a*. CPT-based evaluation of liquefaction potential accounting for soil spatial variability at multiple scales. *Journal of Geotechnical and Geoenvironmental Engineering* **142**, 04015077.

Chen, Q., Wang, C., and Juang, C. H., 2016*b*. Probabilistic and spatial assessment of liquefaction-induced settlements through multiscale random field models. *Engineering Geology* **211**, 135-149.

Cheng, R.C.H., and Traylor, L. 1995. Non-regular maximum likelihood problems. *Journal of the Royal Statistical Society*, Series B, **57**(1), 3-44.

Douglas, J., 2011. Ground motion prediction equations, 1964-2010. Berkeley, CA: *Pacific Earthquake Engineering Research Center*. 444 p.

Farr, T.G. and Kobrick, M., 2000. Shuttle Radar Topography Mission produces a wealth of data. *Eos, Transactions American Geophysical Union*, **81**(48), 583-585.

Farr, T.G., Rosen, P.A., Caro, E., Crippen, R., Duren, R., Hensley, S., Kobrick, M., Paller, M., Rodriguez, E., Roth, L. and Seal, D., 2007. The shuttle radar topography mission. *Reviews of geophysics*, **45**(2). 3p.

FEMA, 2015. *NEHRP recommended seismic provisions for new buildings and other structures Volume I*, FEMA P-1050-1/2015 Edition.

Fumal, T. E. and Tinsley, J. C., 1985. Mapping shear-wave velocities in near-surface geological materials, in *Evaluating Earthquake Hazards in the Los Angeles Region—An Earthquake Perspective*, J. I. Ziony (Editor), *U.S. Geological Survey* Professional Paper 1360, 127-150.

Gentle, J.E., 2002. *Elements of Computational Statistics*, Springer-Verlag, New York.

Gilbert, G.K., 1907. *The San Francisco earthquake and fire of April 18, 1906, and their effects on structures and structural materials* (No. 324). US Government Printing Office.

Givens, G. and Hoeting, J., 2005. *Computational Statistics*. Springer-Verlag, New York.

Gregor, N., Abrahamson, N.A., Atkinson, G.M., Boore, D.M., Bozorgnia, Y., Campbell, K.W., Chiou, B.S.J., Idriss, I.M., Kamai, R., Seyhan, E. and Silva, W., 2014. Comparison of NGA-West2 GMPEs. *Earthquake Spectra*, **30**(3), 1179-1197.

Haldar, A. and Mahadevan, S., 2000. *Probability, Reliability, and Statistical Methods in Engineering Design*. John Wiley & Sons Inc. New York.

Hynes, M. E. and Olsen, R. S., 1999. Influence of confining stress on liquefaction resistance. *Proceedings of the International Workshop on Physics and Mechanics of Soil Liquefaction*, Balkema, Rotterdam, Netherlands, 145-152

Idriss, I.M. and Boulanger, R.W., 2010. SPT-based liquefaction triggering procedures. *Rep. UCD/CGM-10*, *2*.

Iwasaki, T., Tatsuoka, F., Tokida, K., and Yasuda, S., 1978. A practical method for assessing soil liquefaction potential based on case studies at various sites in Japan. *Proceedings 2nd International Conference on Microzonation*, pages 885–896.

Iwasaki, T., Tokida, K., Tatsuoka, F., Watanabe, S., Yasuda, S., and Sato, H. 1982 Microzonation for soil liquefaction potential using simplified methods. *Proceedings of the 3rd International Conference on Microzonation*, Seattle, 3:1310–1330,

Joyner, W. B., Warrick, R. E., and Fumal, T. E., 1981. The effect of Quaternary alluvim on strong ground motion in the Coyote Laoke, California, earthquake of 1979. *Bulletin of the Seismological Society of America* **71**, 1333–1350.

Juang, C. H., Khoshnevisan, S., and Zhang, J., 2015. Maximum likelihood principle and its application in soil liquefaction assessment. In *Risk and Reliability in Geotechnical Engineering*, K.K. Phoon and J. Ching, ed., CRC Press. New York, NY, 181-200.

Juang, C.H., Zhang, J., Khoshnevisan, S., and Gong, W. 2017. Probabilistic methods for assessing soil liquefaction potential and effect. *Proceedings, Georisk 2017*, ASCE, keynote lecture.

Juang, C. H., Li, D. K., Fang, S. Y., Liu, Z., Khor, E. H., 2008. Simplified procedure for developing joint distribution of a_{max} and M_w for probabilistic liquefaction hazard analysis. *Journal of Geotechnical and Geoenvironmental Engineering*, **134**(8):1050-1058.

Juang, C. H., Ching, J., Wang, L., Khoshnevisan, S.; and Ku, C. S., 2013. Simplified procedure for estimation of liquefaction-induced settlement and site-specific probabilistic settlement exceedance curve using cone penetration test (CPT). *Canadian Geotechnical Journal*, **50**(10):1055-1066.

Kayen, R., Moss, R. E. S., Thompson, E. M., Seed, R. B., Cetin, K. O., Der Kiureghian, A., Tanaka, Y., and Tokimatsu, K., 2013. Shear-wave velocity-based probabilistic and deterministic assessment of seismic soil liquefaction potential. *Journal of Geotechnical and Geoenvironmental Engineering* **139**(3), 407-419.

Ku, C.S., Juang, C. H. Chang, C.W., and Ching, J., 2012. Probabilistic version of the Robertson and Wride method for liquefaction evaluation: Development and application. *Canadian Geotechnical Journal*, **49**(1), 27–44.

Lee, V. W., Trifunac, M. D., Todorosvska, M. I., and Novikova, E. I., 1995. Empirical equations describing attenuation of peaks of strong motion, in terms of magnitude, distance, path effects, and site conditions. University of Southern California, Department of Civil Engineering, Los Angeles, CA. Report CE 95-02. 6 p.

Lee, V. W. and Trifunac; M. D., 2010. Should average shear-wave velocity in the top 30 m of soil be used to describe seismic amplification? *Soil Dynamics and Earthquake Engineering* **30**, 1250-1258.

Lee, C. and Tsai, B., 2008. Mapping V_{S30} in Taiwan. *Terrestrial, Atmospheric, and Oceanic Sciences* **19**, 671-82.

Liu, H.P., Boore, D.M., Joyner, W.B., Oppenheimer, D.H., Warrick, R.E., Zhang, W., Hamilton, J.C. and Brown, L.T., 2000. Comparison of phase velocities from array measurements of Rayleigh waves associated with microtremor and results calculated from borehole shear-wave velocity profiles. *Bulletin of the Seismological Society of America*, **90**(3), pp.666-678.

Liu, W., Chen, Q., Wang, C., Juang, C. H., and Chen, G., 2017a. Spatially correlated multiscale V_{S30} mapping and a case study of the Suzhou site. *Engineering Geology*, **220**, 110-122.

Liu, W., Wang, C., Chen, Q., Chen, G., and Juang, C. H., 2017b. Multiscale random field-based shear wave velocity mapping and site classification. In *Proceedings of the Geo-Risk2017 Conference*, Denver, Colorado.

Martin, G. (editor) 1994. Proceedings NCEER, SEAOC, BSSC workshop on site response during earthquakes and seismic code provisions. Univeristy of Southern California, Los Angeles, CA. November 18-20, 1992

Martin, G. and Dobry, R., 1994. Earthquake site response and seismic code provisions. *NCEER Bulletin* **8**, 1-6.

Moss, R. E. S., 2008. Quantifying measurement uncertainty associated with thirty meter shear wave velocity (V_{S30}). *Bulletin of the Seismological Society of America* **98**, 1399-1411.

Mucciarelli, M. and Gallipoli, M.R., 2006. Comparison between Vs30 and other estimates of site amplification in Italy. In *First European Conference on Earthquake Engineering and Seismology*. Geneva, Switzerland.

National Academies of Sciences, Engineering, and Medicine, 2016. *State of the Art and Practice in the Assessment of Earthquake-Induced Soil Liquefaction and Its Consequences*. Washington, DC: The National Academies Press. doi: 1017226/23474.

O'Connell, D.R. and Turner, J.P., 2011. Interferometric multichannel analysis of surface waves (IMASW). *Bulletin of the Seismological Society of America*, **101**(5), 2122-2141.

Odum, J.K., Stephenson, W.J., Williams, R.A. and von Hillebrandt-Andrade, C., 2013. VS30 and Spectral Response from Collocated Shallow, Active-, and Passive-Source VS Data at 27 Sites in Puerto Rico. *Bulletin of the Seismological Society of America*, **103**(5), pp.2709-2728.

Pancha, A., Anderson, J. G., Louie, J. N., & Pullammanappallil, S. K., 2008. Measurement of shallow shear wave velocities at a rock site using the ReMi technique. *Soil Dynamics and Earthquake Engineering*, **28**(7), 522-535.

Park, S. and Elrick, S., 1998. Predictions of shear-wave velocities in southern California using surface geology. *Bulletin of the Seismological Society of America* **88**(3), 677-685.

Parker, G. A., Harmon, J. A., Stewart, J. P., Hashash, Y. M. A., Kottke, A. R., Rathje, E. M., Silva, W. J., and Campbell, K. W., 2017. Proxy-based V_{S30} estimation in central and eastern North America. *Bulletin of the Seismological Society of America* **107**, 1-15.

Petersen, M.D., Moschetti, M.P., Powers, P.M., Mueller, C.S., Haller, K.M., Frankel, A.D., Zeng, Yuehua, Rezaeian, Sanaz, Harmsen, S.C., Boyd, O.S., Field, Ned, Chen, Rui, Rukstales, K.S., Luco, Nico, Wheeler, R.L., Williams, R.A., and Olsen, A.H., 2014. Documentation for the 2014 update of the United States national seismic hazard maps. *U.S. Geological Survey Open-File Report* 2014-1091, 243 p., *https://dx.doi.org/10.3133/ofr20141091*.

Poran, C., Rodriguez-Ordoñez, J., Satoh, T., and Borden, R., 1996. New approach to interpretation of noninvasive surface wave measurements for soil profiling. *Transportation Research Record: Journal of the Transportation Research Board* **1526**, 157-165.

Raftery, A. E., Madigan, D., and Hoeting, J. A., 1997. Bayesian model averaging for linear regression models. *Journal of the American Statistics Association* **92**, 179-191.

Robertson, P. K. and Campanella, R. G., 1985. Liquefaction potential of sands using the CPT. *Journal of Geotechnical Engineering* **111**(3), 384-403.

Robertson, P. K., 1990. Soil classification using CPT. *Canadian Geotechnical Journal*, **27**(1), 151–158.

Robertson, P. K. and Wride, C. E., 1998. Evaluating cyclic liquefaction potential using the cone penetration test. *Canadian Geotechnical Journal*, **35**(3):442–459.

Robertson, P. K., 2009a. Performance based earthquake design using the CPT. *Proceedings IS-Tokyo*, 3–20.

Robertson, P. K., 2009b. Interpretaiton of cone penetration tests—a unified approach. *Canadian Geotechnical Journal* **46**(11), 1337-1355.

Ronold, K.O. and Bjerager, P., 1992. Model uncertainty representation in geotechnical reliability analyses. *Journal of geotechnical engineering*, **118**(3), pp.363-376.

Ross, S.M., 2014. *Introduction to probability models*. Academic press.

Scasserra, G., Stewart, J. P., Kayen, R. E., and Lanzo G., 2009. Database for earthquake strong motion studies in Italy. *Journal of Earthquake Engineering* **13**, 852-881.

Schmertmann, J.H., 1978. *Guidelines for Cone Penetration Test.(Performance and Design)* (No. FHWA-TS-78-209 Final Rpt.).

Schwarz, G., 1978. Estimating the dimension of a model. *The Annals of Statistics* **6**, 461-464.

Seed, H. B. and Idriss, I. M. 1971. Simplified procedure for evaluating soil liquefaction potential. *Journal of the Soil Mechanics and Foundations Division, ASCE* **90**(SM9), 1249-1273.

Seed, H. B., 1979. Soil liquefaction and cyclic mobility evaluation for level ground during earthquakes. *Journal of Geotechnical Engineering Division*. ASCE, **105**(2), 201-255.

Seed, H. B. and Idriss, I. M. 1982. *Ground motions and soil liquefaction during earthquakes.* Earthquake Engineering Research Institute.

Seed, H. B., Tokimatsu, K., Harder, L. F., and Chung, R. M., 1985. Influence of SPT procedures in liquefaction resistance evaluations. *Journal of Geotechnical Engineering* **111**(12), 1425-1445.

Seyhan, E., Stewart, J. P., Ancheta, T. D., Darragh, R. B., and Graves, R. W., 2014. NGA-West2 site database. *Earthquake Spectra* **30**, 1007-1024.

Sonmez, H., 2003. Modification of the liquefaction potential index and liquefaction susceptibility mapping for a liquefaction-prone area (Inegol, Turkey). *Environmental Geology*, **44**(7), pp.862-871.

Stuedlein, A. W., 2010. Shear-wave velocity correlations for Puyallup River alluvium. *Journal of Geotechnical and Geoenvironmental Engineering* **136**, 1298-1304.

Thompson, E. M., Baise, L. G., and Kayen R. E., 2007. Spatial correlation of shear-wave velocity in the San Francisco Bay Area sediments. *Soil Dynamics and Earthquake Engineering* **27**, 144-52.

Thompson, E. M., Wald, D. J., and Worden, C. B., 2014. A V_{S30} map for California with geologic and topographic constraints. *Bulletin of the Seismological Society of America* **104**, 2313-2321.

Tinsley, J. C. and Fumal, T. E., 1985. Mapping quaternary sedimentary deposits for areal variations in shaking response, in *Evaluating Earthquake Hazards in the Los Angeles Region – An Earth Science Perspective*. J. I. Ziony (Editor), *U.S. Geological Survey Professional Paper 1360*, 101-126.

Wald, D. J. and Allen, T. I., 2007. Topographic slope as a proxy for seismic site conditions and amplification. *Bulletin of the Seismological Society of America* **97**, 1379-1395.

Whitman, R. V., 1971. Resistance of soil to liquefaction and settlement. *Soils and Foundations* **11**(4), 59-59.

Wills, C. J., and Silva W., 1998. Shear wave velocity characteristics of geologic units in California. *Earthquake Spectra* **14**, 533-556.

Wills, C.J., Petersen, M., Bryant, W.A., Reichle, M., Saucedo, G.J., Tan, S., Taylor, G. and Treiman, J., 2000. A site-conditions map for California based on geology and shear-wave velocity. *Bulletin of the Seismological Society of America*, **90**(6B), S187-S208.

Wills, C. J., and Clahan, K. B., 2006. Developing a map of geologically defined site-conditions categories for California. *Bulletin of the Seismological Society of America* **96**, 1483-1501.

Wills, C. J., and Gutierrez, C., 2011. Investigation of geographic rules for improving site-conditions mapping. *California Geological Survey Final Technical Report 20* (Award No. 07HQGR0061).

Wills, C. J., Gutierrez, C. I., Perez, F. G., and Branum D. M., 2015. A Next Generation V_{S30} Map for California Based on Geology and Topography. *Bulletin of the Seismological Society of America* **105**, 3083-3091.

Yong, A., Hough, S. E., Iwahashi, J., and Braverman, A., 2012. Terrain-based site conditions map of California with implications for the contiguous United States. *Bulletin of the Seismological Society of America* **102**,114-128.

Yong, A., Thompson, E. M., Wald, D., Knudsen, K. L., Odum, J. K., Stephenson, W. J., and Haefner, S., 2015. Compilation of V_{S30} data for the United States: U.S. Geological Survey Data Series 978.

Youd, T. L., Idriss, I. M., Andrus, R. D., Arango, I., Castro, G., Christian, J., Dobry, R., Finn, D. W. L., Harder Jr, L. F., Hynes, M. E., Ishihara, K., Koester, J., Liao, S., Marcuson, W. I., Martin, G., Mitchell, J., Moriwaki, Y., Power, M., Robertson, P., Seed, R., and Stokoe, K. I., 2001. Liquefaction resistance of soils: summary report from the 1996 NCEER and 1998 NCEER/NSF workshops on evaluation of liquefaction resistance of soils. *Journal of Geotechnical and Geoenvironmental Engineering*, **127**(4):297–313.

Zhang, J., Zhang, L.M. and Tang, W.H., 2009. Bayesian framework for characterizing geotechnical model uncertainty. *Journal of Geotechnical and Geoenvironmental Engineering*, **135**(7), pp.932-940.

Zhang, J., Tang, W.H., Zhang, L.M. and Huang, H.W., 2012. Characterising geotechnical model uncertainty by hybrid Markov Chain Monte Carlo simulation. *Computers and Geotechnics*, **43**, pp.26-36.

Zhang, J., Huang, H. W., Juang, C. H., and Su, W. W., 2014. Geotechnical reliability analysis with limited data: Consideration of model selection uncertainty. *Engineering Geology* **181**, 27-37.

APPENDIX A

This appendix contains sensitivity plots prepared in Chapter 5 for the uncertainty analysis. The sensitivity analysis was conducted for all 15 geologic units that were investigated in the study. The plots show that uncertainty can positively or negatively affect the results of the model ranking, and that the results vary by geologic unit. More investigation is needed to understand the causes for the fluctuations in performance due to uncertainty beyond the explanation provided in Chapter 5.

Although the thresholds are slightly different, it is clear that similar behavior to that which was demonstrated in Chapter 5 is observed here as well.

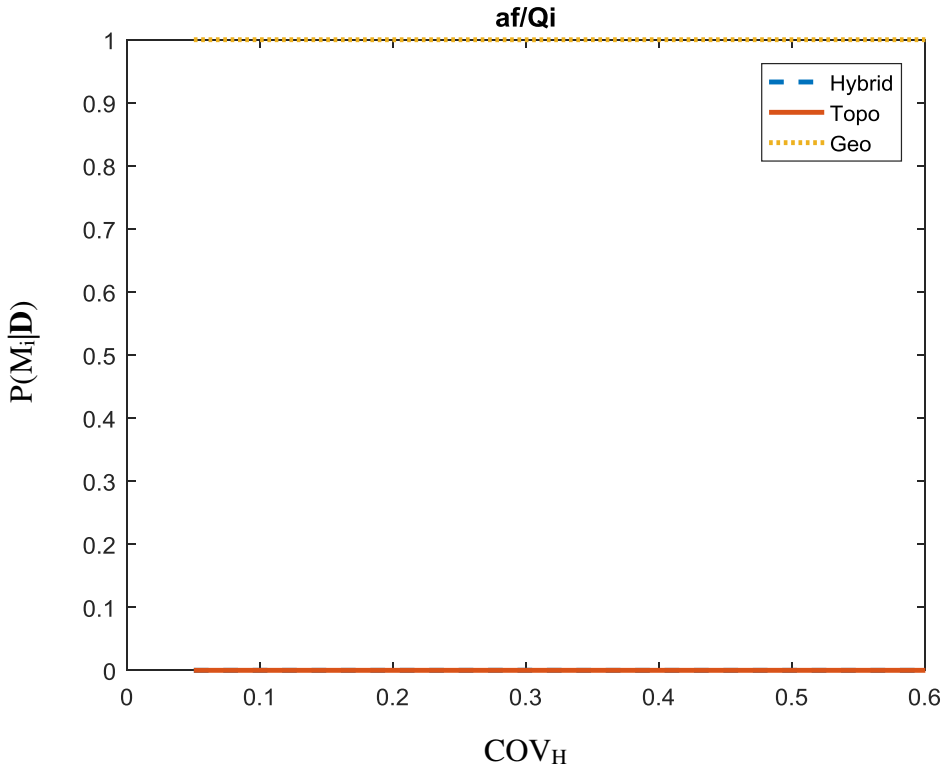

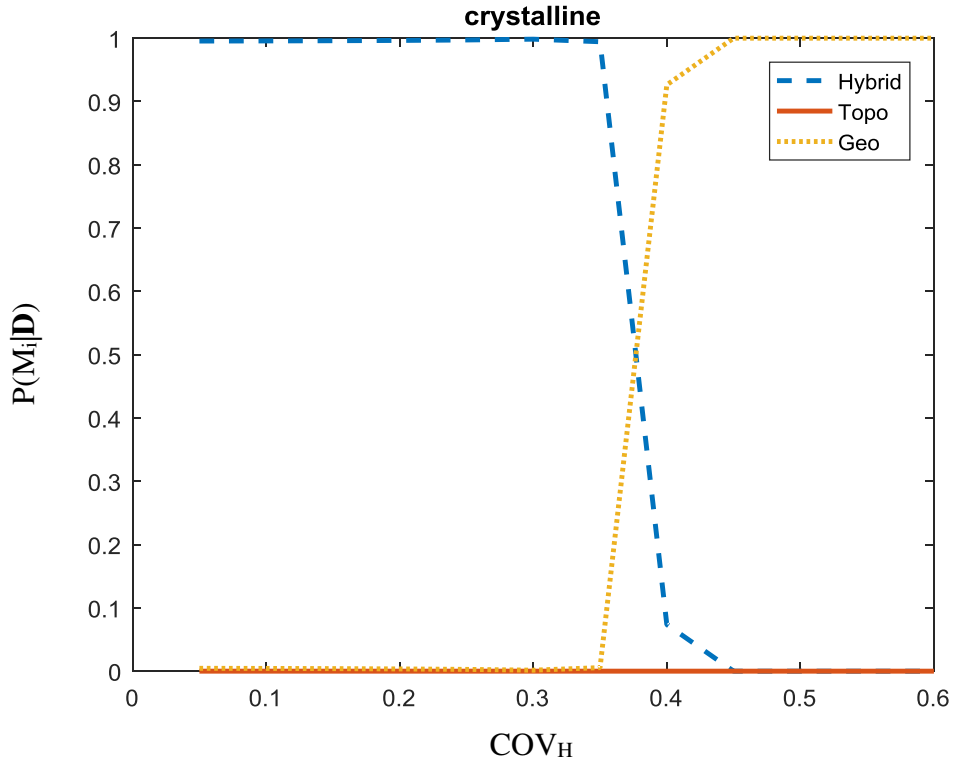
crystalline
Hybrid
Topo
Geo
P(M_i|D)
COV_H
0
0.1
0.2
0.3
0.4
0.5
0.6
0.7
0.8
0.9
1

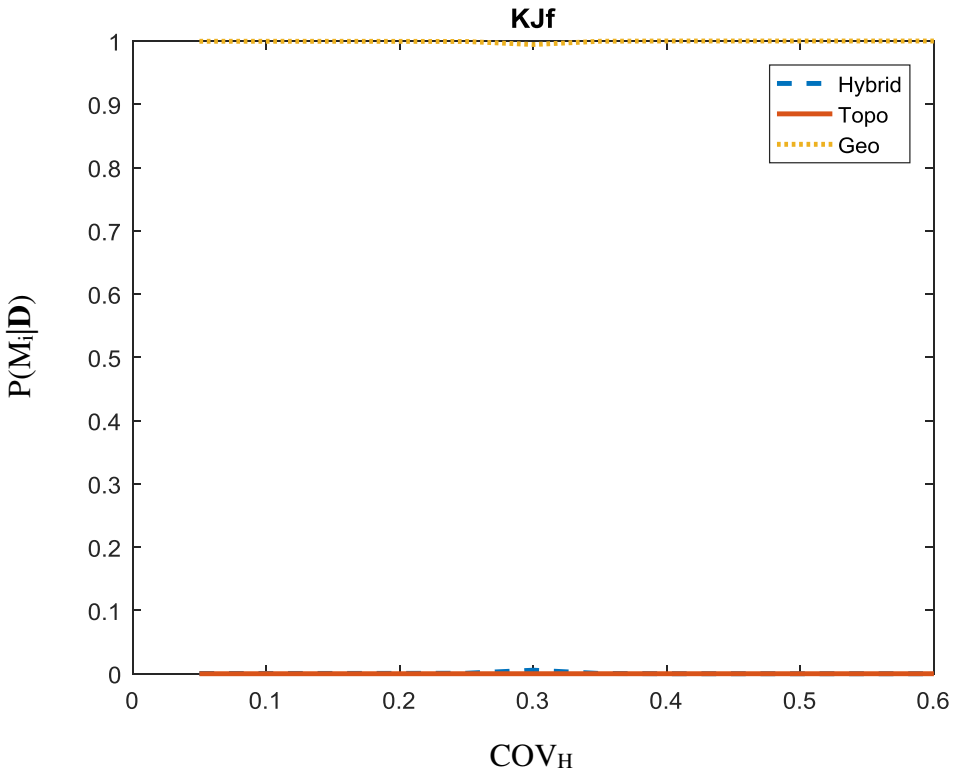
KJf
Hybrid
Topo
Geo
P(M_i|D)
COV_H
0
0.1
0.2
0.3
0.4
0.5
0.6
0.7
0.8
0.9
1

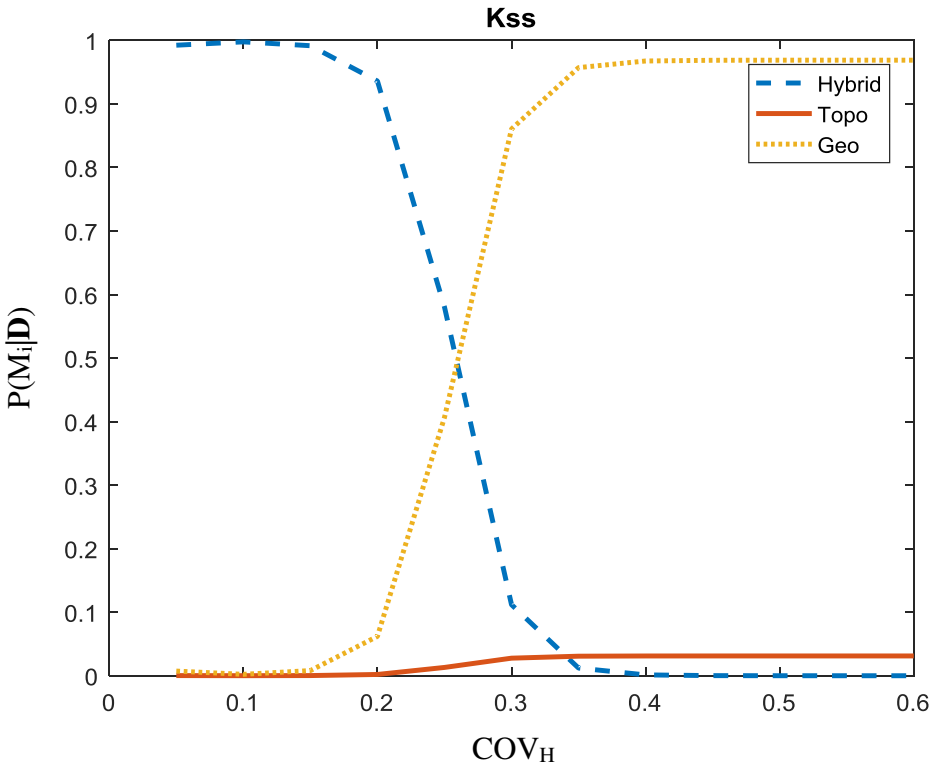
Kss
Hybrid
Topo
Geo
P(M_i|D)
COV_H
0
0.1
0.2
0.3
0.4
0.5
0.6
0.7
0.8
0.9
1

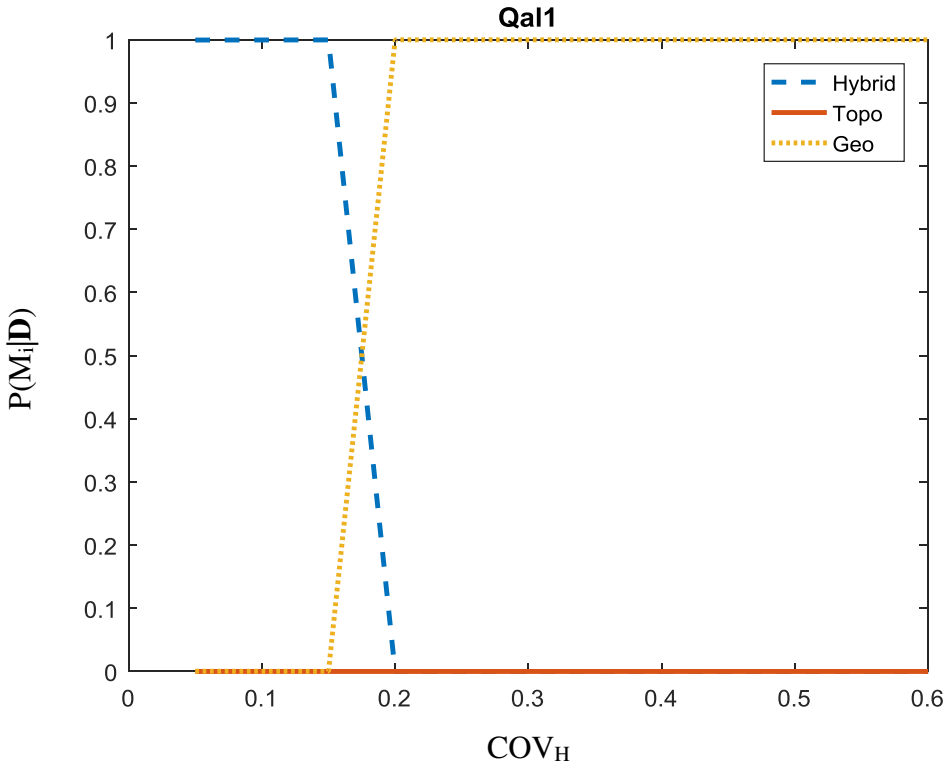
Qal1
Hybrid
Topo
Geo
P(M_i|D)
COV_H
0
0.1
0.2
0.3
0.4
0.5
0.6
0.7
0.8
0.9
1

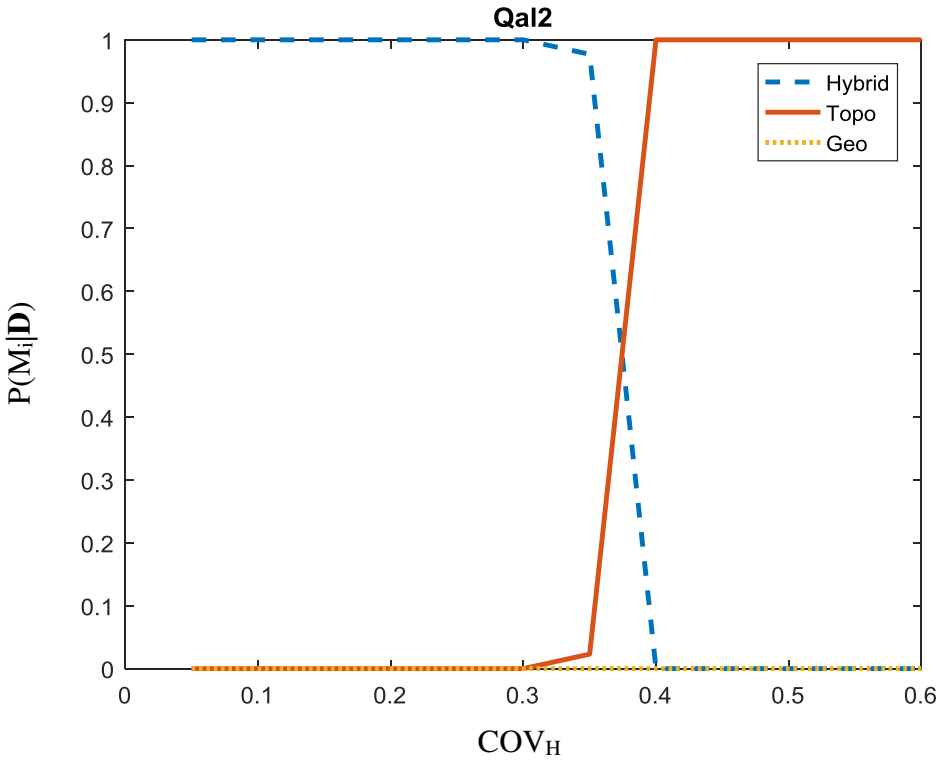
Qal2
Hybrid
Topo
Geo
P(M_i|D)
COV_H
0
0.1
0.2
0.3
0.4
0.5
0.6
0.7
0.8
0.9
1

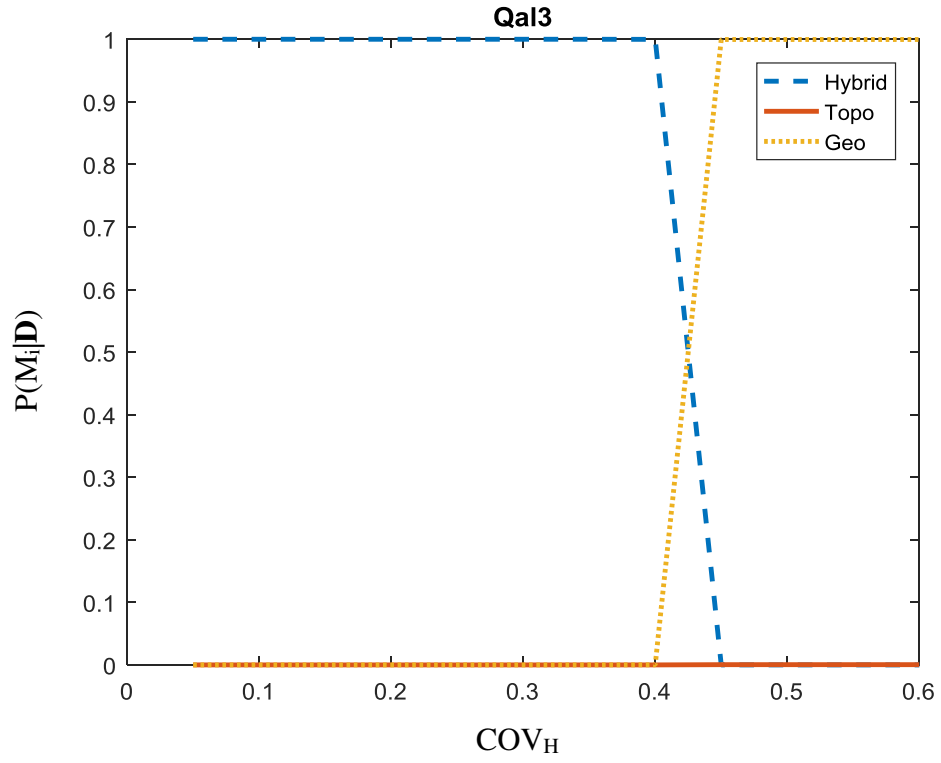
Qal3
Hybrid
Topo
Geo
P(M_i|D)
COV_H
0
0.1
0.2
0.3
0.4
0.5
0.6
0.7
0.8
0.9
1

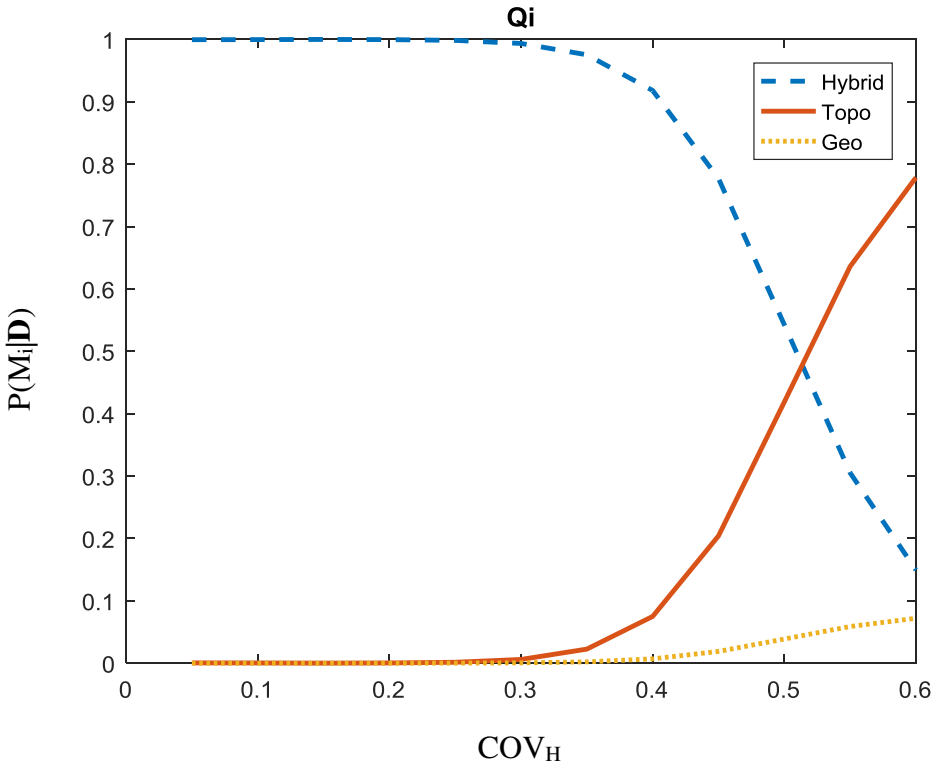
Qi
Hybrid
Topo
Geo
P(M_i|D)
COV_H
0
0.1
0.2
0.3
0.4
0.5
0.6
0.7
0.8
0.9
1

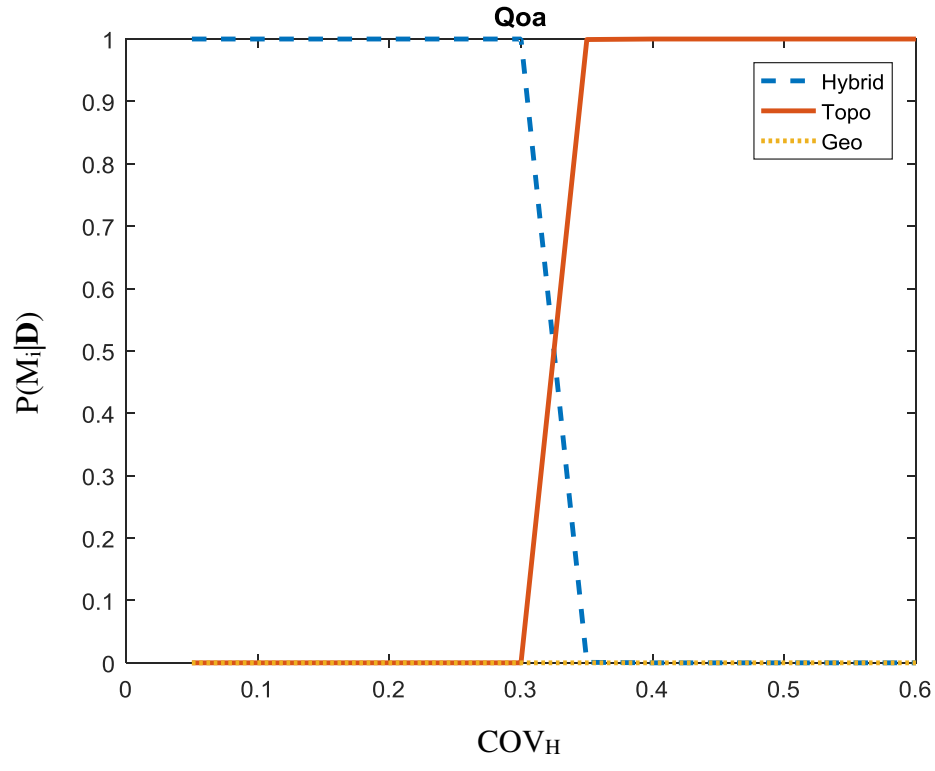
Qoa
Hybrid
Topo
Geo
P(M_i|D)
COV_H
0
0.1
0.2
0.3
0.4
0.5
0.6
0.7
0.8
0.9
1

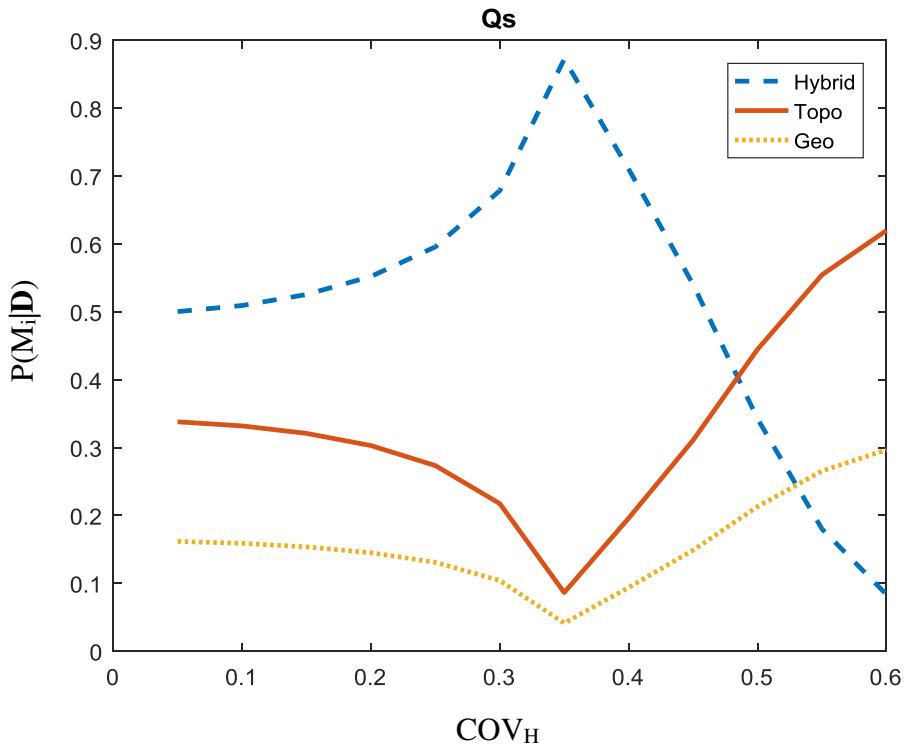
Qs
Hybrid
Topo
Geo
P(M_i|D)
COV_H
0
0.1
0.2
0.3
0.4
0.5
0.6
0.7
0.8
0.9

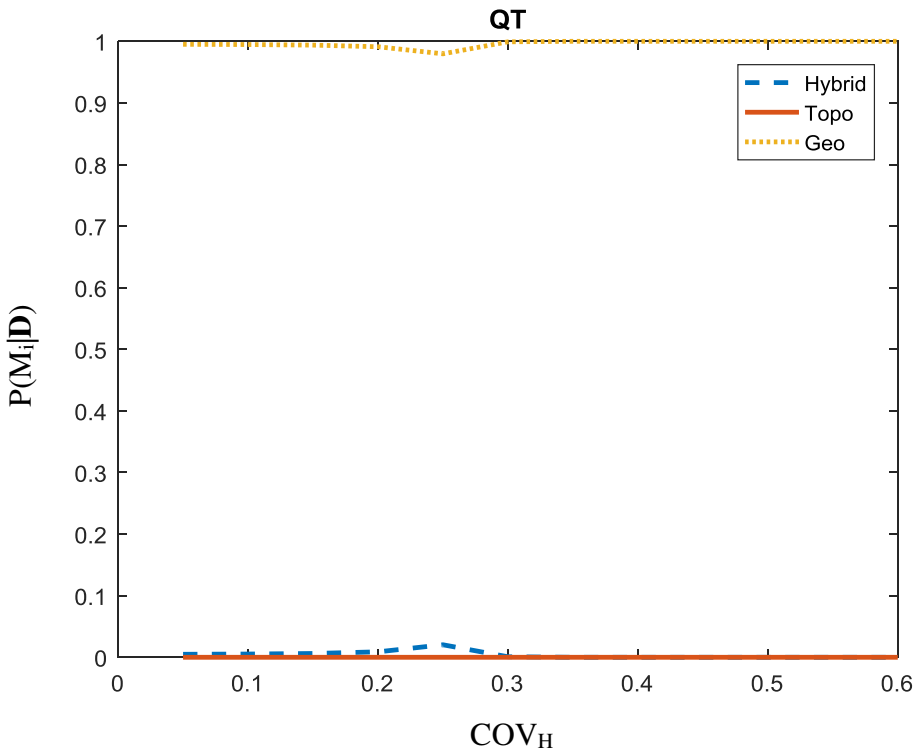
QT
Hybrid
Topo
Geo
P(M_i|D)
COV_H
0
0.1
0.2
0.3
0.4
0.5
0.6
0.7
0.8
0.9
1

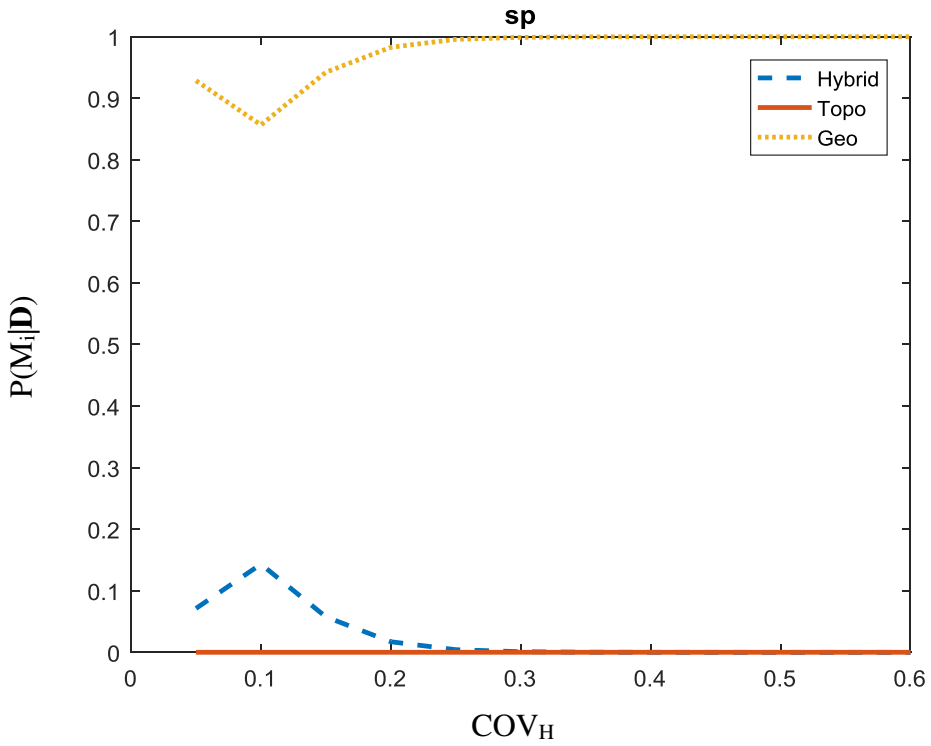
sp
Hybrid
Topo
Geo
P(M_i|D)
COV_H
0
0.1
0.2
0.3
0.4
0.5
0.6
0.7
0.8
0.9
1

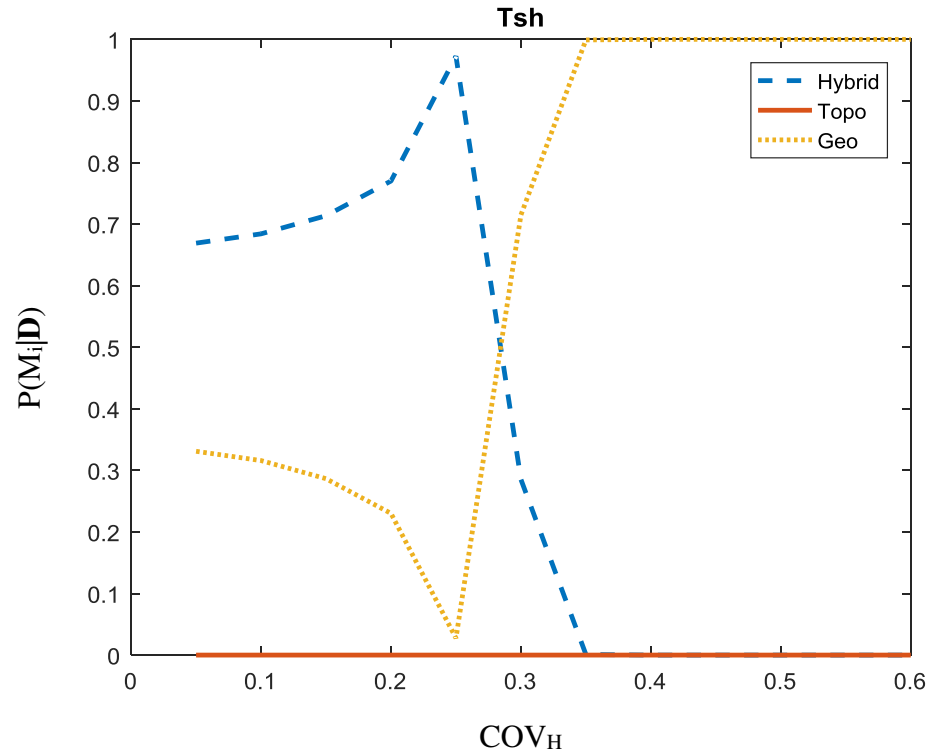
Tsh
Hybrid
Topo
Geo
P(M_i|D)
COV_H
0
0.1
0.2
0.3
0.4
0.5
0.6
0.7
0.8
0.9
1

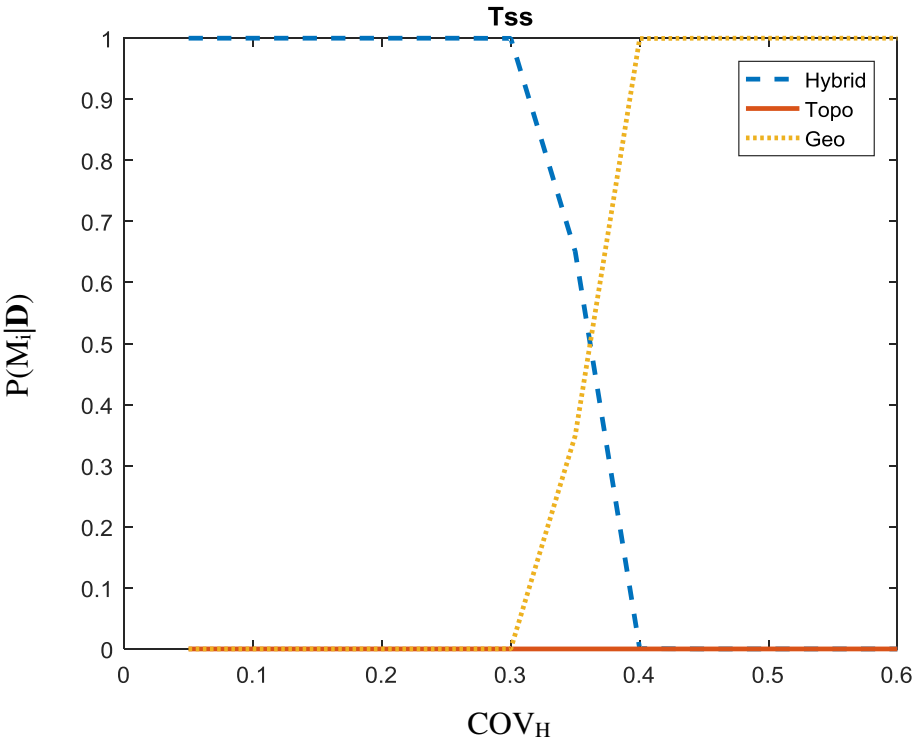
Tss
Hybrid
Topo
Geo
P(M_i|D)
COV_H
0
0.1
0.2
0.3
0.4
0.5
0.6
0.7
0.8
0.9
1

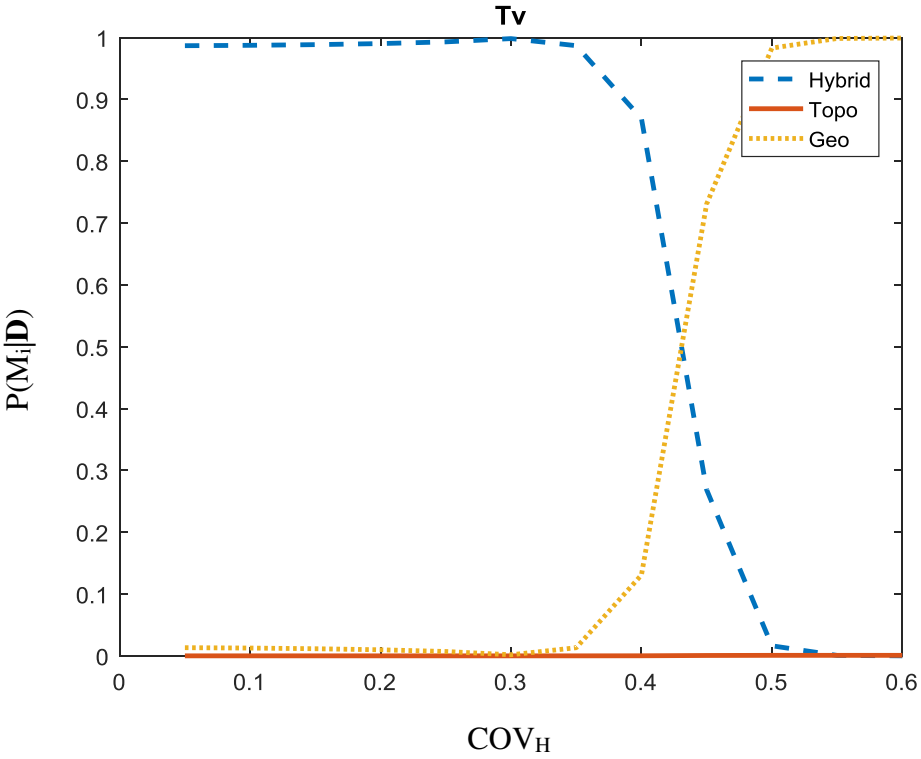
Tv
Hybrid
Topo
Geo
P(M_i|D)
COV_H
0
0.1
0.2
0.3
0.4
0.5
0.6
0.7
0.8
0.9
1

APPENDIX B

This appendix includes preliminary MATLAB code that can be used to automatically perform liquefaction hazard quantification calculations. It was developed to run using the API for the USGS 2008 deaggregation tool and hazard curve tool, which are no longer available.

```
%%%CPT-data interpreter script which can be used to perform
calculations%%%
%%%related to liquefaction-induced damage, such as expected settlement
%%%
%%%and probability of exceeding threshold settlement values
%%%

%%%               Written by Andrew Brownlow 1/31/2017
%%%

clear
clc
%Navigate to appropriate folder
%This is where the CPT data is stored
cd('./CPT_data/')

%The year should be defined for the current study, and is needed to
%communicate with the USGS deaggregation server
%Note: years is the string version of the exposure time
years = '50';
year = 50;

%%%Read Vs30 Data from provided file. This is a file containing
location
%%%data and Vs30 values. The current map (San_Francisco.xyz) was
obtained
%%%from the USGS Global Vs30 model website. This map is pre-defined,
and
%%%available at
http://earthquake.usgs.gov/hazards/apps/vs30/predefined.php
%%%A custom version of this map can be generated using the tool from
the
%%%same source http://earthquake.usgs.gov/hazards/apps/vs30/custom.php

%This input can be changed by referencing a different file. The code
for
%reading and interpreting this input is in the findVs30.m function. If
this
%line is uncommented, it should be commented out in the findVs30.m
function
```

```
Vs30Data = load('../Vs30/San_Francisco.xyz');

%Obtain input file
filelist = dir('*.txt');
%Create output matrix
%The number hard-coded into the columns dimension corresponds to the
number
%of outputs desired from the location-specific output matrix, which can
be
%used to generate an EP curve
locationmat = {'Longitude','Latitude','Expected LPI','Expected
Settlement (cm)'};
epcurvedata =
{'Longitude','Latitude','P(S>0.01cm)','P(S>0.025cm)','P(S>0.05cm)','P(S
>0.1cm)','P(S>0.25cm)','P(S>0.5cm)','P(S>1cm)','P(S>2cm)','P(S>3cm)','P
(S>4cm)','P(S>5cm)','P(S>6cm)','P(S>7cm)','P(S>8cm)','P(S>10cm)','P(S>1
2.5cm)','P(S>15cm)','P(S>20cm)'};
%Start of runtime measurement
tic


%This is the overarching loop of the script; for each iteration of the
%loop, one CPT data file is read from the CPT_data directory, and all
%functions and calculations are performed. This includes downloading
%location-specific deaggregation files and hazard curves from the USGS
%website, as well as all geotechnical calculations. A new directory is
%generated for each iteration of the loop to correspond to each CPT
data
%file/location of interest.
for iii = 1:length(filelist)
    filename = filelist(iii).name;
    %Read CPT data in file, and give output of UTM X- and Y-
coordinates,
    %water table depth, Vs30 (currently hard-coded for the test so I
don't
    %have to worry about inputs), depth, qc, fs, longitude, and
latitude
    [UTM_X, UTM_Y, water, vs30, z, qc, fs, lon, lat, site] =
read_CPT_data(filename, Vs30Data);


    %Make a new folder (directory) with name of current site
    mkdir(site{3});


    %Deaggregation download: inputs loop
    for jjj = 1:6
        switch jjj
            case 1
                %contact USGS deaggregation website and input the
correct
                %hazard information for each location
```

```
                percents = '01';
                percent = 1;
                deaggi(jjj,:) = {[site{3} '_' percents '_' years], lat,
lon, percent, vs30, year, 1, 1, 1};
            case 2
                percents = '02';
                percent = 2;
                deaggi(jjj,:) = {[site{3} '_' percents '_' years], lat,
lon, percent, vs30, year, 1, 1, 1};
            case 3
                percents = '05';
                percent = 5;
                deaggi(jjj,:) = {[site{3} '_' percents '_' years], lat,
lon, percent, vs30, year, 1, 1, 1};
            case 4
                percents = '10';
                percent = 10;
                deaggi(jjj,:) = {[site{3} '_' percents '_' years], lat,
lon, percent, vs30, year, 1, 1, 1};
            case 5
                percents = '20';
                percent = 20;
                deaggi(jjj,:) = {[site{3} '_' percents '_' years], lat,
lon, percent, vs30, year, 1, 1, 1};
            case 6
                percents = '50';
                percent = 50;
                deaggi(jjj,:) = {[site{3} '_' percents '_' years], lat,
lon, percent, vs30, year, 1, 1, 1};

        end
    end

    %create format of text to be written to text file
    formatspec = '%s %g %g %g %g %g %g %g %g\n';
    %create new text file named pars inside folder for current site
    fileID = fopen(['./' site{3} '/pars.txt'], 'w');
    %get dimensions of deaggregation input matrix
    [nrows, ncols] = size(deaggi);
    for row = 1:nrows
        fprintf(fileID, formatspec, deaggi{row,:});
    end
    fclose(fileID);

    %Copy python script to newly created site folder
    copyfile('../deaggregations.py',[site{3} '/']);
    copyfile('../goodman.py',[site{3} '/']);
    copyfile('../goodman.pyc',[site{3} '/']);


    %Navigate into the appropriate current site's directory, run the
python
    %script to create the deaggregation files in a new directory named
```

```
    %downloads within each site's directory
    cd([site{3}])
    system('C:\Python27\python deaggregations.py');

    %create string versions of lat and lon
    lats = num2str(lat);
    lons = num2str(lon);


    %Hazard curve download from USGS website
    websave([site{3}
'.csv'],['http://geohazards.usgs.gov/hazardtool/curves.php?format=2&lat
=' lats '&lon=' lons
'&site=760&period=0p00'],weboptions('Timeout',Inf));

    %Transpose .csv file of hazard curve to be in columns without
column
    %headers.  This is necessary for the upcoming functions to work
    %properly.
    %First, get the field ID to open current site's downloaded hazard
curve
    %.csv file
    fid = fopen([site{3} '.csv']);
    dataformat = '%*s %*s %*s %*s %*s %q %q %q %q %q %q %q %q %q %q %q
%q %q %q %q %q %q %q %q';
    allcsv = textscan(fid,dataformat,'delimiter',',');
    allcsv = [allcsv{:}];
    for rowi=1:2
        for coli = 1:length(allcsv)
            hazcurvs(coli,rowi) = allcsv(rowi+1,coli);
        end
    end
    fclose(fid);
    hazcurvi = str2double(hazcurvs);
    csvwrite([site{3} '.csv'], hazcurvi);


    %Calculate Joint Distribution of Mw and a_max using MwAmax
function.
    sitename = site{3};
    [Grid_Mw,Grid_amax,p_Amax_Mw] = MwAmax(sitename);


    s_limit = 10 ;
    [settlement, settlement_matrix,
settlement001,settlement0025,settlement005,settlement01,settlement025,s
ettlement05,settlement1,settlement2,settlement3,settlement4,settlement5
,settlement6,settlement7,settlement8,settlement10,settlement12_5,settle
ment15,settlement20, LPI, LPI5plus] =
calc(Grid_Mw,Grid_amax,p_Amax_Mw,s_limit,qc,fs,z, water);
```

```
    %Navigate back to CPT_data input file to allow main loop to
continue
    %with next iteration
    cd ..


    %Temporary output while I test the code; currently writes latitude
    %and longitude to a matrix. Will be expanded to include outputs of
LPI
    %probability and settlement as a final result. (Settlement in cm)
    locationmat(iii+1,:) = {lon, lat, LPI, settlement};
    epcurvedata(iii+1,:) = {lon, lat,
settlement001,settlement0025,settlement005,settlement01,settlement025,s
ettlement05,settlement1,settlement2,settlement3,settlement4,settlement5
,settlement6,settlement7,settlement8,settlement10,settlement12_5,settle
ment15,settlement20};%for settlementX values, X is defined in calc.


end

xlswrite('ExpectedResponse.xlsx',locationmat);
xlswrite('Settlement_EPCurve.xlsx',epcurvedata);

locationmatheader = ['Longitude','Latitude','Expected LPI','Expected
Settlement (cm)'];
epcurvedataheader =
['Longitude','Latitude','P(S>0.01cm)','P(S>0.025cm)','P(S>0.05cm)','P(S
>0.1cm)','P(S>0.25cm)','P(S>0.5cm)','P(S>1cm)','P(S>2cm)','P(S>3cm)','P
(S>4cm)','P(S>5cm)','P(S>6cm)','P(S>7cm)','P(S>8cm)','P(S>10cm)','P(S>1
2.5cm)','P(S>15cm)','P(S>20cm)'];
fid = fopen('ExpectedResponse.csv', 'w');
fprintf(fid, 'Longitude,Latitude,Expected LPI,Expected Settlement
(cm)\n');
fclose(fid);


%End of runtime measurement
toc
cd('../')
```